

The hydrological change under extreme drought in the United States: Separating climate and landscape impacts

Xinbai Xie



The hydrological change under extreme drought in the United States: Separating climate and landscape impacts

by

Xinbai Xie

to obtain the degree of Master of Science
at the Delft University of Technology,
to be defended publicly on Wednesday July 8, 2020 at 9:00 am.

Student number: 4792130

Project duration: October, 2019 – July, 2020

Thesis committee:	Dr. M. Hrachowitz	TU Delft (Chairman)
	Dr. ir. R. J. van der Ent	TU Delft
	Dr. ir. S. G. J. Heijman	TU Delft

An electronic version of this thesis is available at <http://repository.tudelft.nl/>.



Acknowledgements

This thesis describes my research about exploring hydrological change induced by extreme drought events in basins across the United States. It is also the final product of my graduation project for the Master of Science at the Delft University of Technology.

First of all, I would like to thank Markus Hrachowitz, my supervisor and the chair of my thesis committee. With your suggestions, support, guidance and supervision, I could keep the right way in my research, solve the problems I encountered throughout the process and learn how to be a hydrologist to take control and make decisions about my project. Your encouragement, concern and enthusiasm are much appreciated, and it has been great to have you as my supervisor. In addition, I would also like to thank the other members of the committee, Ruud van der Ent and Bas Heijman. Thank you for your feedback, comments, help and contributions to my research. You provided me with various ideas about my research, which made it more creative and of higher quality.

I am thankful to all my colleagues in Water Management, most of whom are also my friends. With their help, I spent two years studying in the Netherlands full of challenges and difficulties, as well as joy and happiness. I want to mention Xiaopei in particular, my classmate and even my friend. We are always the best partners, no matter in study or life. We always support and encourage each other. I am glad that I met you in the Netherlands.

Thank you, Yanwen, my roommate. You gave me a lot of support and help in the two years, especially the hard time of lockdown due to COVID-19. Although we are from different faculties, we always encourage each other. You were the one that I could rely on during that hard time.

Furthermore, Mom and Dad, thank you for supporting every decision I made and always believing in me. I love you.

Enjoy your reading!

Xinbai Xie
Delft, July 2020

Abstract

Current climate change characterized by increasing temperature has led to an increase in the intensity and frequency of extreme droughts that have more prolonged and profound ecohydrological and social impacts. By paying attention to the hydrological change before and after extreme drought and the patterns of drought recovery of ecological hydrological system, it is possible to better understand the consequences of extreme drought on ecohydrological system. Both climate change and landscape change have an influence on catchment hydrological condition. The drought-related hydrological change is, therefore, the combination of changes induced by these two drivers. To further explore extreme drought impacts and the root causes of hydrological change under extreme drought events, it is necessary to separate the impact of drought-related climate change from the impact of landscape change. This study aims to characterize the variations in hydroclimatic conditions before and after extreme drought by studying the hydroclimatic movements in Budyko space, explore post-drought ecohydrological system recovery, and further separate and investigate the effects of climate change and landscape change on catchment hydrological conditions.

Monthly Standard Precipitation Evapotranspiration Index (SPEI) at a 12-month timescale was used to characterize and define the extreme drought events. The Budyko framework was applied to study the hydroclimatic changes of 63 basins in the United States induced by extreme drought events from 1990 to 2013 by quantifying the hydroclimatic movements in Budyko space. The climate effect on precipitation partitioning was distinguished from the landscape effect that is mainly related to vegetation response to extreme drought events. The contributions of precipitation and potential evaporation were quantified to further understand the effect of climate change which is caused by alterations of these climatic variables. To understand the effect of drought-related vegetation change on catchment precipitation partitioning, Normalized Difference Vegetation Index (NDVI) was applied to examine the response of vegetation to drought in terms of alteration in vegetation greenness and patterns of vegetation recovery.

There were significant hydroclimatic changes in the basins before and after extreme drought. In post-drought period, more precipitation tended to be partitioned into evaporation in most of the basins. Change in streamflow was larger than the change in evaporation. 63.5% of all the basins experienced wetter conditions and more precipitation after drought. All basins gradually recovered in post-drought period, but not fully restored to their pre-drought states. The hydrological change under extreme drought was not explained by climate change alone in these basins, suggesting the existence of landscape drivers. The climate and landscape effects on precipitation partitioning could either enhance or counteract each other. The landscape drivers contributed more to drought-related change in catchment precipitation partitioning. In terms of the climatic effect that associated with the change in aridity index, the drought-related climate change affects catchment precipitation partitioning by changing the precipitation and potential evaporation, among which precipitation is a more crucial climatic driver. From a vegetation-related landscape perspective, vegetation greenness reverted to pre-drought level within three years in most of the basins. The rapid or slow recovery, regrowth and even degradation of vegetation in post-drought period cause landscape-driven changes in catchment precipitation partitioning through directly changing vegetation transpiration and streamflow.

This study gives insight into change in hydrological conditions before and after extreme drought and possible causes based on climate change and landscape change, vegetation change in particular. It could help to better understand the impacts of extreme droughts on ecohydrological system.

Contents

- 1 Introduction..... 1**
 - 1.1 Background 1
 - 1.2 Research objective and questions 3
 - 1.3 Thesis outline 3
- 2 Literature study..... 4**
 - 2.1 Background information of drought..... 4
 - 2.1.1 Drought definition 4
 - 2.1.2 Drought recovery..... 5
 - 2.2 Application of Budyko framework..... 5
 - 2.3 Climate change and its effect 6
 - 2.4 Drought-related vegetation change and its effect 7
- 3 Materials and methods..... 9**
 - 3.1 Study areas 9
 - 3.1.1 Basin dataset..... 9
 - 3.1.2 Basin selection..... 10
 - 3.2 Data 11
 - 3.2.1 Meteorological data and its processing 11
 - 3.2.2 Remote sensing data and its processing 12
 - 3.3 Methods..... 13
 - 3.3.1 Definition of extreme drought event 13
 - 3.3.2 Budyko framework..... 15
 - 3.3.3 Decomposition method for separating of climate and landscape impacts..... 16
 - 3.3.4 Detection of ecohydrological system recovery in post-drought period..... 19
 - 3.3.5 Detection of vegetation changes and responses 19
- 4 Results 21**
 - 4.1 Characteristics of extreme drought events 21
 - 4.2 Hydroclimatic movements in Budyko space..... 21
 - 4.3 Climate-driven movement and climatic effect 26
 - 4.4 Relationship and interaction between climate and landscape effects 28

4.5 Recovery of ecohydrological system in post-drought period	32
4.6 Vegetation change and its effect on landscape-driven change.....	36
5 Discussion.....	39
5.1 Definition of pre-drought, drought and post-drought periods	39
5.2 Drought recovery of ecohydrological system.....	40
5.3 Drought-related climate change and climatic effect.....	40
5.4 Vegetation-related landscape effect on precipitation partitioning	41
5.5 Other possible landscape drivers	42
5.6 Uncertainty and limitation.....	42
6 Conclusion.....	44
References	49
Appendix	55
Appendix A: Catchment characteristics of 63 basins	55
Appendix B: Time series of monthly SPEI at a 12-month timescale of 63 basins	57
Appendix C: Drought characteristics and pre- and post-drought periods	79
Appendix D: Relative changes of streamflow and evaporation	81

1 Introduction

1.1 Background

The severity of droughts has been subject to an increasing trend worldwide, which could be ascribed to the rapid and steep increase in temperature (Sheffield and Wood, 2008; Dai, 2013). Extreme drought events have become increasingly frequent (Beniston and Stephenson, 2004). Compared to mean hydrological conditions or even mild and moderate droughts, extreme droughts have more significant impacts on ecological environment and human society, which is manifested from diverse aspects including water resources, ecosystems, agriculture, energy, and economy, etc. (Wigley, 1985). More recent attention of hydrologic research has focused on characteristics of extreme drought events and drought impacts on ecohydrological system (Cavin et al., 2013; Espinoza et al., 2011; Young et al., 2017; Yang et al., 2017). Understanding and evaluating the influences of extreme drought events on ecohydrological system is of great importance to predict future hydrological extremes, improve integrated water management and strengthen extreme droughts mitigation measures.

Many previous studies on the impacts of extreme droughts paid particular attention to hydrological impacts and climate features during extreme droughts (Espinoza et al., 2011; Potter and Chiew, 2011; Marengo and Espinoza, 2016; Spinoni et al., 2017). Besides, since plants are an essential part of ecohydrological system and play a crucial role in energy and water cycles, considerable efforts have already been made to evaluate the influences of extreme droughts mainly on forest. These studies linked the tree mortality and degradation to extreme droughts and investigated tree recovery from extreme drought effects (Liang et al., 2003; Cavin et al., 2013; Zhao et al., 2015; Serra-Maluquer et al., 2018). However, most recent studies have not taken the spatial heterogeneity of extreme drought characteristics into account and only focused on a single extreme drought event. For instance, Zhao et al. (2015) used a set drought period from January 2009 to December 2010 throughout the study areas in their extreme drought investigation. The extreme drought events could differ in onset, offset and other characteristics among different basins. Understanding the general patterns of different extreme drought events occurring in various watershed systems is, therefore, necessary for basin-scale hydrology. Besides, identifying drought periods for individual basins is also needed. Moreover, there are still uncertainty of effects of extreme droughts on ecohydrological system in post-drought period. The response of ecohydrological system to extreme droughts in post-drought period directly implies the recovery of ecohydrological system from extreme droughts, which is of great importance for extreme drought management, extreme drought risk evaluation and post-drought development. Besides, it is possible to better understand the impacts of extreme droughts on ecohydrological system by investigating the changes in hydroclimatic conditions before and after extreme drought.

The changes in hydrological and climatic conditions are the response of ecohydrological system to variations in water fluxes and water resources on land induced by drought. The partitioning of precipitation into evaporation and streamflow shows the conversion and interaction between the water fluxes in water cycles. Budyko framework (Budyko, 1974), which builds a connection between water and energy balance and describes water cycles implied by evaporative index as a function of climate implied by aridity index, is

widely applied to detect the hydroclimatic change and determine the effects of global climatic and environmental changes on land water fluxes. (Renner et al., 2012; Van der Velde et al., 2014; Jaramillo and Destouni, 2014). Moreover, it has been generally recognized that different environmental drivers, mainly including climate change and landscape change, can cause alterations in the water balance, resulting change in water partitioning. (Zhao et al., 2015; Jaramillo and Destouni, 2014). Climate change has an impact on precipitation partitioning by changing precipitation and potential evaporation, while landscape change directly affect the partitioning of precipitation into river runoff and evaporation (Tomer and Schilling, 2009). Nevertheless, the two essential effects are difficult to disentangle empirically. Budyko framework is therefore required to further distinguish the combined effect of climate and landscape changes. The climatic effect on catchment precipitation partitioning that is represented by changes in the aridity index is, therefore, supposed to be separated from the effect of landscape change. Similarly, extreme droughts might lead to both climate and landscape changes. Yang et al. (2017) found that both climate and catchment landscape controlled the recovery of hydrologic system from extreme droughts. The hydrological change in ecohydrological system before and after extreme drought might also be the result of drought-related climate change and landscape change simultaneously. Therefore, when investigating hydrological change under the influence of extreme drought, different driving factors should be considered. Despite this, to date, only a few studies have explored the impacts of extreme droughts on ecohydrological system from a perspective of different drivers. The combined impact of drought-related climate and landscape changes on variations of precipitation partitioning is still challenging to be separate, and the dominant effect among the two effects remains largely unknown. Therefore, it is interesting to get more insight into the catchment hydrological response to extreme drought and distinguish climate and landscape impacts on catchment precipitation partitioning by using the Budyko framework.

In addition, separating the climate- and landscape-driven changes in water partitioning is also of great importance for understanding in deep how extreme droughts affect ecohydrological system and how ecohydrological system recovers from extreme drought as well. More importantly, this provides a direction for exploration of essential causes of hydrological change in case of extreme droughts and helps to analyze the catchment hydrological response to climate and landscape changes respectively. For the causes, from a climatic perspective, the drought-induced variations in precipitation and potential evaporation, expressed by in terms of changes in aridity index, could cause the alterations in precipitation partitioning (Han et al., 2018). For instance, Vose et al. (2016) found that less precipitation was partitioned into runoff after drought, which was the result of post-drought runoff reduction due to reduced rainfall amounts. On the other hand, under a natural and unregulated condition, vegetation change plays a dominant role in landscape change, leading to hydrological change through mainly affecting evapotranspiration (Jaramillo et al., 2018). The vegetation response to drought, especially drought-related vegetation die-off and recovery, might cause the different changes in precipitation partitioning in different geohydrological conditions through directly affecting evaporation, transpiration, and canopy interception and also indirectly changing runoff (Guardiola-Claramonte et al., 2011; Adams et al., 2012). Therefore, it is necessary to further quantify and explore drought-related climate effect and landscape effect, vegetation-related impact in particular, on catchment precipitation partitioning respectively to better understand the root causes of hydrological change before and after extreme drought.

1.2 Research objective and questions

This research aims to quantify the variations in hydroclimatic condition before and after extreme drought events through detecting the hydroclimatic movements in Budyko space by applying a previous application of Budyko framework (Jaramillo and Destouni, 2014; Jaramillo et al., 2018; Van der Velde et al., 2014), and detect the recovery of ecohydrological system in post-drought period. A crucial relevant aim is to separate the dominant effects, namely climate and landscape impacts, on catchment precipitation partitioning and further explore the effects of climatic variables and drought-induced vegetation change to investigate the causes of hydrological change induced by extreme drought. This leads to the main research question:

How do hydrological conditions change between pre- and post-drought periods under extreme drought events and what causes these changes?

To answer the main research question, the following sub-questions will be answered:

1. How do hydroclimatic conditions change before and after extreme drought event?
2. What are the relationship and interaction between climate and landscape effects on change in catchment precipitation partitioning?
3. What are the patterns of post-drought ecohydrological system recovery?
4. How does drought-related climate change affect catchment precipitation partitioning?
5. How does drought-related vegetation change affect catchment precipitation partitioning?

1.3 Thesis outline

Chapter 2 discusses more information and knowledge already presented in other relevant studies. The materials and methods used in this study are explained in Chapter 3. This includes the details of study areas and the used data. Besides, preliminary data processing and selection of study objects (basins, and then extreme drought events) are described. Chapter 3 also contains the methods used and the details of how to use the available data and information to answer the research questions. The results are given in Chapter 4. Chapter 5 consists of discussions of the connection between the results of this study and the theories discussed in Chapter 2, some other related assumptions and further discussions based on the results, and descriptions of other possible factors that might limit and affect the results. Finally, the conclusions of this study are summarized and some recommendations and suggestions for future research are provided in the last chapter.

2 Literature study

Relevant background information and an overview of the current knowledge presented in other studies that are related to this study are described in this chapter. The background information of drought, including drought definition and drought recovery of ecohydrological system, is discussed in section 2.1. Next, the application of the Budyko framework to detect hydroclimatic change in previous studies is presented. Section 2.3 discusses the background information on the effect of climate change on catchment hydrological condition. Section 2.4 summarizes the background information of drought-induced vegetation change, especially post-drought vegetation response, and its effect on hydrological response.

2.1 Background information of drought

2.1.1 Drought definition

The American Meteorological Society (1997) divided the definitions of drought and drought varieties into four parts: meteorological, agricultural, hydrological and socioeconomic. Meteorological drought refers to precipitation deficit or reduction that is unusually extreme over a prolonged period. Insufficient soil moisture that has an influence on plants, especially crops, during growth season can result in agricultural drought. Hydrological drought, which usually occurs after meteorological and agricultural drought, refers to a reduction in surface or subsurface water supply after prolonged precipitation deficit. Socioeconomic drought refers to water deficit affecting human life and relates the economic demand of water supply to the other three droughts. Drought is often represented and quantified in sense of drought indicators. Streamflow drought index (SDI) is widely utilized to quantify hydrological drought based on streamflow data (Nalbantis and Tsakiris, 2009). Standardized precipitation index (SPI), Standardized Precipitation Evapotranspiration Index (SPEI) and Palmer Drought Severity Index (PDSI) are commonly used for quantification and definition of meteorological drought. SPI and SPEI have mathematical similarities, following similar calculation principles. The SPI is a drought indicator, focusing on precipitation deficit, which is based solely on precipitation data (McKee et al., 1993), while the SPEI captures the water balance, takes the impact of temperature into account (Vicente-Serrano et al., 2010) and avoids the inherent probability distribution fitting problem of SPI due to the presence of zero precipitation (Wu et al., 2007). The PDSI based on soil water balance has been widely applied to quantify prolonged drought and aridity changes, which is more complex and superior to SPI and SPEI (Sheffield, 2004; Dai, 2011). It depends on more factors, which means that more various data, including precipitation, temperature and soil information, is needed for the calculation. The drought event definition is usually accomplished through the method of McKee et al. (1993). A drought event starts when the value of the drought indices is less than -1 and ends when the value of the drought indices is positive. During the drought, the value of the drought indices keeps negative. The characteristics of drought are identified by means of theory of runs based on drought indices time series suggested by (Yevjevich, 1969).

In addition, in terms of the definition of extreme drought, there has been no consensus. There have been different definition methods in recent research. For example, Spinoni et al. (2017) defined an extreme drought event as the event during which the drought indices reach at least once a value below -2. Some other studies defined the extreme drought events based on drought years. The extreme drought year was regarded as when

the drought indices of are less than -2 for at least one month within vegetation growing season within that year (Silvio et al., 2015; George et al., 2017). Besides, Serra-Maluquer et al. (2018) defined extreme drought years as the years with the lowest drought indices among their time series. For different research objectives, these studies, therefore, have their own methods of identifying extreme drought.

2.1.2 Drought recovery

Drought has an great influence on both human and natural systems (Mishra and Singh, 2010). It has been fully recognized that ecohydrological system displays resilience after drought, that is, the ability of self-regulation to recover itself to pre-drought state (Bêche et al., 2009; Martorell et al., 2014; Hoover et al., 2014; Schwalm et al., 2017). A crucial metric of post-drought catchment hydrological response to drought event and impacts of drought is recovery time, that is, how long it takes for the ecohydrological system to return to its pre-drought state. Schwalm et al. (2017) suggested that the pattern of recovery time shows great spatial heterogeneity on a global scale, but ecohydrological system is able to recover rapidly within six months in most regions. Moreover, the larger the severity of a drought event is, the longer recovery time will be. The drought recovery is not only controlled by climatic conditions, but also by catchment properties that are associated with catchment hydrographical properties, vegetation conditions and in-drought hydrological changes (Mishra and Singh, 2010). Yang et al. (2017) and Schwalm et al. (2017) found that the situation of precipitation after drought might be the most predominant factor for drought recovery, while catchment landscape, especially vegetation condition implied by gross primary productivity, plays a crucial but secondary role in affecting drought recovery. The effects of other hydroclimatic conditions and catchment characteristics on drought recovery are relatively small. As a part of ecohydrological system, vegetation plays a critical role in hydrological response of catchment to drought; thus more and more attention has been focused on post-drought vegetation recovery. Li et al. (2019) found that vegetation greenness and vegetation productivity can restore within six months in most of Southwest China, with recovery time varying with vegetation types. Other studies found that some vegetation species can restore from drought after 1-5 years, while others need a longer time for recovery and keep low growth rate for decades in Spain (Camarero et al., 2011; Antonio Gazol and Camarero, 2016; Yin and Bauerle, 2017). In summary, ecohydrological system has the resilience to return itself to the pre-drought condition, and the recovery time could vary with geographical space, characteristics of drought events and catchment properties.

2.2 Application of Budyko framework

The Budyko framework is diffusely used to quantify the mean annual partitioning of precipitation into runoff and evaporation, expressed as evaporative index, as a function of climatic conditions expressed as the aridity index, a ratio of potential evaporation to precipitation (Budyko, 1974). This empirical relationship between aridity index and evaporative index, implying long term equilibrium water and energy balance, is represented by Budyko curve, different formulations of which have been derived based on various characteristics of catchment and climate (Lu Zhang et al., 2008). Since more recent attention has focused on changes in water cycles under climate change (Sivapalan et al., 2011), the Budyko framework has been widely applied for identifying patterns of catchment hydrological response and detecting the hydroclimatic change in recent studies. Van der Velde et al. (2014) applied the Budyko framework to detect and compare the hydroclimatic change in three different regions, including mountains, forests and agricultural areas in Sweden. A large and growing body of literature has investigated the effect of change in climatic conditions on the hydrological

response of river basin in terms of streamflow variation by using Budyko framework (Arora, 2002; Roderick and Farquhar, 2011; Renner et al., 2012). Besides, Yang and Yang (2011) further separated the contributions of different climatic variables, including air temperature, precipitation, wind speed and net radiation, to the elasticity of streamflow to deeply evaluate the climatic effects on streamflow. In addition, there is a large volume of studies investigating the relationship between changes in land use and land cover, especially vegetation changes, and alteration of hydrological conditions in terms of evapotranspiration change (Zhang et al., 2001) and streamflow change (Oudin et al., 2008) by using Budyko framework. Nevertheless, most of these studies only focused on an individual driver of hydrological change. The alterations in land cover and climate variables caused by climate change and human activities might affect the hydrological process of river basin simultaneously; hence, it has been realized that it is necessary to understand catchment hydrological response to the combination of these alterations (Xu et al., 2014). Therefore, the Budyko framework is required to further distinguished the combined effect of climate change and landscape change on catchment precipitation partitioning (Zhang et al., 2001). For instance, Wang and Hejazi (2011), Williams et al. (2012) and Creed et al. (2014) utilized the Budyko framework to distinguish catchment hydrological response to climate and landscape changes. More importantly, on the basis of these theories, Van der Velde et al. (2014), Jaramillo and Destouni (2014) and Jaramillo et al. (2018) further improved the application of the Budyko framework to explore catchment hydroclimatic change by studying change trajectory in Budyko space and separate different change drivers. This improved application allows comprehensive analytical change assessment without excessive amounts of various data, compared to other approaches which rely on complex models (Gudmundsson et al., 2016). On the whole, the application of Budyko framework in previous studies above might offer thinking and methods for exploring drought-related hydroclimatic change and catchment hydrological response to climate and landscape changes induced by extreme droughts for this study.

2.3 Climate change and its effect

The causes of the changes in catchment hydrological conditions are usually divided into climate change and landscape change (Jaramillo and Destouni, 2014), among which climate change refers to precipitation change and potential evaporation change that is further related to changes in temperature, radiation, wind speed and water vapor. The impacts of climate change are directly evaluated by the change in aridity index in Budyko framework (Jaramillo et al., 2018). Some studies focused on the climatic effect that is related to changes in aridity index on precipitation partitioning for understanding hydrological response to climate change. Considering only the effect of climate change, an increase in aridity index can lead to more precipitation partitioned into evaporation, while the reduction in aridity index can lead to less precipitation partitioned into evaporation (Jaramillo and Destouni, 2014; Jaramillo et al., 2018). Other studies estimated the effects of climate change on hydrological response in terms of runoff change based on the change in aridity index (Arora, 2002; Liu et al., 2013). The essence of change in aridity index is the changes in water fluxes, including precipitation and potential evaporation. Changes in these climatic variables are interactive and not independent. In terms of factors affecting aridity index, Li et al. (2017) and Sun et al. (2017) found that change in potential evaporation plays a dominant role in the change in aridity index in Southwest China, instead of precipitation change, which means that the alteration of potential evaporation contributes more to climate effect on hydrological response. However, Huo et al. (2013) found that contribution of the alteration in precipitation to the change in aridity index is more than that of the alteration in potential evaporation, which shows the opposite. For different watershed systems, the climatic effect on hydrological response can

vary significantly in time and space that depends on watershed characteristics (Vose et al., 2016). Hydrological response to climate change is complex and still needs further exploration. However, much uncertainty still exists about the drought-related changes in climatic conditions, especially changes in post-drought period, and their effects on catchment hydrological response and catchment water balance behavior. Similarly, the hydrological response to drought is represented directly by runoff response to drought through reduction or increase in precipitation and indirectly by evapotranspiration response to drought through variation in evaporative energy and water availability. Therefore, understanding the hydrological change induced by climatic drivers before and after extreme drought event and the effect of drought-related climate change can be obtained by using similar approaches used in previous studies mentioned above.

2.4 Drought-related vegetation change and its effect

Drought-related changes in vegetation, whether vegetation productivity reduction, plant mortality, changes in vegetation species or vegetation recovery and regrowth, can affect catchment hydrological response (Saft et al., 2015), as vegetation plays a vital role in controlling some hydrological fluxes, including transpiration, evaporation, canopy interception, streamflow and infiltration, etc. (Schlesinger and Jasechko, 2014). Catchment hydrological response to drought can be either aggravated or alleviated by how vegetation responds to drought (Vose et al., 2016). The understanding of post-drought vegetation change and relevant hydrological condition change, especially the alterations of runoff and transpiration, are mainly derived from using simulation models or synthesizing from studies with field sampling and indicators of vegetation activity and growth analyzing. For example, Mueller et al. (2005) found that both higher mortality following drought among mature pinyon compared to young pinyon and the post-drought transformation of the remaining pinyon could lead to lower runoff after drought through field sampling in 11 sites of San Francisco volcanic field. Vicente-Serrano et al. (2013) found that lower runoff after drought than before could be explained by the conversions of plant species towards the species that can extract water more efficiently. Other studies found that slow regrowth following drought could cause a rise in runoff (Adams et al., 2012; Saft et al., 2015). Therefore, after vegetation die-off and degradation induced by drought, the recruitment and restoration of vegetation can result in either decrease or increase in streamflow, which depends on vegetation recovery and regrowth dynamics, especially the water consumption during regrowth (Brown et al., 2005). Besides, post-drought vegetation change can also affect the catchment hydrological conditions in terms of transpiration variation. In the post-drought period, when soil moisture is sufficient and water stress is alleviated, more water could be available for vegetation to support transpiration for increasing vegetation biomass and thus rapid recovery (Helman et al., 2017; Han et al., 2018). Except for the improvement of climatic conditions, Julio Camarero et al. (2018) further found that the increasing vegetation biomass with more transpiration could also be explained by the reduction in competition among vegetation communities. The vegetation mortality induced by drought could lead to less competition for resources among the surviving vegetation (Callaway and Walker, 1997), promoting vegetation recovery. Other studies found that the drought resilience might decline, and post-drought vegetation regrowth could be slow due to the existence of legacy effects of drought (Anderegg et al., 2015; Julio Camarero et al., 2018), which can lead to reduced transpiration (Saft et al., 2015). For the legacy effects of drought on vegetation, there are still some studies with opposite conclusions. Instead of leading to slow regrowth and further degradation of vegetation, legacy effects of drought could cause a strong resilience of vegetation (Gazol et al., 2017; Wu et al., 2018), which might lead to the opposite hydrological response. In summary, vegetation response to drought can lead to a different hydrological response, directly presented by different variations in streamflow and vegetation transpiration.

Fully understanding how the post-drought vegetation change, especially restoration or further degradation, affects catchment hydrological response still presents a considerable challenge due to limited data and other limitations and uncertainties.

3 Materials and methods

This chapter describes the materials and methods used in this study. Section 3.1 describes the information of the study areas with details of catchment properties and criteria of basin selection. The used data, including meteorological data and remote sensing data, and its processing are discussed in section 3.2. All the methods used to answer the research questions are mentioned in section 3.3.

3.1 Study areas

3.1.1 Basin dataset

534 small and medium basins spanning the entire continental United States were used as preliminary research objects in this study. The locations of these basins are shown in Figure 3.1. The area of all basins is less than 1000 km². These 534 basins are part of the basin data set of unregulated basins used in a hydrologic model performance assessment study in the United States (Newman et al., 2015). The spatial features of basin network were created by the Geospatial Fabric for national hydrological modelling, which is allowed for measurement of total basin area upstream of the streamflow gauge (Viger, 2014). Elevation contour polygon shapefiles of the basins were also created by Geospatial Fabric dataset based on the digital elevation model (DEM). These basins cover an extensive variety of hydrological and climatic conditions, ranging from wet to dry and from cool to hot basins. Most of the basins have minimal human interference on land use change, water distribution and water withdrawal. The basin shapefile dataset was obtained from Camels dataset (<https://ral.ucar.edu/solutions/products/camels>).



Figure 3.1: Location map and spatial distribution of the 534 basins in the continental United States.

3.1.2 Basin selection

The hydrological cycle of basin is supposed to follow the long-term water balance. The long-term water balance for a basin can be expressed as:

$$\bar{P} - \bar{E}_a - \bar{Q} = \Delta S = 0 \quad (3.1)$$

Where \bar{P} is the long-term mean annual precipitation, \bar{E}_a is the long-term mean annual actual evaporation, \bar{Q} is the long-term mean annual streamflow at the basin outlet, ΔS is change in water storage within the basin.

Over a long-term period, the water storage change (ΔS) should be significantly smaller than other water fluxes, which permits the assumption of zero long-term water storage change. From the perspective of energy constraint, the actual evaporation should not be larger than the potential evaporation which represents the energy input and maximum amount of water evaporated under ideal conditions. Therefore, to satisfy such an energy constraint, Equation 3.1 can be rewritten as:

$$\bar{P} - \bar{Q} = \bar{E}_a < \bar{E}_p \quad (3.2)$$

Where \bar{E}_p is the long-term mean annual potential evaporation.

With the meteorological data used in this study, including precipitation, potential evaporation and streamflow, the long-term hydrological cycle of basin should therefore meet the following requirement:

$$\bar{P} - \bar{E}_p - \bar{Q} < 0 \quad (3.3)$$

Therefore, basins that fail to meet the above condition are excluded in this study. In addition, this study focuses on the hydrological change between pre- and post-drought periods in case of extreme drought events, hence only the basins where experienced extreme drought events are kept for the analysis in this study. The details of both the drought definition and drought event selection are discussed in Chapter 3.3.1. After checking the long-term water balance behavior of the basins and selecting drought events, 63 basins that meet all the requirements were selected from the 534 basins as final research objects in this study. The spatial distribution and locations of the 63 basins are indicated in Figure 3.2. The long-term mean hydroclimatic conditions of the 63 basins are shown in Figure 3.3. Over the period 1981-2013, most of the 63 basins experienced energy limited conditions implied by aridity index (E_p/P) less than 1, which denotes that these basins were in relatively humid conditions with the actual evaporation more constrained by energy availability than by water availability. According to the long-term aridity index, these 63 basins are divided into three climatic regions, including humid, sub-humid and semi-arid/arid regions. The classification of climatic regions based on the aridity index is shown in Table 3.1. For the 63 basins, the humid, sub-humid and semi-arid/arid basins account for 41%, 41% and 18% of them respectively. The detailed hydrological, geographical and land cover characteristics of the 63 basins are shown in Appendix A.

Table 3.1: Climatic region classification based on long-term aridity index (AI) (modified from the climatic region classifications of Ponce et al. (2000) and Arora (2002))

Climatic region	Range of aridity index (AI)
Humid	$AI \leq 0.7$
Sub-humid	$0.7 < AI \leq 1$
Semi-arid/arid	$1 < AI$

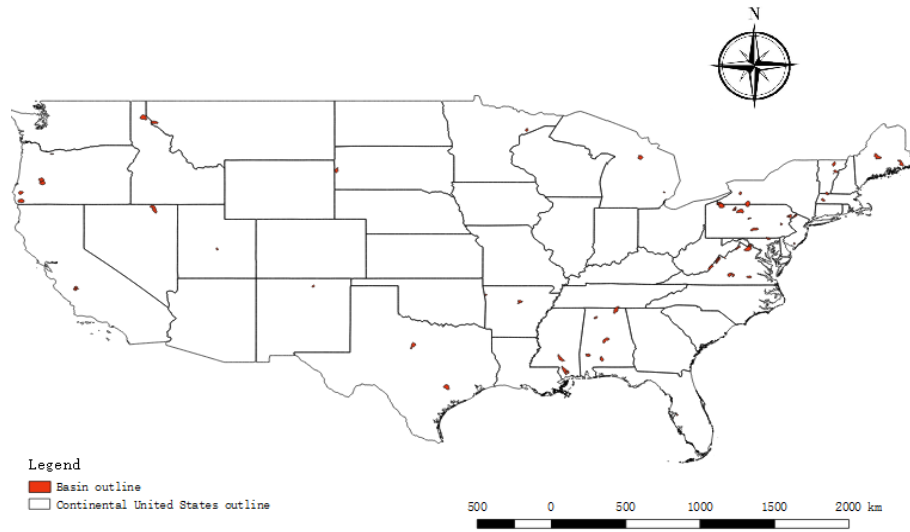


Figure 3.2: Location map and spatial distribution of the 63 basins in continental United States.

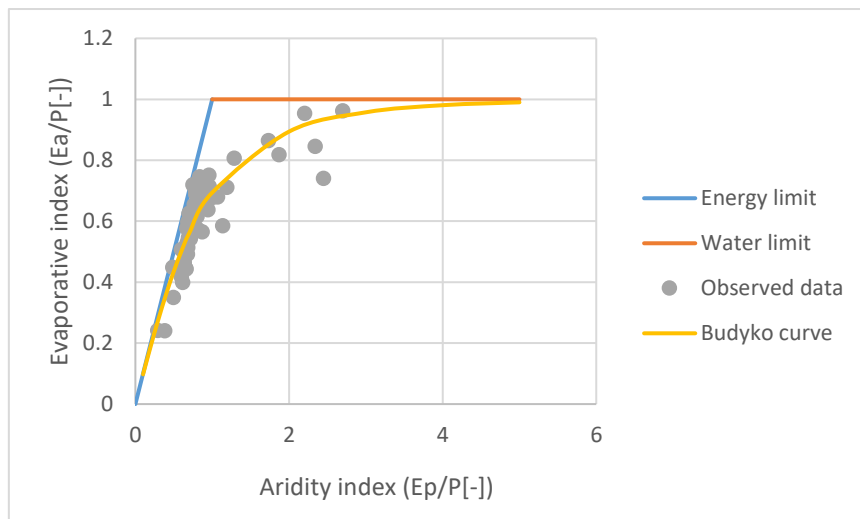


Figure 3.3: Long-term mean hydroclimatic conditions of the 63 basins over the period 1981-2013 illustrated in Budyko space, in terms of aridity index (E_p/P) and evaporative index (E_a/P) based on annual mean meteorological data. The Budyko curve represents the relationship based on Budyko equation between evaporative index and aridity index. The corresponding relationship is physically limited by water demand (energy limit, $E_a < E_p$) and water supply (water limit, $E_a < P$).

3.2 Data

3.2.1 Meteorological data and its processing

The meteorological data used in this study consists of daily areal average forcing data for basins (precipitation, potential evaporation and maximum and minimum temperature) and daily streamflow from 1981 to 2013. All of the data used in this study is part of the dataset used or the model outputs in the study of Newman et al. (2015). The daily forcing data, including precipitation and maximum and minimum temperature, was derived from the Daymet dataset that is a daily and gridded ($1 \times 1 \text{ km}^2$ spatial resolution) dataset with the

North American spatial extent. The Daymet dataset was obtained from the Oak Ridge National Laboratory Distributed Active Archive Center (https://daac.ornl.gov/cgi-bin/dsviewer.pl?ds_id=1328). The USGS Geo Data Portal (GDP) produced area-weighted forcing data through weighting calculations (Blodgett et al., 2011). In this study, due to the lack of data, daily areal average potential evaporation of each basin is the average value of 10 different daily Priestly–Taylor-estimated potential evaporation values of the basin which are the model outputs in the study of Newman et al. (2015). Daily streamflow data for gauges that are located at the outlets of the basins was obtained from the USGS National Water Information System server (<https://waterdata.usgs.gov/usa/nwis/sw>). After obtaining all the data, each daily meteorological data for each basin was summed to obtain monthly and annual meteorological data based on calendar year which were used for checking long-term water balance of the basins, SPEI calculation and the analysis of hydroclimatic change between pre- and post-drought periods.

3.2.2 Remote sensing data and its processing

In this study, Normalized Difference Vegetation Index (NDVI) was utilized to quantify the change in aboveground vegetation greenness and vegetation growth affected by extreme drought events at different sub periods, including pre-drought, in-drought and post-drought periods. The images of the NDVI composites were generated from the daily observations of multiple Advanced Very High Resolution Radiometer (AVHRR), and these observations have been synthesized together to create almost cloudless images that can show maximum vegetation greenness. The images of NDVI across the contiguous United States have a spatial resolution of 1 km and a weekly step from 1981 to 2013 obtained from the USGS EarthExplorer (<https://earthexplorer.usgs.gov>). However, it is found that there is great data missing in NDVI composites before 1990. AVHRR NDVI Composites before 1990 are thus not available in most of continental United States. Therefore, in this study, only NDVI composites from 1990 to 2013 were used for analysis, which led to the constraint of drought event selection. This is discussed in detail in Chapter 3.3.1.

To scale the NDVI results to byte data range and save virtual memory, the value of NDVI downloaded directly from the USGS EarthExplorer has already been scaled to the range of 0 to 200, which means that a value of 0 represents the theoretical value of -1, a value of 200 represents the theoretical value of +1. In this study, to analyze more efficiently and show the vegetation greenness condition more clearly and directly, the range of NDVI value was converted to the original range, namely from -1 to +1, through data processing. A value close to 0 indicates no green vegetation, while a value close to +1 denotes the highest possible density of green leaves. NDVI dataset for each basin was obtained by extracting each basin shapefile from the NDVI image with a continental United States spatial extent. For each basin, the weekly NDVI dataset was aggregated to monthly and annual NDVI datasets. The areal average NDVI for each basin is the average of NDVI values on all pixels within the basin. All the NDVI dataset processing was accomplished by using ArcGIS 10.7 Python (ArcGIS10.7 with the Spatial Analyst extension and Python).

3.3 Methods

3.3.1 Definition of extreme drought event

Computation of SPEI

Standardized Precipitation Evapotranspiration Index (SPEI) (Vicente-Serrano et al., 2010) is a recently developed drought indicator for meteorological drought. It is based on water balance which is the difference between monthly precipitation and potential evaporation. Compared to Standardized Precipitation Index (SPI) that has mathematical similarities with SPEI, the SPEI takes water balance into account and includes the effect of temperature variability on drought evaluation. In addition, the SPEI is multiscalar and suitable for drought detection and monitor under global warming, compared to Palmer Drought Severity Index (PDSI) which is also based on water balance (Vicente-Serrano et al., 2010). Besides, the calculation of the PDSI needs more various data, which is more complicated than that of SPEI. Therefore, in this study, due to the advantages of SPEI and the limitation of data, SPEI was utilized to define, identify and monitor the crucial characteristics of extreme droughts, including start, end, duration, severity and intensity.

Monthly precipitation and potential evaporation data were utilized to calculate the monthly SPEI time series for all the basins. SPEI can be computed on a range of timescales from 1 to 48 months, but 1, 3, 6, 9, 12 and 24 months are commonly used. In this study, extreme drought events were identified by using SPEI at 12-month timescale. Therefore, a 12-month SPEI value is computed by using the cumulative difference between precipitation and potential evaporation over the preceding 12 months. The underlying reason is that 12-month SPEI can reflect a medium-term tendency in water deficit and surplus patterns, annual water condition and hydrological impacts of drought. In addition, 12-month SPEI is better for the explanation of the anomaly of hydrological variables than SPEI at shorter or longer time scales which might be too sensitive to drought events or lead to missing some drought events (Spinoni et al., 2014). The monthly SPEI series at 12-month timescale for each basin were computed by using the SPEI package of R software. This package was developed by Vicente-Serrano et al. (2010), with available relevant documentation of the package at <http://hdl.handle.net/10261/10002>. The details of SPEI calculation, with more complete descriptions in Vicente-Serrano et al. (2010), are shown as follows.

The water deficit or surplus for the month i , expressed by the difference between precipitation (P) and potential evaporation (Ep), is calculated according to:

$$D_i = P_i - Ep_i \quad (3.4)$$

Commonly, Ep in Equation 3.4 is calculated based on temperature and latitude data by using Thornthwaite method. However, in this study, monthly areal average potential evaporation data was used directly for the calculation of water deficit or surplus, due to maximum assurance of accuracy.

The calculated D_i values are aggregated at 12-month time scale. The accumulative difference for month j in year i is computed according to:

$$X_{i,j} = \sum_{l=1+j}^{12} D_{i-1,l} + \sum_{l=1}^j D_{i,l}, \text{ if } j < 12 \quad (3.5)$$

$$X_{i,j} = \sum_{l=j-11}^j D_{i,l}, \text{ if } j = 12 \quad (3.6)$$

Where $D_{i,l}$ is the difference between precipitation and potential evaporation in the first month of year i .

The accumulated difference series is normalized by log-logistic distribution. The probability density function is expressed as:

$$f(x) = \frac{\beta}{\alpha} \left(\frac{x-\gamma}{\alpha}\right)^{\beta-1} \left[1 + \left(\frac{x-\gamma}{\alpha}\right)^{\beta}\right]^{-2} \quad (3.7)$$

where α , β and γ are the parameters of log-logistic distribution which can be obtained according to (Singh et al., 1993):

$$\alpha = \frac{(w_0 - 2w_1)\beta}{\Gamma(1+1/\beta)\Gamma(1-1/\beta)} \quad (3.8)$$

$$\beta = \frac{2w_1 - w_0}{6w_1 - w_0 - 6w_2} \quad (3.9)$$

$$\gamma = w_0 - \alpha\Gamma(1 + 1/\beta)\Gamma(1 - 1/\beta) \quad (3.10)$$

The probability distribution function of the accumulated difference series is written as:

$$F(x) = \left[1 + \left(\frac{\alpha}{x-\gamma}\right)^{\beta}\right]^{-1} \quad (3.11)$$

Then SPEI can be computed as the standardized values of the probability distribution function $F(x)$ according to:

$$SPEI = W - \frac{2.515517 + 0.802853W + 0.010328W^2}{1 + 1.432788W + 0.189269W^2 + 0.001308W^3} \quad (3.12)$$

Where $W = \sqrt{-2\ln(1 - F(x))}$ for $F(x) \geq 0.5$, $W = \sqrt{-2\ln(F(x))}$ for $F(x) < 0.5$.

Identification of extreme drought event

The monthly SPEI series at 12-month timescale were utilized to define drought event based on the method suggested by McKee et al. (1993). The categories of drought based on the values of SPEI are shown in Table 3.2. To pay attention to the conditions when drought event is supposed to be the dominant driver of hydroclimatic change, -1 was selected as the truncation threshold. In this study, a drought event begins when SPEI first reaches below -1 or less and ends when SPEI returns above 0. During the drought, the value of the SPEI keeps negative. During the drought event, if SPEI reaches at least once a value less than -2, it is regarded as an extreme drought event. Once the drought event is defined, its characteristics, including duration, severity and intensity, can be identified. The drought duration is equal to the number of months between the start (included) and the end (excluded) month of the drought event; the drought severity is the accumulative value of the SPEI time series during the drought event; the drought intensity is equal to the lowest SPEI value during the drought event (Yevjevich, 1969).

Since the NDVI dataset is only available from 1990 to 2013, the extreme drought events occurring in this period were used for analysis in this study. Pre- and post-drought periods are consecutive five years before and after extreme drought event respectively. Based on the definition of drought in this study, pre-drought period (5 years before extreme drought) for a basin ends in the month which is before the starting month of the drought event and has a SPEI above -1 followed by a value of -1 or less. In comparison, post-drought period (5 years after extreme drought) for a basin begins in the month which follows the last month of the

drought duration and has a positive SPEI. 5 years is enough to allow ecohydrological system to reach hydrological stable state and vegetation recovery after drought (Julio Camarero et al., 2018; Helman et al., 2017). Furthermore, a more extended period of more than five years might lead to the pre- or post-drought period exceeding the given period from 1990 to 2013. This might cause the comparison of hydroclimatic conditions and vegetation responses in pre- and post-drought periods impossible, due to the missing meteorological and vegetation greenness data. In addition, to avoid the influence of the consecutive drought events on the hydroclimatic conditions and vegetation responses in the pre- and post-drought periods of each of the drought events, only the drought event with no other drought events occurring in the five years before or after it was used for analysis in this study. Actually, since the frequency of the extreme drought event is low, it is rare that the period between two consecutive extreme drought events is less than five years. Therefore, this constraint of drought event has no significant effect on the analysis in this study.

Table 3.2: Drought categories based on SPEI values (modified from drought categories based on SPI of Mckee et al. (1993)).

Level	Drought Category	SPEI Values
0	No drought	$0 \leq \text{SPEI}$
1	Mild drought	$-1.0 < \text{SPEI} < 0$
2	Moderate drought	$-1.5 < \text{SPEI} \leq -1.0$
3	Severe drought	$-2.0 < \text{SPEI} \leq -1.5$
4	Extreme drought	$\text{SPEI} \leq -2.0$

3.3.2 Budyko framework

This study seeks to detect the changes in hydroclimatic conditions before and after extreme drought event by using the Budyko framework (Budyko, 1974). The Budyko framework describes water and energy balance on land through the relationship between the aridity index (E_p/P) and evaporative index (E_a/P). It also represents that the evaporation in a basin is limited by water supply (precipitation) or water demand (potential evaporation). The catchment precipitation partitioning is represented by the evaporative index in Budyko space, and the climatic condition is denoted by the aridity index. To detect the hydroclimatic conditions in the pre- and post-drought periods respectively and their changes, the mean annual water and energy balance in the two comparative periods were analyzed based on the meteorological data in the five years before and after the extreme drought event for each basin. According to the former application of the Budyko framework (Van der Velde et al., 2014; Jaramillo and Destouni, 2014; Jaramillo et al., 2018), the total hydroclimatic movement of the scatter in Budyko space before and after extreme drought for each basin was represented by a vector (v) with both magnitude (m) and direction (θ) to capture and illustrate the hydroclimatic change. The vector has horizontal and vertical components represented by the changes in aridity index ($\Delta(E_p/P)$) and evaporative index ($\Delta(E_a/P)$) respectively, as shown in Figure 3.4. The direction and magnitude of total hydroclimatic movement are calculated according to:

$$\theta = b - \arctan\left(\frac{\Delta(E_a/P)}{\Delta(E_p/P)}\right) \quad (3.13)$$

$$m = \sqrt{(\Delta(E_a/P))^2 + (\Delta(E_p/P))^2} \quad (3.14)$$

Where θ is in degrees starting upper vertical and clockwise, with a range from 0 to 360°. b is a constant ($b = 90^\circ$ when $\Delta(E_p/P) > 0$ and $b = 270^\circ$ when $\Delta(E_p/P) < 0$).

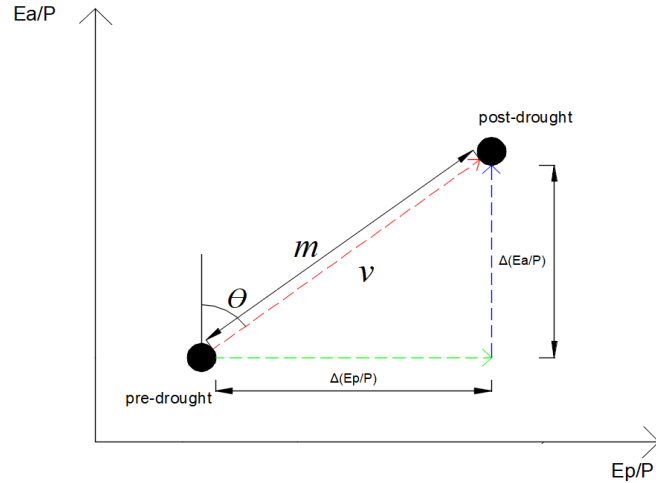


Figure 3.4: Schematic representation of total hydroclimatic movement in Budyko space between pre-drought period (5 years before extreme drought event) and post-drought period (5 years after extreme drought event) represented by a vector. The red arrow represents the vector of the total hydroclimatic movement with magnitude (m) and direction (θ). The green arrow represents the horizontal component of the vector, which is denoted by change in aridity index ($\Delta(Ep/P)$). The blue arrow represents the vertical component of the vector, which is denoted by change in evaporative index ($\Delta(Ea/P)$).

In this study, wind rose of direction and magnitude, suggested by Jaramillo and Destouni. (2014), was used to illustrate the total hydroclimatic movements and climate-driven movements (discussed in detail in Chapter 3.3.3) for the 63 basins to show general patterns of the total hydroclimatic change and hydroclimatic change directly induced by drought-related climate change. A wind rose denotes the combination of changes in the evaporative index and aridity index for all the basins. The variability of hydroclimatic changes represented by movements in Budyko space might be oversimplified by such a wind rose, since the two critical characteristics of movement in Budyko space, namely magnitude and direction, depend on the unique hydroclimatic condition of each basin (Jaramillo et al., 2018). Nevertheless, it is a simple and easy way to illustrate and detect the general trends of the hydroclimatic changes between pre- and post-drought periods in large sets of basins. Besides, using wind rose can make the identification of the occurrence of other drivers of change except for climatic drivers more easily.

3.3.3 Decomposition method for separating of climate and landscape impacts

Separating climate and landscape effects on catchment precipitation partitioning

The impact of drought-related landscape change on precipitation partitioning before and after extreme drought was distinguished from the impact of drought-related climate change through the decomposition method. A basin that experienced the hydroclimatic change from pre-drought period (t_1) to post-drought period (t_2) can be denoted in Budyko space by a point moving from its initial state (t_1 : $(Ep/P)_1$, $(Ea/P)_1$) to a new state (t_2 : $(Ep/P)_2$, $(Ea/P)_2$) as indicated in Figure 3.5. Under the effect of climate change alone implied by the change in aridity index ($\Delta(Ep/P)$), the point will move along the Budyko curve to a new state (t_{2*} : $(Ep/P)_{2*}$, $(Ea/P)_{2*}$). Hence, the immediate climate-driven change in precipitation partitioning for each basin is represented by the change in evaporative index induced by climate change ($\Delta(Ea/P)_{\text{climate}}$). The climate determined evaporative index ($(Ea/P)_{\text{climate}}$) can be calculated by using the Budyko equation (Budyko, 1974):

$$\left(\frac{E_a}{P}\right)_{\text{climate}} = \left[\frac{E_p}{P} \tanh\left(\frac{1}{E_p}\right) \left(1 - e^{-\frac{E_p}{P}}\right)\right]^{\frac{1}{2}} \quad (3.15)$$

However, in reality, catchment hydrological change, namely the change in catchment precipitation partitioning, is the result of the combination of climate change and landscape change. Therefore, due to the effect of landscape change, the basin will turn to a new and different state instead of following the Budyko curve, with the point moving to a new location $(t_2: (E_p/P)_2, (E_a/P)_2)$. The total precipitation partitioning change induced by both climate and landscape changes is therefore represented by an observed total change in the evaporative index $(\Delta(E_a/P))$. The landscape-driven change represented by the change in landscape determined evaporative index $(\Delta(E_a/P)_{\text{landscape}})$ can be calculated according to:

$$\Delta\left(\frac{E_a}{P}\right)_{\text{landscape}} = \Delta\left(\frac{E_a}{P}\right) - \Delta\left(\frac{E_a}{P}\right)_{\text{climate}} \quad (3.16)$$

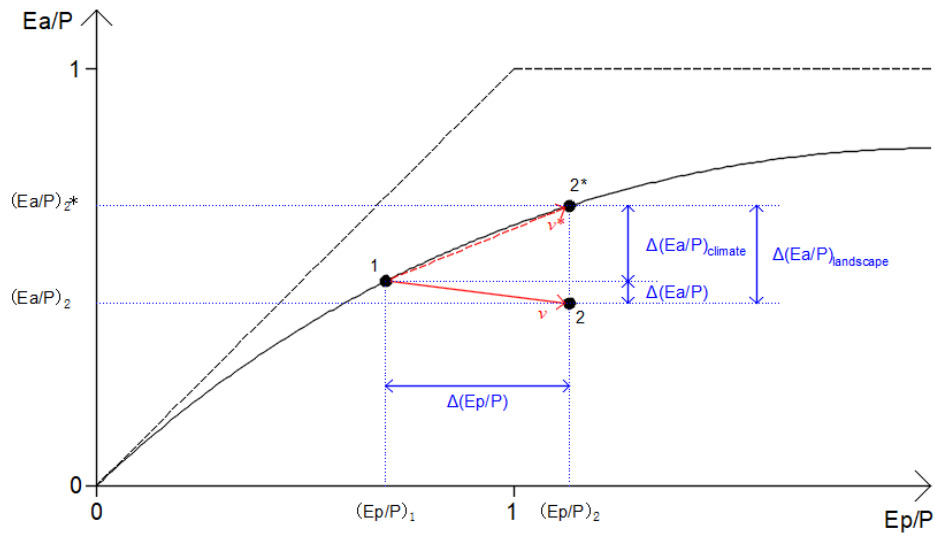


Figure 3.5: Schematic representation of the hydroclimatic movement in the two comparison periods in Budyko space and the separation of climate and landscape effects on precipitation partitioning. The t_1 and t_2 represent pre-drought period (5 years before extreme drought event) and post-drought period (5 years after extreme drought event) respectively. The total hydroclimatic movement in Budyko space is denoted by a vector (v). The change in precipitation partitioning ($\Delta(E_a/P)$) is divided into climate-driven component ($\Delta(E_a/P)_{\text{climate}}$) and landscape-driven component ($\Delta(E_a/P)_{\text{landscape}}$). The climate-driven movement can be represented by a vector (v^*). The curve in the figure is the Budyko curve that describes the relationship between aridity index and evaporative index based on Budyko equation.

The hydroclimatic movement in Budyko space due to climatic effect, representing the climate-driven hydroclimatic change, was expressed as a vector (v^*). The corresponding magnitude (m_c) and direction (θ_c) of climate-driven movement can be calculated by using Equation 3.13 and 3.14 based on the aridity index and climate determined evaporative index of each basin. Same as the total movements in Budyko space between the two comparative periods, the climate-driven movements of the basins were also synthesized as a wind rose. However, landscape-driven movements cannot be synthesized as a wind rose. As shown in Figure 3.6(a), after decomposing the vector for total movement in Budyko space into two parts, the vector for landscape-driven movement is in the direction that goes vertical downward in basins moving downward and rightward (and by analogy also for basins moving downward and leftward). In a similar way, the vector for landscape-driven movement is in the direction that goes vertical upward in basins moving upward and

rightward as indicated in Figure 3.6(b), and by analogy also for basins moving upward and leftward. Under a constant climatic condition, the landscape drivers have an influence directly on evaporation and runoff, thus on the evaporative index, which leads to an upward or downward movement in Budyko space. Therefore, the direction of landscape-driven movement is always in the direction of 0 or 180° in Budyko space, and the magnitude of landscape-driven movement (m) is equal to the absolute value of change in landscape determined evaporative index ($|\Delta(Ea/P)_{landscape}|$). Hence, wind rose cannot be used to illustrate the landscape-driven change in hydroclimatic conditions between pre- and post-drought periods.

In this study, boxplot was used for quantifying the general patterns of the impacts of climate and landscape on changes in precipitation partitioning between pre- and post-drought periods and detecting the interactions and relationship between these two drivers in such a broad set of basins. It was also used to quantify the alterations of precipitation and potential evaporation to further understand the effect of climate change that associated with change in aridity index.

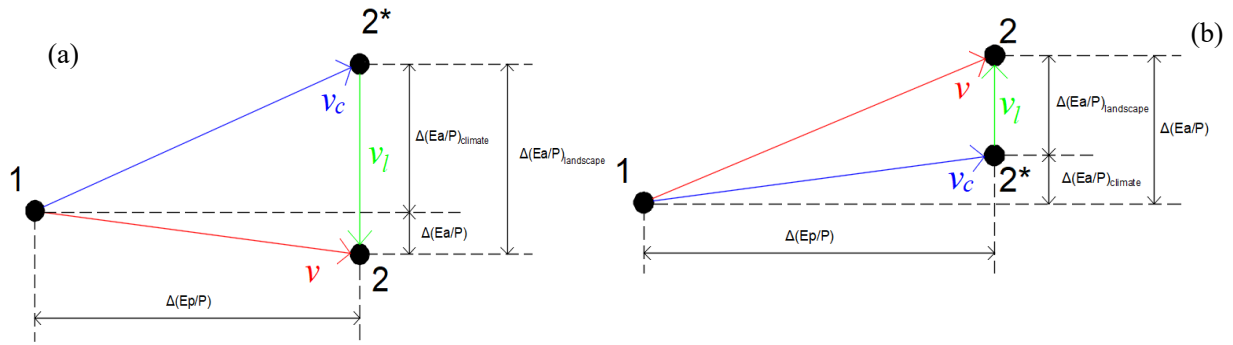


Figure 3.6: Schematic representations of the hydroclimatic movement in Budyko space. The blue arrow represents the vector for total hydroclimatic movement. The red and green arrows represent the vectors for climate-driven movement and landscape-driven movement respectively. **(a)** Hydroclimatic movement in Budyko space in basins moving downward and rightward. **(b)** Hydroclimatic movement in Budyko space in basins moving upward and rightward.

Separating climate and landscape effects on streamflow change

To further investigate the change in catchment precipitation partitioning and determine the effects of drought related climate and landscape changes, the changes in streamflow before and after extreme drought events were also quantified. The climate effect on changes in streamflow was therefore separated from the landscape effect.

As shown in Figure 3.5 and 3.6, the landscape change can directly affect the catchment precipitation partitioning, leading a vertical component, while climate change can cause both horizontal and vertical components. Thus, the streamflow change induced by landscape change is calculated first. The streamflow can be expressed as a function of the evaporative index:

$$Q = P\left(1 - \frac{Ea}{P}\right) \quad (3.17)$$

As shown in Figure 3.5, the landscape determined streamflow change can be calculated by

$$\Delta Q_{landscape} = P_2 \left[\left(\frac{Ea}{P} \right)_{2*} - \left(\frac{Ea}{P} \right)_2 \right] \quad (3.18)$$

The total change in streamflow driven by the combined effect of climate and landscape changes (ΔQ) is the difference between mean annual streamflow in pre- and post-drought periods. The streamflow change driven by climate effect before and after extreme drought events can be computed by subtracting the landscape-driven streamflow change from the total streamflow change:

$$\Delta Q_{climate} = \Delta Q - \Delta Q_{landscape} \quad (3.19)$$

The boxplot was also used for quantifying the general patterns of the climate and landscape impacts on alterations in river runoff before and after extreme drought event in the 63 basins in this study.

3.3.4 Detection of ecohydrological system recovery in post-drought period

To understand patterns of drought recovery of ecohydrological system, the variation tendency of total precipitation partitioning change driven by the combined effect of drought-related climate and landscape changes over time in the post-drought period for the 63 basins was analyzed. The mean annual precipitation partitioning condition in the pre-drought period (5 years before extreme drought event) in a basin, represented by the evaporative index in Budyko framework, was regarded as a baseline state for that basin. The mean annual precipitation partitioning conditions for different cumulative post-drought periods, namely 1, 2, 3, 4, and 5 years after extreme drought event, were quantified respectively for each basin. The differences in evaporative index between the baseline period and different individual cumulative post-drought periods (1-5 years after drought) represent the changes in catchment water balance behavior for different cumulative post-drought periods. If the absolute values of the differences in the evaporative index for the basins show a declining tendency over time, it means that the basins revert to their pre-drought state gradually. Meanwhile, the variation trends in climate-driven change ($\Delta(Ea/P)_{climate}$) and landscape-driven change ($\Delta(Ea/P)_{landscape}$) over time after drought were also analyzed respectively by the same method above to understand drought recovery under different effects.

In addition, the magnitude (m) of total hydroclimatic movement in Budyko space, as shown in Figure 3.4, represents the extent of hydroclimatic condition change in a basin. A larger magnitude indicates that a more remarkable change in hydroclimatic conditions between pre- and post-drought periods. A decrease in the magnitude of hydroclimatic movement over time after drought also denotes the recovery of a basin from drought impact. Therefore, the variation trend of magnitudes of hydroclimatic movements in Budyko space with the increasing cumulative post-drought periods (1-5 years) was quantified to understand the drought recovery patterns in the 63 basins. Similarly, variation trends of magnitudes of climate-driven movements (m_c) and landscape-driven movements (m_l) in Budyko space over time were also quantified respectively by the same method above to understand drought recovery under different effects. Here, as discussed in Chapter 3.3.2 and 3.3.3, the magnitudes of total movement (m) and climate-driven movement (m_c) for each basin were calculated according to Equation 3.14, while the magnitude of landscape-driven movement (m_l) is equal to the absolute value of change in landscape determined evaporative index ($|\Delta(Ea/P)_{landscape}|$).

3.3.5 Detection of vegetation changes and responses

As a dominant part of landscape change, vegetation change induced by drought was quantified to understand the mechanism of landscape effect, especially vegetation-related landscape effect, on catchment hydrological change in case of extreme drought events. The possible effects of vegetation responses to extreme drought events on catchment precipitation partitioning were analyzed. In order to access vegetation changes and responses to extreme droughts in these basins, NDVI was utilized to quantify the variations in aboveground

vegetation greenness. The vegetation changes and responses for each basin were quantified by comparing the mean annual NDVI in three sub-periods: pre-drought period (5 years before extreme drought event), in-drought period and post-drought period (5 years after extreme drought event). The general trends and patterns of vegetation changes and responses implied by changes in vegetation greenness for the 63 basins were synthesized in boxplots.

Besides, the patterns of vegetation recovery time for all the 63 basins were quantified for the analysis of vegetation response to drought in the post-drought period, showing vegetation recovery and vegetation response to possible drought legacy effects. The mean annual NDVI in the pre-drought period (5 years before extreme drought event) in a basin is regarded as a baseline level of vegetation greenness. The annual mean NDVI in the first, second, third, fourth and fifth year after drought for each basin was computed respectively, displaying the average level of vegetation greenness during an individual year. Since there might be significant variations in vegetation greenness between growing season and non-growing season and also different seasons with different climatic conditions, the annual mean NDVI in post-drought period was used as the average level of vegetation greenness for comparison in this study, instead of using the original weekly NDVI or the aggregated monthly NDVI. If the annual mean NDVI is equal to or more than its baseline level, it can be assumed that vegetation has already recovered to its pre-drought state. Therefore, in this study, the vegetation recovery time is defined roughly as the first time (in year) after drought when the value of annual mean NDVI anomalies is not less than its pre-drought level.

4 Results

The results of this study are presented in this chapter which is divided into six sections. Section 4.1 describes the extreme drought events that occurred in these 63 basins. The hydroclimatic changes represented by movements in Budyko space before and after extreme drought event are presented in section 4.2. The climate-driven movements in Budyko space and relevant climatic effect on catchment precipitation partitioning are discussed in section 4.3. The landscape-driven change in catchment precipitation partitioning and its relationship to climate-driven change are presented in section 4.4. Section 4.5 discusses post-drought recovery patterns of the basins based on variation tendencies of precipitation partitioning change and movement magnitudes over time in the post-drought period. The last section describes drought-related vegetation change and its effect on catchment precipitation partitioning change.

4.1 Characteristics of extreme drought events

Monthly SPEI was calculated over a 12-month time scale. Appendix B shows the SPEI time series of each of the 63 basins. From 1981 to 2013, there was an obvious increase ($p < 0.05$) in the changes in the values of monthly SPEI in 41% of these basins, while an evident decrease ($p < 0.05$) in 16% of these basins. The variation trend of SPEI value in other basins was not noticeable ($p > 0.05$). Over the period from 1990 to 2013, only one extreme drought event has occurred in most of the basins. However, in some basins, there existed extreme drought events at the beginning of 1990 or the end of 2013. These drought events are not included in this study, since the analysis for pre- and post-drought periods is impossible due to the lack of meteorological and vegetation greenness data. After these extreme events were removed, only one extreme drought event per basin was analyzed for follow-up research. The 63 basins are located throughout the whole continental United States; hence it shows great differences and spatial heterogeneity in the start, end, duration and intensity of these extreme droughts. The main characteristics of the extreme drought events are shown in Appendix C. Most of the extreme drought events occurred in 1995-1996, 1999-2000, 2001-2003 and 2007-2008, lasting for several months or even several years. Around 92% of all the extreme drought events are prolonged droughts with a duration of more than one year. These extreme drought events lasted at least nine months and at most 54 months, with a mean duration of 22 months. The mean severity of the extreme drought events is -29.7, with a minimum value of -9.1 and a maximum value of -63.23. The mean intensity of the extreme drought events is -2.26, with a minimum value of -2.00 and a maximum value of -2.82. The pre- and post-drought periods are five years before and after the extreme drought event in each basin respectively. The details of pre- and post-drought periods for each basin are also showed in Appendix C.

4.2 Hydroclimatic movements in Budyko space

The hydroclimatic conditions of the 63 basins in pre- and post-drought periods were indicated by scatters in Budyko space as shown in Figure 4.1. The catchment precipitation partitioning into evaporation is represented by evaporative index (E_a/P), while aridity index (E_p/P) denotes the catchment climatic condition. Basins experienced upward or downward movements, as well as leftward or rightward movements in Budyko space. The various trajectories of movement indicate that all 63 basins have experienced different

hydroclimatic conditions in pre- and post-drought periods and had different responses to the extreme droughts. In order to better and clearly understand the general patterns of the hydroclimatic changes in the 63 basins, the characteristics of the movements in Budyko space were illustrated in the wind rose.

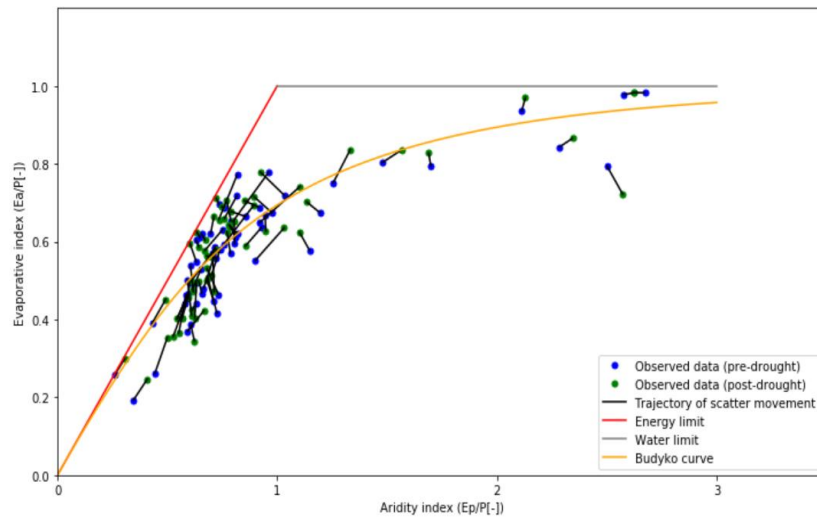


Figure 4.1: Changes in hydroclimatic conditions in Budyko space. The observed mean hydroclimatic conditions of the 63 basins in pre-drought period (5 years before extreme drought event, blue points) and post-drought period (5 years after extreme drought event, green points) clarified in Budyko space, in terms of aridity index (E_p/P) and evaporative index (E_a/P) based on annual mean meteorological data. The black line between the blue and green scatter represents the trajectory of hydroclimatic movement for each basin. The Budyko curve represents the relationship based on Budyko equation between evaporative index and aridity index. The corresponding relationship is physically limited by water demand (energy limit, $E_a < E_p$) and water supply (water limit, $E_a < P$).

The wind rose of total hydroclimatic movements shows the directions and magnitudes of movements of the 63 basins from pre-drought period to post-drought period as indicated in Figure 4.2(a). This wind rose indicates that between the two comparative periods the total hydroclimatic movement spectrum extended over all directions. There is no unified pattern of movements in Budyko space of all of the 63 basins. There were movements in all direction intervals. Different combinations of changes in the evaporative and aridity index led to various movements with different directions and magnitudes in Budyko space. The occurrence of different directional movements denotes that basins have different and unique responses to extreme drought events, since different basins have different catchment properties, climatic and hydrological conditions and land cover types. The magnitude of total hydroclimatic movement in Budyko space between pre- and post-drought periods is an indicator of sensitivity of the basin to climate and landscape changes induced by the extreme drought event. A massive magnitude of total hydroclimatic movement denotes that significant drought-related climate change and landscape change have occurred in that basin leading large basin hydroclimatic change. The basin could be more sensitive to the drought-induced climate change and landscape change. This means that there might be large effects of extreme drought event on catchment hydroclimatic conditions, thus on catchment water and energy balance. Moreover, the magnitude of movement might help to explain the meaning of the direction of movement, especially the direction of movement with relatively larger magnitudes. As shown in Figure 4.2(a), the total hydroclimatic movements in Budyko space with relatively larger magnitudes (between 0.1 and 0.3) fell into all the direction intervals. Nevertheless, most of the basins with larger movement magnitudes experienced the movement in the range

of directions both $0 < \theta < 90^\circ$ and $180^\circ < \theta < 270^\circ$.

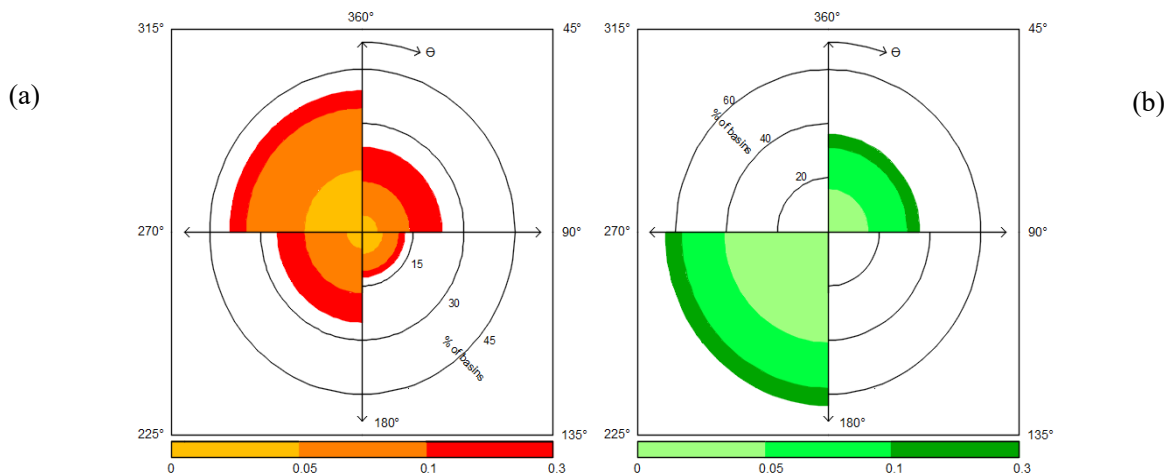


Figure 4.2: Hydroclimatic movements in Budyko space in the 63 basins between pre-drought period (5 years before extreme drought event) and post-drought period (5 years after extreme drought event) as a result of the combination of changes in aridity index (E_p/P) and evaporative index (E_a/P). **(a)** Wind rose of total hydroclimatic movements of the 63 basins driven by combined effect of climate change and landscape change. **(b)** Wind rose of hydroclimatic movements of the 63 basins driven by climatic effect alone. The direction range of movement ($0 < \theta < 360^\circ$) is divided into four 90° interval paddles, grouping all basins moving in each direction interval. The directions (θ) start from the upper vertical and clockwise. The magnitude (m) of movements in Budyko space is represented by the intensity of color intervals. For instance, the red part in the third quadrant in Figure 4.2(a) indicates that around 8% of the basins moved in the range of directions $255^\circ < \theta < 270^\circ$, with magnitudes between 0.1 and 0.3.

Under the combined effect of drought-related climate change and landscape change, around 61.9% of all the basins experienced an increase in the evaporative index (E_a/P), moving them upwards in Budyko space as shown in Figure 4.2(a), which denotes that more proportion of precipitation was released as evaporation after extreme drought events. More water fluxes and resources on land might be released through vegetation transpiration, canopy interception and surface evaporation in post-drought period, which led to less water turning into river runoff. Basins with increased evaporative index experienced river runoff reduction ($\Delta Q < 0$) and evaporation increase ($\Delta E_a > 0$) after drought compared with pre-drought state, as indicated in Figure 4.3(a, b). A decreased evaporative index means the opposite condition that more precipitation was partitioned into streamflow and less into evaporation. Basins with decreased evaporative index experienced an increase in river runoff ($\Delta Q > 0$) and a decrease in evaporation increase ($\Delta E_a < 0$), as shown in Figure 4.3 (a, b). For the 63 basins, the relative change is more considerable for river runoff with a mean value of 18.2% than evaporation with a mean value of 8.6% as shown in Appendix D. In the process of changing precipitation partitioning, the change in streamflow was therefore relatively larger than the change in evaporation in these basins.

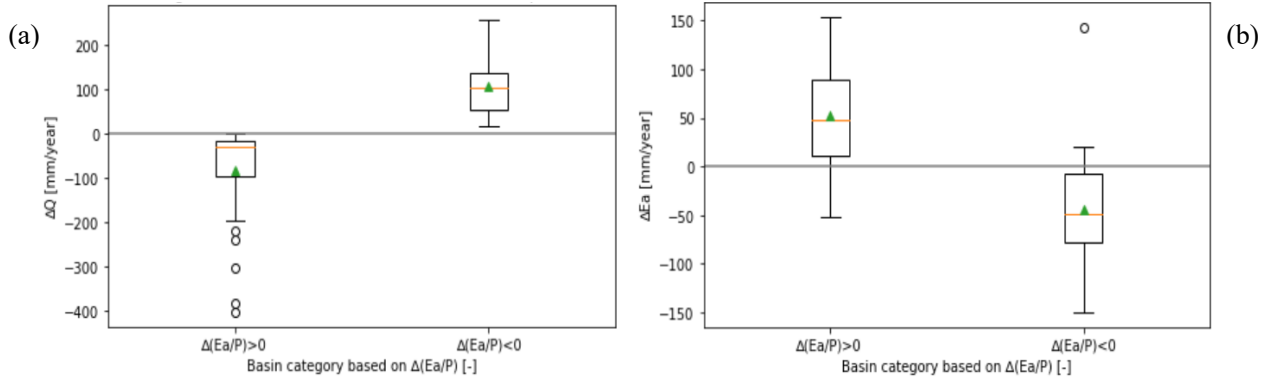


Figure 4.3: (a) Changes in river runoff between pre-drought period (5 years before extreme drought event) and post-drought period (5 years after extreme drought event) in basins with increased evaporative index (left) and decreased evaporative index (right). (b) Changes in evaporation between pre-drought period (5 years before extreme drought event) and post-drought period (5 years after extreme drought event) in basins with increased evaporative index (left) and decreased evaporative index (right). The horizontal orange line in boxplot represents the median of the changes. The green triangle represents the mean value of the changes. The black circles represent the outliers. The gray line represents the marginal line where runoff change (ΔQ) or evaporation change (ΔEa) is equal to 0.

In addition, in terms of changes in climatic conditions between pre- and post-drought periods, 63.5% of the 63 basins experienced decreased aridity index (Ep/P), moving them leftward in Budyko space as indicated in Figure 4.2(a). These basins experienced more energy limited conditions after extreme drought events, with higher water availability and less proportion of energy turning into sensible heat flux. After drought, the actual evaporation in these basins was, therefore, more constrained by energy availability for evaporation than by water availability. This implies that these basins became wetter with more water availability after extreme drought events, compared with pre-drought period. Moreover, the basins with decreased aridity index experienced an increase or decrease in average temperature between the two comparative periods, with a temperate difference at $-0.023 \pm 0.79^\circ\text{C}$, as shown in Figure 4.4. Therefore, there was no unified change pattern of the average temperature in these basins. Basins with increased aridity index experienced the opposite condition that the watershed system tended to still suffer from water deficit and aridity in post-drought period. These basins experienced more water limited conditions after extreme drought events, with less water availability and more fraction of energy turning into sensible heat flux. The actual evaporation in these basins was, therefore, more limited by the amount of water that has entered the basins as precipitation. Besides, the dryer conditions were also accompanied by higher temperature in most of these basins after extreme drought events, as indicated in Figure 4.4.

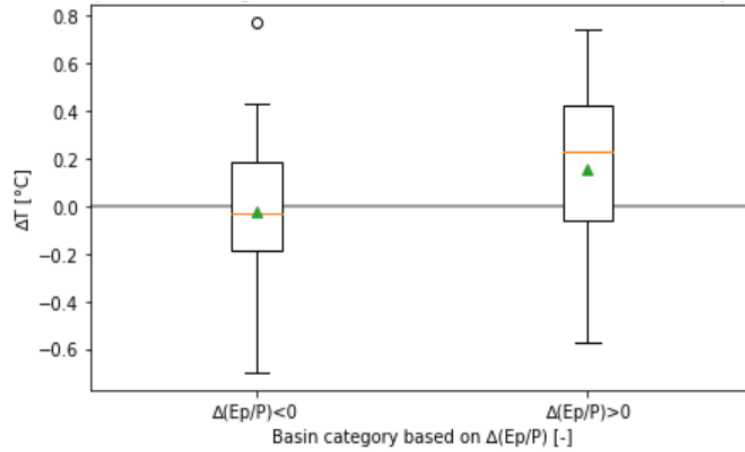


Figure 4.4: Changes in average temperature between pre-drought period (5 years before extreme drought event) and post-drought period (5 years after extreme drought event) in basins with decreased aridity index (left) and increased aridity index (right). The horizontal orange line in boxplot represents the median of temperature changes. The green triangle represents the mean of temperature changes. The black circles represent the outliers. The gray line represents the marginal line where the temperature change (ΔT) is equal to 0.

Table 4.1: Proportion of basins with increased (or decreased) evaporative index and increased (or decreased) aridity index for humid, sub-humid and semi-arid/arid regions.

Climatic region	$\Delta(Ea/P) > 0$	$\Delta(Ea/P) < 0$	$\Delta(Ep/P) > 0$	$\Delta(Ep/P) < 0$
Humid	50%	50%	38%	62%
Sub-humid	62%	38%	23%	77%
Semi-arid/arid	91%	9%	64%	36%

Moreover, as mentioned in Chapter 3.1.2, the 63 basins have been divided into three climatic regions according to the long-term aridity index. Different climatic regions also show different patterns of changes in hydroclimatic conditions before and after extreme drought. As indicated in Table 4.1, in terms of changes in hydrological conditions, most semi-arid/arid basins experienced an increased evaporative index after drought, which means that more precipitation was partitioned into evaporation. A large part of sub-humid basins also experienced an increased evaporative index, but the difference in the proportions of basins with increased and decreased evaporation index for these basins is obviously lower than that for semi-arid/arid basins. For humid basins, the number of basins with increased evaporative index is the same as that of basins with decreased evaporative index. In addition, most humid and sub-humid basins became wetter after drought. These basins might be able to increase and improve catchment water availability rapidly after drought as a result of the restored precipitation. In contrast, most semi-arid/arid basins experienced more arid conditions after drought. Therefore, the change in climatic conditions within a basin under extreme drought might be affected by the long-term climatic condition of the basin. Besides, post-drought climatic condition has a great influence on the post-drought development of agriculture within the basin. For different climate regions, farmers might therefore need to take corresponding measures to deal with the impact of climate change caused by extreme drought on agriculture. For humid and sub-humid basins, since these basins tend to become more humid with increased precipitation after drought, the soil moisture and irrigation water might be relatively less affected in post-drought period. However, semi-arid/arid basins are more likely to experience more arid conditions, which may affect the soil moisture and irrigated water supply within a few years after drought, and thus the crop growth. Therefore, for semi-arid/arid basins, farmers might need to

take some measures, such as planting drought-tolerant crop, taking water-saving irrigation measures (e.g. drip and sprinkler irrigation technologies), building water storage cellars and cultivating when rainfall returns to normal, to mitigate the influence of post-drought climate conditions on agriculture.

4.3 Climate-driven movement and climatic effect

As shown in Figure 4.2(a, b), the wind rose of climate-driven movements in Budyko space differs significantly from that of total movements. The range of possible directions of climate-driven movements (θ_c) for the 63 basins is only either $0^\circ < \theta < 90^\circ$ or $180^\circ < \theta < 270^\circ$. Most of the 63 basins experienced a wetter condition after drought, which led to the actual evaporation more limited by energy availability.

Table 4.2: Mean relative changes of precipitation and potential evaporation for basins with increased or decreased aridity index

Basin category	P [%]	Ep [%]
$\Delta(Ep/P) < 0$	6.68	1.36
$\Delta(Ep/P) > 0$	6.80	1.04

Under the influence of climatic drivers alone, a decrease in aridity index ($\Delta(Ep/P) < 0$) only led to a decrease in evaporative index ($\Delta(Ea/P) < 0$) as indicated in Figure 4.2(b, $180^\circ < \theta < 270^\circ$). These basins experienced wetter conditions after drought. This more energy-limited condition after extreme drought events, therefore, decreased the fraction of precipitation partitioned into evaporation. The actual evaporation was more limited by potential evaporation. The mean annual precipitation was higher in post-drought period at 1265 ± 791 mm yr⁻¹, compared to a value of 1208 ± 741 mm yr⁻¹ in pre-drought period, as shown in Figure 4.5(a). Compared to the change in potential evaporation, the change in precipitation was relatively more obvious. The increase of precipitation ($P < 0.5$) was relatively larger than the decrease of potential evaporation ($P > 0.5$), with mean annual potential evaporation at 922 ± 471 mm yr⁻¹ and 917 ± 465 mm yr⁻¹ in pre- and post-drought periods respectively as indicated in Figure 4.5(b). The mean relative change was larger for precipitation at 6.68% than for potential evaporation at 1.36% for basins with decreased aridity index, as shown in Table 4.2. Therefore, the general decrease in aridity index was caused by the increase in precipitation from pre-drought period to post-drought period. The increase in precipitation after extreme drought events in these basins has, thus, directly caused more river runoff. As shown in Figure 4.6, basins with the more humid conditions after drought experienced an increase in river runoff induced by climate effect.

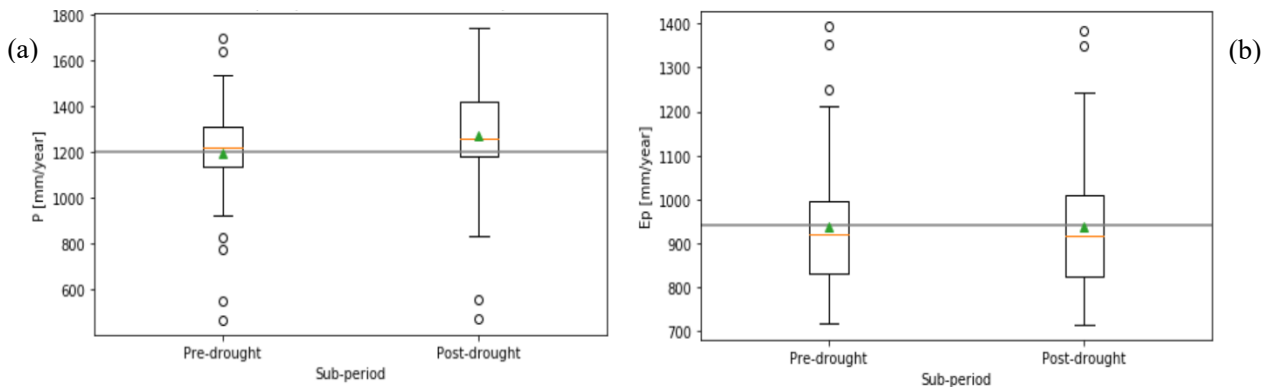


Figure 4.5: (a) The mean annual precipitation in basins with decreased aridity index ($\Delta(Ep/P) < 0$) in pre-drought period (5

years before extreme drought event, left) and post-drought period (5 years after extreme drought event, right), with the long term (33-year) mean annual precipitation shown by the horizontal gray line. (b) The mean annual potential evaporation in basins with decreased aridity index ($\Delta(Ep/P) < 0$) in pre-drought period (5 years before extreme drought event, left) and post-drought period (5 years after extreme drought event, right), with the long term (33-year) mean annual potential evaporation shown by the horizontal gray line. The horizontal orange line in boxplot represents the median. The green triangle represents the mean value. The black circles represent the outliers.

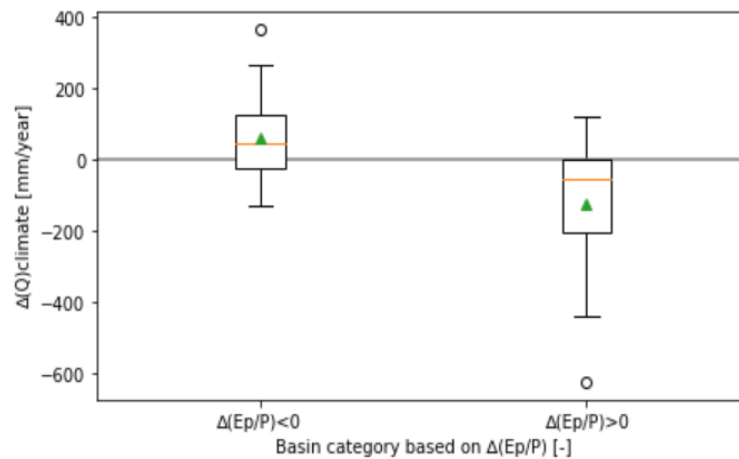


Figure 4.6: Changes in river runoff induced by drought-related climate change between pre-drought period (5 years before extreme drought event) and post-drought period (5 years after extreme drought event) in basins with decreased aridity index (left) and increased aridity index (right). The horizontal orange line in boxplot represents the median of the changes. The green triangle represents the mean value of the changes. The black circles represent the outliers. The gray line represents the marginal line where runoff change ($\Delta Q_{\text{climate}}$) is equal to 0.

In addition, in the absence of the effect of landscape drivers, the increase in aridity index ($\Delta(Ep/P) > 0$) only resulted in the increase in the evaporative index ($\Delta(Ea/P) > 0$) as shown in Figure 4.2(b, $0^\circ < \theta < 90^\circ$). These basins experienced more arid conditions in post-drought period. This more water-limited condition after extreme drought event therefore increased the fraction of precipitation partitioned into evaporation. The actual evaporation was more constrained by water available for evaporation that has entered the basins as precipitation. In these basins, increased aridity index was mainly caused by the reduced precipitation ($p < 0.5$), the change of which was comparatively greater than the change in potential evaporation ($p > 0.5$) as indicated in Figure 4.7(a, b). The mean relative change of precipitation was larger at 6.80% than that of potential at 1.04% for basins with increased aridity index as shown in Table 4.2. Therefore, the general increase in aridity index was mainly the result of the decrease in precipitation from pre-drought period to post-drought period. The decrease in precipitation after extreme drought events in these basins has, thus, directly caused less river runoff. As shown in Figure 4.6, basins with the drier condition after drought experienced a decrease in river runoff induced by climate effect. Under such a dry condition of the basins, the increase in temperature (Figure 4.4) was expected to enhance evaporation by increased soil evaporation and/or vegetation transpiration; thus, less water turned into river runoff.

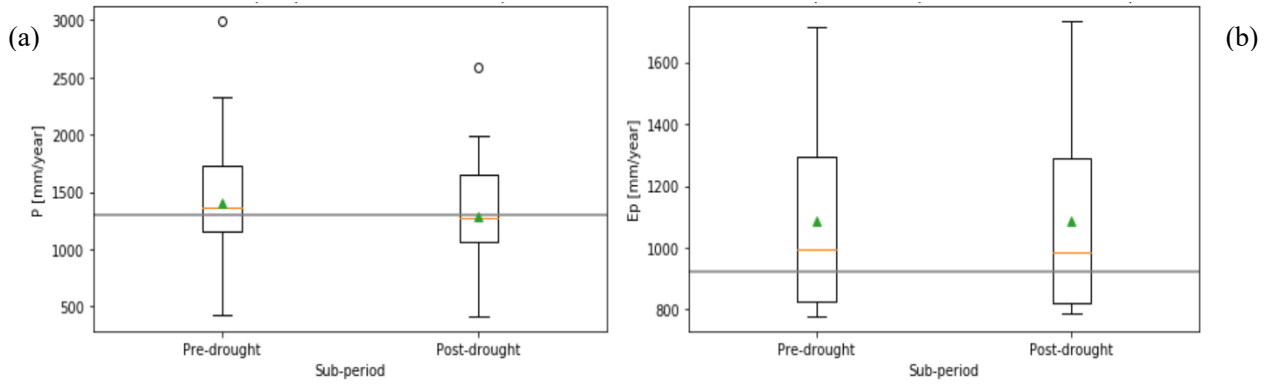


Figure 4.7: (a) The mean annual precipitation in basins with increased aridity index ($\Delta(Ep/P) > 0$) in pre-drought period (5 years before extreme drought event, left) and post-drought period (5 years after extreme drought event, right), with the long term (33-year) mean annual precipitation shown by the horizontal gray line. (b) The mean annual potential evaporation in basins with increase aridity index ($\Delta(Ep/P) > 0$) in pre-drought period (5 years before extreme drought event, left) and post-drought period (5 years after extreme drought event, right), with the long term (33-year) mean annual potential evaporation shown by the horizontal gray line. The horizontal orange line in boxplot represents the median. The green triangle represents the mean value. The black circles represent the outliers.

Regardless of whether the aridity index increased or decreased from pre-drought period to post-drought period, the contribution of precipitation to the alteration in the aridity index was larger than that of potential evaporation. Therefore, the change of water balance behavior driven by drought-related climate change between pre- and post-drought periods was more ascribed to the change in precipitation and less due to change in potential evaporation that is related to some meteorological factors, including wind speed, temperature, solar radiation and water vapor. The climate drivers have directly caused more changes in river runoff in the 63 basins, leading to changes in catchment precipitation partitioning. Furthermore, as shown in Figure 4.2(a, b), the directions of total hydroclimatic movements with larger magnitudes were in the same direction intervals as the directions of climate-driven hydroclimatic movements ($0^\circ < \theta < 90^\circ$ or $180^\circ < \theta < 270^\circ$). The basins with hydroclimatic movement directions in these direction intervals generally experienced a relatively larger change in precipitation. It is inferred that, to a large extent, these relatively large magnitudes were caused by relatively large changes in precipitation.

Moreover, there were obvious differences between wind roses of climate-driven hydroclimatic movements and total hydroclimatic movements in Budyko space, as indicated in Figure 4.2(a, b). The occurrence of total movements outside the range of directions of climate-driven movements, therefore, reflects the impact of drought-related landscape drivers. The change in catchment precipitation partitioning in the basins might not be explained exclusively by drought-related climatic drivers that relate to the variation in aridity index. Therefore, climate change induced by extreme drought events is not the only or the most crucial driver in the change of precipitation partitioning between pre- and post- drought period in these 63 basins.

4.4 Relationship and interaction between climate and landscape effects

Basins with total movement directions in the same direction intervals had similar patterns of the relationship and interaction between climate effect and landscape effect on change in catchment precipitation partitioning. The basins were therefore divided into four parts based on the combination of alterations in evaporative index

and aridity index to analyze the landscape-driven change in catchment precipitation partitioning and its relationship to climate-driven change separately.

Table 4.3: Mean contribution of climate and landscape effects on catchment precipitation partitioning

Range of directions in total change spectrum	Climate effect [%]	Landscape effect [%]
$0^\circ < \theta < 90^\circ$	52.0	48.0
$90^\circ < \theta < 180^\circ$	12.0	88.0
$180^\circ < \theta < 270^\circ$	43.4	56.6
$270^\circ < \theta < 360^\circ$	25.9	74.1
Average	33.3	66.7

Basins with both increased aridity index and evaporative index ($0^\circ < \theta < 90^\circ$, Figure 4.2(a)) have experienced an increase in the climate-driven component of precipitation partitioning ($\Delta(Ea/P)_{\text{climate}} > 0$) between pre- and post-drought periods as indicated in Figure 4.8. They have also experienced landscape-driven increases ($\Delta(Ea/P)_{\text{Landscape}} > 0$), which enhanced the climate-driven increases. In these basins, the climate effect on precipitation partitioning was relatively higher than landscape effect, with 52% and 48 % of the total change in evaporative index driven by climate and landscape respectively, as shown in Table 4.3. However, the difference between the contributions of the two drivers to changes in precipitation partitioning is not very large.

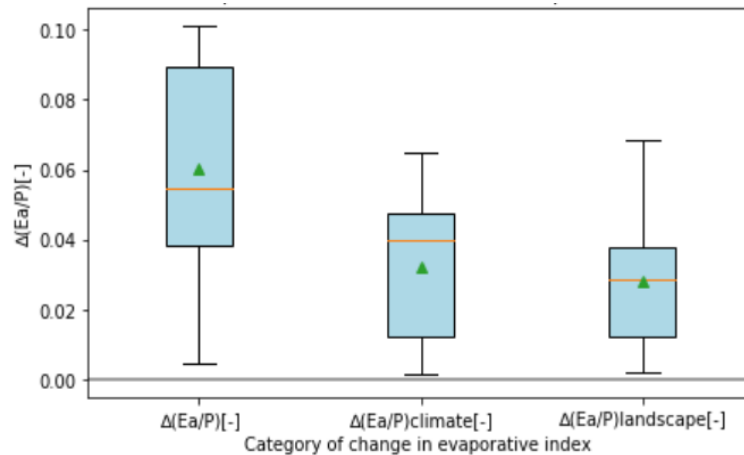


Figure 4.8: Climate and landscape effects on change in precipitation partitioning in basins with both increased aridity index and evaporative index. Distribution of changes between pre-drought period (5 years before extreme drought event) and post-drought period (5 years after extreme drought event) in the evaporative index ($\Delta(Ea/P)$), and its climate-driven component ($\Delta(Ea/P)_{\text{climate}}$) and landscape-driven component ($\Delta(Ea/P)_{\text{landscape}}$). The horizontal orange line in boxplot represents the median. The green triangle represents the mean value.

Basins with increased aridity index but decreased evaporative index ($90^\circ < \theta < 180^\circ$, Figure 4.2(a)) have experienced an increasing climatic effect driven by a more arid condition which was counteracted by a decreasing landscape effect between the two periods as indicated in Figure 4.9. The counteracting effects apply to mean value, median and interquartile ranges of changes in the evaporative index of these basins. The directions of total hydroclimatic movements were significantly different from that of climate-driven movements in these basins. The landscape drivers contributed more to change in catchment precipitation partitioning in these basins than climatic drivers, with 88% and 12 % of the total change in precipitation

partitioning driven by landscape and climate respectively, as shown in Table 4.3. Even though in this drier condition, more water was turned into evaporation and less into river runoff after drought events under the influence of climate change, total change showed a decreasing trend implied by a decreased evaporative index, since landscape-driven decreases overshadowed the climate-driven increases.

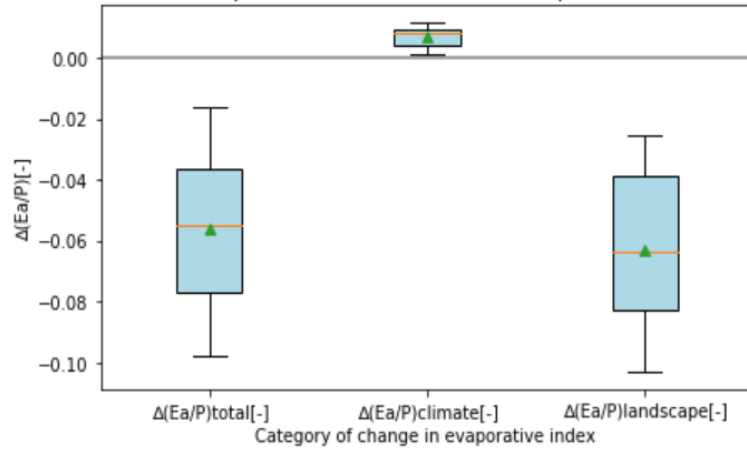


Figure 4.9: Climate and landscape effects on change in precipitation partitioning in basins with increased aridity index and decreased evaporative index. Distribution of changes between pre-drought period (5 years before extreme drought event) and post-drought period (5 years after extreme drought event) in the evaporative index ($\Delta(Ea/P)$), and its climate-driven component ($\Delta(Ea/P)_{climate}$) and landscape-driven component ($\Delta(Ea/P)_{landscape}$). The horizontal orange line in boxplot represents the median. The green triangle represents the mean value.

Basins with both decreased aridity index and evaporative index ($180^\circ < \theta < 270^\circ$, Figure. 4.2(a)) have undergone a reducing climatic effect induced by wetter conditions with more precipitation. The climate-driven decreases were enhanced by the landscape-driven decreases between pre- and post-drought periods, as indicated in Figure 4.10. The mean contribution of landscape effect on precipitation partitioning was relatively larger than that of climate effect, with 56.2% and 43.4% respectively, as shown in Table 4.3. In these basins, the total hydroclimatic movements had the same directions as climate-driven movements. However, the magnitudes of total movements are larger than that of climate-driven movements mainly due to landscape effect.

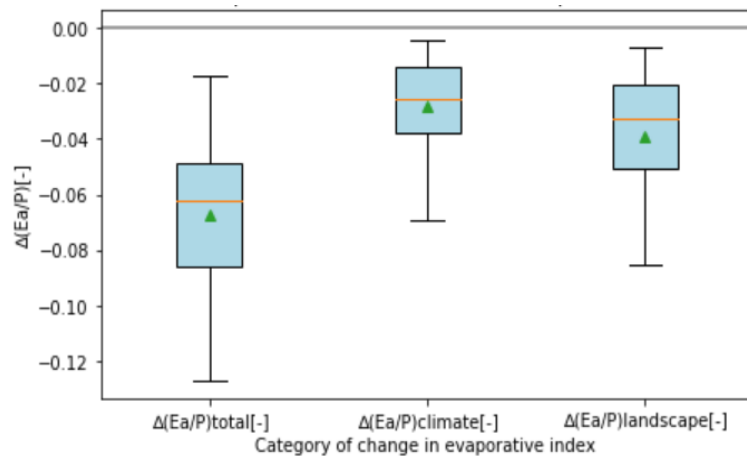


Figure 4.10: Climate and landscape effects on change in precipitation partitioning in basins with both decreased aridity index and evaporative index. Distribution of changes between pre-drought period (5 years before extreme drought event) and post-

drought period (5 years after extreme drought event) in the evaporative index ($\Delta(Ea/P)$), and its climate-driven component ($\Delta(Ea/P)_{\text{climate}}$) and landscape-driven component ($\Delta(Ea/P)_{\text{landscape}}$). The horizontal orange line in boxplot represents the median. The green triangle represents the mean value.

Basins with decreased aridity index and increased evaporative index ($270^\circ < \theta < 360^\circ$, Figure. 4.2(a)) have experienced a decreasing climate effect. After extreme drought events, these basins became wetter with more precipitation, which led to climate-driven decreases in catchment precipitation partitioning. However, this decreasing climate-driven change was counteracted by the increasing landscape-driven change; hence, the total change was still positive with more precipitation partitioned into evaporation, as indicated in Figure 4.11. The counteracting effects also apply to mean value, median and interquartile ranges of variations in evaporative index of these basins. The contribution of landscape factors to the changes of catchment precipitation partitioning was significantly greater, as shown in Table 4.3. This directly resulted in the total hydroclimatic movements outside the direction range of climate-driven movements in these basins.

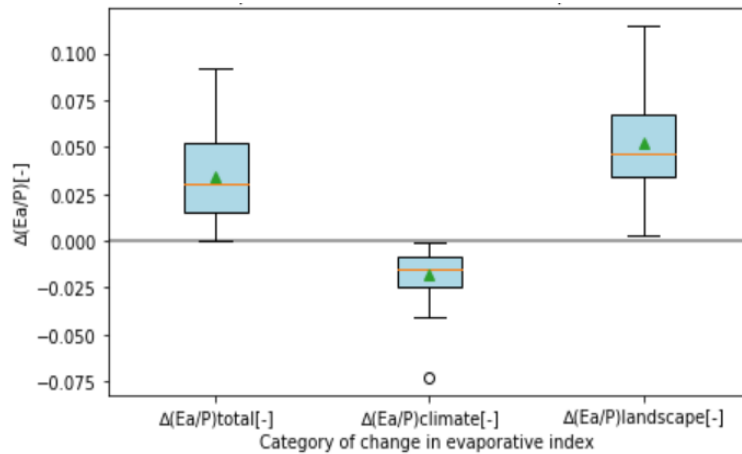


Figure 4.11: Climate and landscape effects on change in precipitation partitioning in basins with decreased aridity index and increased evaporative index. Distribution of changes between pre-drought period (5 years before extreme drought event) and post-drought period (5 years after extreme drought event) in the evaporative index ($\Delta(Ea/P)$), and its climate-driven component ($\Delta(Ea/P)_{\text{climate}}$) and landscape-driven component ($\Delta(Ea/P)_{\text{landscape}}$). The horizontal orange line in boxplot represents the median. The green triangle represents the mean value.

All in all, before and after extreme drought event, all 63 basins had the hydrological change that cannot be explained by drought-related climate drivers alone; hence it must take the impact of drought-related landscape change into account. The climate and landscape effects on change in catchment precipitation partitioning could either enhance or counteract each other in the 63 basins. Nevertheless, the total changes in precipitation partitioning in all the basins were always consistent with the landscape-driven change, that is, the variation trends were the same. For most basins, landscape drivers contributed more to the changes in precipitation partitioning between pre- and post-drought periods. The landscape change induced by drought, therefore, played a more significant role in hydrological change between pre- and post-drought periods in these basins compared to drought-related climate change.

4.5 Recovery of ecohydrological system in post-drought period

After extreme drought event, total changes in the evaporative index ($\Delta(Ea/P)$) in the 63 basins driven by the combination of drought-related climate and landscape changes showed a slight increase with time as shown in Figure 4.12. The median of total change increased from 0.006 in one year after drought to 0.015 in five years after drought, while the mean value increased from -0.004 to 0.003. Compared to pre-drought state, more precipitation was therefore partitioned into evaporation over time in five years after extreme drought events in these basins. The interquartile range implied by the width of the boxplot decreased slightly over time, which implies that there was less variability in the middle 50% of the total changes in the evaporative index. The maximum of the boxplot decreased and the minimum increased with time in post-drought period. The absolute values of changes tended to decrease regardless of whether there was a positive or negative total change in the basins, which implies that the changes between pre- and post-drought periods gradually abated. Therefore, generally speaking, the water balance behavior of the basins gradually returned to the pre-drought level over time after drought.

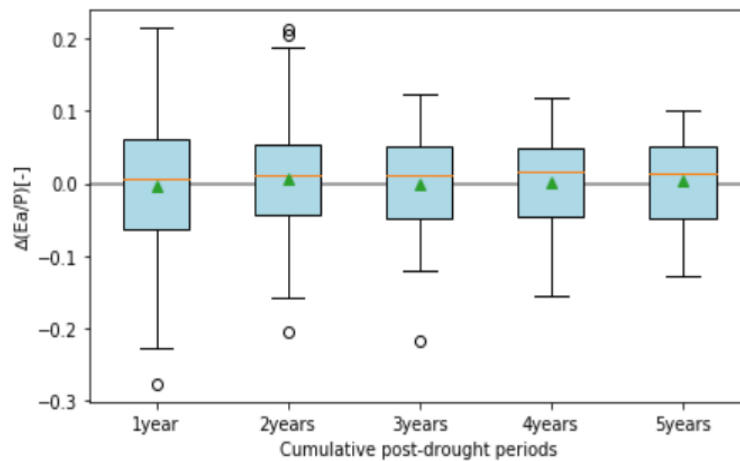


Figure 4.12: Variation tendency of total changes in evaporative index ($\Delta(Ea/P)$) driven by the combination of drought-related climate and landscape changes with increasing cumulative post-drought periods in the 63 basins. The horizontal orange line in boxplot represents the median. The green triangle represents the mean value. The black circles represent the outliers.

The drought recovery of ecohydrological system is affected by both climate and landscape factors. From the perspective of climate change, after extreme drought events, the changes in aridity index ($\Delta(Ep/P)$) of the basins showed a downward trend as indicated in Figure 4.14. The median value of aridity index change decreased from 0.037 in one year after drought to -0.016 in five years after drought, while the mean value also decreased from positive to negative. Therefore, most basins changed to a more humid state over time in post-drought period. This is a relative shift of ecohydrological system from wet conditions before drought to dry conditions during drought and then to wet conditions after drought. The interquartile range decreased significantly, which denotes that more data points were distributed around the median. Both the decrease of maximum and the increase of minimum of the boxplot with time in post-drought period were noticeable. The absolute values of changes in aridity index showed a decreasing tendency over time, which implies that climate variables, including precipitation and potential evaporation, returned gradually to a relatively normal level, namely the pre-drought level. Therefore, the drought-induced changes in climatic conditions before and after extreme drought events weakened over time. The effect of extreme droughts on the climatic conditions of these basins were gradually decreasing with time in post-drought period.

Under the gradually wetting conditions of the basins, climate-driven changes in the evaporative index ($\Delta(Ea/P)_{\text{climate}}$) decreased from 0.015 ± 0.213 in one year after drought to -0.008 ± 0.073 in five years after drought as shown in Figure 4.13. The mean value fluctuated slightly, decreasing first and then increasing. The interquartile range decreased dramatically over time, which implies that there was less variability in the middle 50% of the climate-driven changes in the evaporative index. The maximum of the boxplot decreased and the minimum increased with time in post-drought period. The absolute values of climate-driven changes tended to decline regardless of whether there was a positive or negative climate-driven change in the basins, which indicates that the impact of drought-related climate change on catchment water balance behavior might weaken over time after drought. Therefore, the basins recovered from extreme droughts gradually.

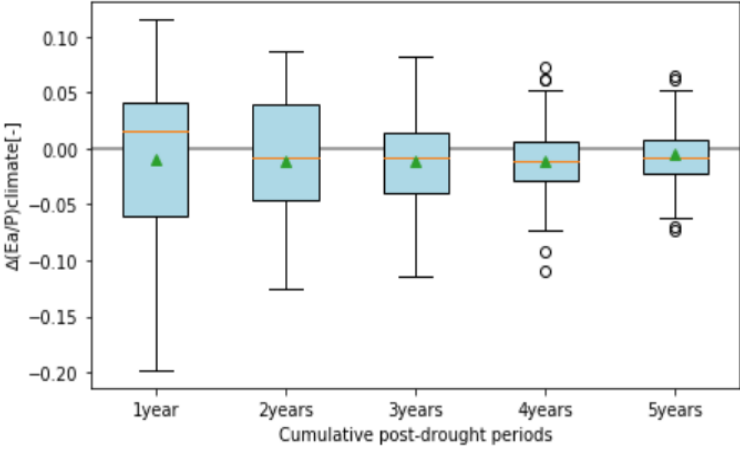


Figure 4.13: Variation tendency of climate-driven changes in evaporative index ($\Delta(Ea/P)_{\text{climate}}$) with increasing cumulative post-drought periods in the 63 basins. The horizontal orange line in boxplot represents the median. The green triangle represents the mean value. The black circles represent the outliers.

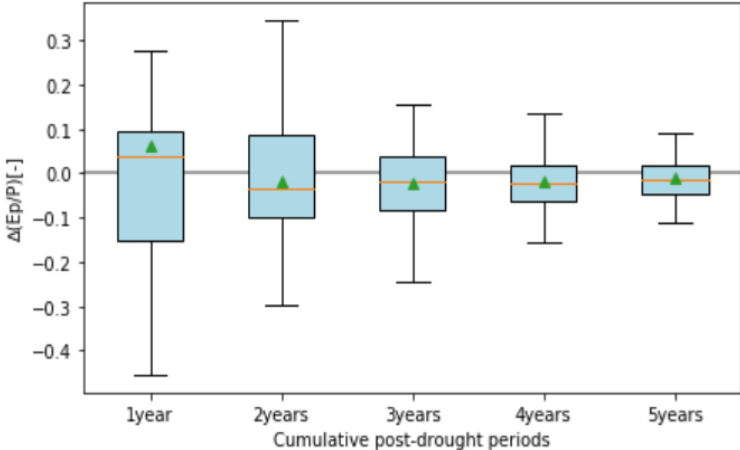


Figure 4.14: Variation tendency of changes in aridity index ($\Delta(Ep/P)$) with increasing cumulative post-drought periods in the 63 basins. The horizontal orange line in boxplot represents the median. The green triangle represents the mean value. The black circles represent the outliers.

Landscape-driven changes in the evaporative index ($\Delta(Ea/P)_{\text{landscape}}$) also showed a similar variation trend over time after extreme drought events. The landscape-driven changes in the evaporative index increased slightly from 0.010 ± 0.267 in one year after drought to 0.017 ± 0.120 in five years after drought as shown in Figure 4.17. The mean value fluctuated with time in post-drought period. The interquartile range of

landscape-driven change decreased slightly. The maximum of the boxplot also decreased and the minimum increased with time in post-drought period. The absolute values of landscape-driven changes in evaporative index tended to decline, even though landscape-driven changes could be positive or negative due to different vegetation responses to drought combined with the effect of other drought-related landscape changes. The changes in landscape in these basins between pre- and post-drought periods might diminish over time after drought. The impact of landscape change induced by extreme drought events on catchment water balance behavior might weaken over time after drought. Therefore, the basins recovered gradually from extreme droughts.

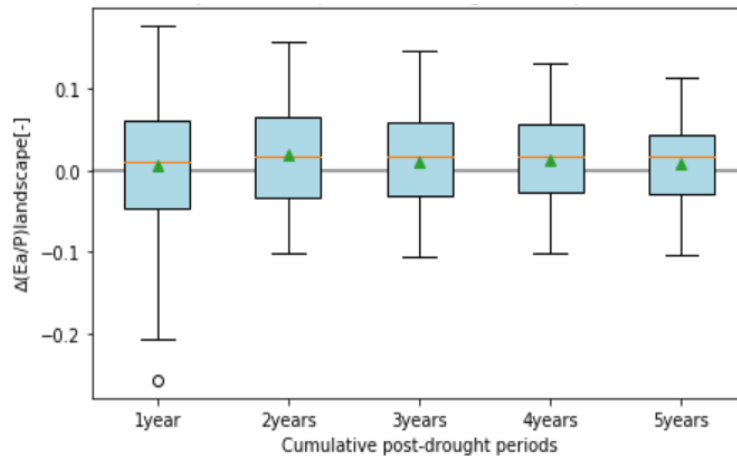


Figure 4.17: Variation tendency of landscape-driven changes in evaporative index ($\Delta(Ea/P)_{\text{landscape}}$) with increasing cumulative post-drought periods in the 63 basins. The horizontal orange line in boxplot represents the median. The green triangle represents the mean value. The black circles represent the outliers.

In addition, the magnitude of hydroclimatic movement in Budyko space indicates the sensitivity of basin to both drought-related climate and landscape changes. The larger the magnitude of hydroclimatic movement in Budyko space is, the greater drought-induced climate and landscape changes the basin might experience. As shown in Figure 4.18, the magnitudes of total hydroclimatic movements decreased significantly over time in post-drought period, which means that the hydroclimatic changes in these basins before and after extreme drought events gradually weakened over time. The effects of extreme droughts weakened gradually with time after drought; hence these basins experienced a recovery after drought. Furthermore, magnitudes of movement induced by climate change (m_c) and landscape change (m_l) also showed an apparent decline with increasing cumulative post-drought periods as indicated in Figure 4.19 and 4.20 respectively, which denotes that both of the drought-related climate effect and landscape effect weakened over time in post-drought period. Therefore, the decreasing trends of magnitudes of movements in Budyko space driven by the combined effect or single effect also prove that the impacts of extreme droughts on hydroclimatic conditions of these basins weakened over time and these basins gradually recovered from drought.

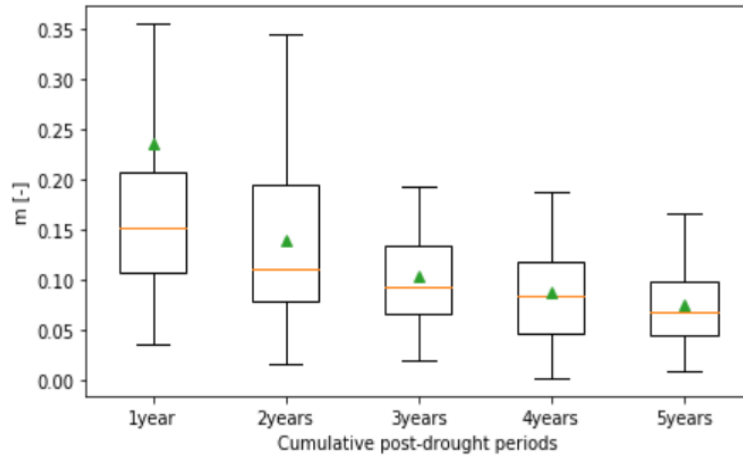


Figure 4.18: Variation tendency of magnitudes of total hydroclimatic movements in Budyko space (m) with increasing cumulative post-drought periods in the 63 basins. The horizontal orange line in boxplot represents the median. The green triangle represents the mean value. The black circles represent the outliers.

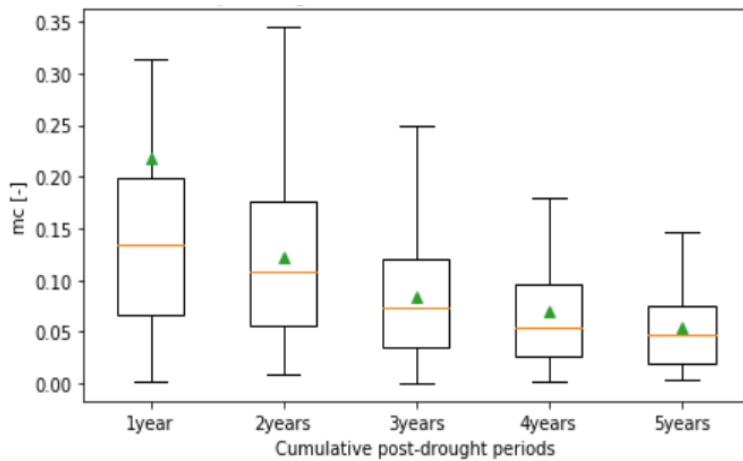


Figure 4.19: Variation tendency of magnitudes of climate-driven hydroclimatic movements in Budyko space (m_c) with increasing cumulative post-drought periods in the 63 basins. The horizontal orange line in boxplot represents the median. The green triangle represents the mean value. The black circles represent the outliers.

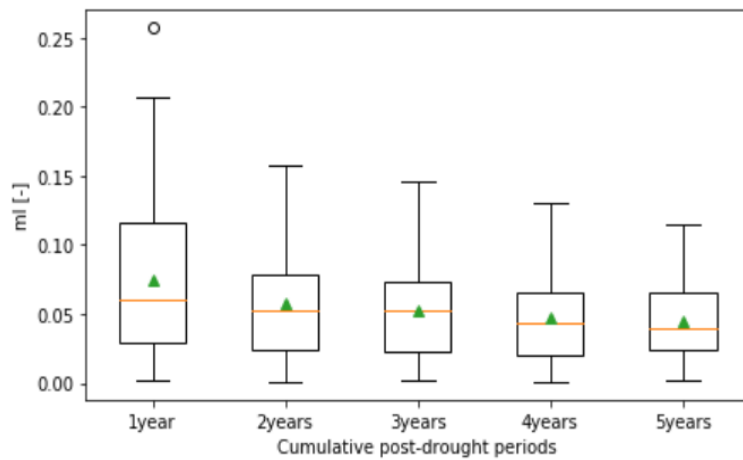


Figure 4.20: Variation tendency of magnitudes of landscape-driven hydroclimatic movements in Budyko space (m_l) with increasing cumulative post-drought periods in the 63 basins. The horizontal orange line in boxplot represents the median. The green triangle represents the mean value. The black circles represent the outliers.

The differences between pre- and post-drought states of the basins diminished gradually with increasing cumulative post-drought periods. Basins returned to their pre-drought states gradually over time in post-drought period. However, the absolute values of changes in the evaporative index and the magnitudes of hydroclimatic movements did not reach zero or a smaller value in five years after extreme drought events. There were still differences in hydrological, climatic and landscape conditions of the basins between pre- and post-drought periods. This means that these basins might need more time for drought recovery, or the basins might revert to a new relatively stable state instead of fully recovering to pre-drought state.

4.6 Vegetation change and its effect on landscape-driven change

The extreme drought events inhibited vegetation growth, implied by the NDVI decreasing from pre-drought period to in-drought period as shown in Figure 4.21. The mean annual NDVI was significantly lower ($P < 0.05$) during drought at 0.45 ± 0.25 , compared to a value of 0.49 ± 0.26 in pre-drought period. The mean value of NDVI decreased from 0.48 to 0.45. During drought, vegetation decrement might be the result of persistent water deficit with less precipitation and higher temperature (Han et al., 2018). The decline of vegetation greenness during drought denotes that extreme drought events might impose stress on vegetation community, which could lead to the reduction in aboveground vegetation biomass and productivity, thus vegetation growth reduction and even vegetation die-off.

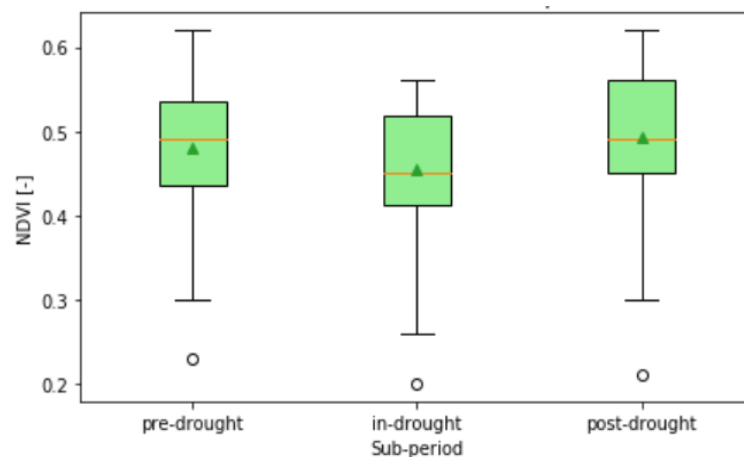


Figure 4.21: The mean annual Normalized Difference Vegetation Index (NDVI) of the 63 basins at different periods, including pre-drought period (5 years before extreme drought event), in-drought period and post-drought period (5 years after extreme drought event). The horizontal orange line in boxplot represents the median. The green triangle represents the mean value. The black circles represent the outliers.

In general, ecohydrological system has a certain degree of resilience to return to its pre-drought state after an extreme drought event. As an important part of ecohydrological system, vegetation also has the resilience to drought. In post-drought period, vegetation greenness recovered in the basins. As indicated in Figure 4.21, compared with drought period, vegetation greenness showed an obvious increase ($P < 0.01$) with a mean annual NDVI value of 0.49 ± 0.28 in post-drought period. In the five years after drought, vegetation experienced a slight increase ($P > 0.1$) in vegetation greenness which returned to or even went beyond its pre-drought level. Nevertheless, vegetation greenness in around 3.2% of the basins has not yet recover completely to its pre-drought state, showing a slight decline in mean annual NDVI before and after extreme drought event.

The recovery time of vegetation in the post-drought period is controlled by the inherent resilience of vegetation, the drought intensity and environmental conditions after drought, including water availability, nutrients and light (Gessler et al., 2017; Choat et al., 2018). In general, after drought, vegetation greenness was able to restore from drought effects and revert to its pre-drought level within one year in more than 50 % of all the basins as shown in Figure 4.22. Basins with different patterns of hydroclimatic changes showed different patterns on recovery time of vegetation greenness. Similar to section 4.5, the basins were therefore divided into four parts based on the combination of alterations in evaporative index and aridity index to analyze patterns of the recovery time of vegetation greenness separately.

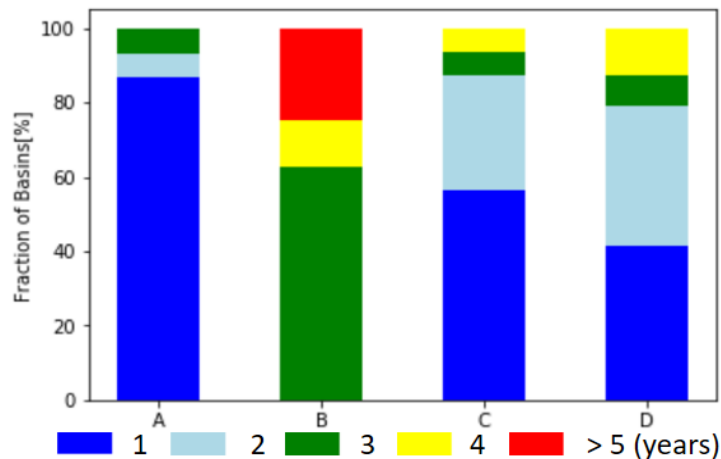


Figure 4.22: The recovery time of vegetation in the 63 basins and the fraction of basins with specific recovery time in diverse kinds of basins. Basin categories: A: basins with both increased aridity and evaporative index, B: basins with increased aridity index and decreased evaporative index, C: basins with both decreased aridity and evaporative index, D: basins with decreased aridity index and increased evaporative index. The different colors represent the different recovery time (in year) of vegetation greenness.

As shown in Figure 4.22, vegetation greenness recovered relatively faster in basins with both increased aridity and evaporative index, with NDVI recovering to its pre-drought state within one year in more than 80% of these basins. In these basins, there was still water shortage after drought, compared with pre-drought period. In such a drier condition after extreme drought events, vegetation might have higher hydrological resilience to extreme droughts to restore itself to pre-drought state in post-drought period. With high resilience, vegetation might recover rapidly. Therefore, the landscape-driven increases in the evaporative index ($\Delta(Ea/P)_{\text{landscape}}$) might be the result of the increased vegetation transpiration due to an increase in vegetation biomass during the process of the rapid recovery and regeneration in the post-drought period.

Vegetation needed a longer time to revert its greenness in basins with increased aridity index and decreased evaporative index. In 62.5% of these basins, vegetation returned to its pre-drought level NDVI within three years. However, vegetation greenness was still below its pre-drought level in five years after drought in 25% of these basins. The post-drought NDVI was higher than the drought NDVI, but lower than the pre-drought NDVI, which means that there was a recovery in vegetation greenness, but vegetation in these basins might need more than five years to revert to its pre-drought state. This might be related to vegetation species in the basins, such as slow-growing vegetation, which needs more investigation. It could be hypothesized that as a

result of the legacy effects of extreme droughts, for instance, more arid climatic condition with less moisture availability and reduction of soil nutrients, the vegetation degradation and slow regeneration may occur simultaneously, which could lead to a decrease in vegetation transpiration from pre-drought period to post-drought period. The landscape-driven decreases in the evaporative index might be the result of the decrease in vegetation transpiration due to less vegetation cover compared with pre-drought period. The reduced vegetation cover may be mainly due to the slow regrowth and recovery of the vegetation community in the post-drought period. In addition, changes in vegetation induced by extreme droughts might also affect water balance behavior by causing changes in streamflow. The basins with decreased evaporative index induced by landscape change, experienced an increase in river runoff between pre- and post-drought periods as presented in Figure 4.23. Vegetation degradation during extreme drought events and slow regrowth in post-drought period might decrease the soil water holding capacity, which may explain the higher runoff. Therefore, higher runoff due to the response of vegetation to drought is another possible factor in the decrease in evaporative index driven by landscape.

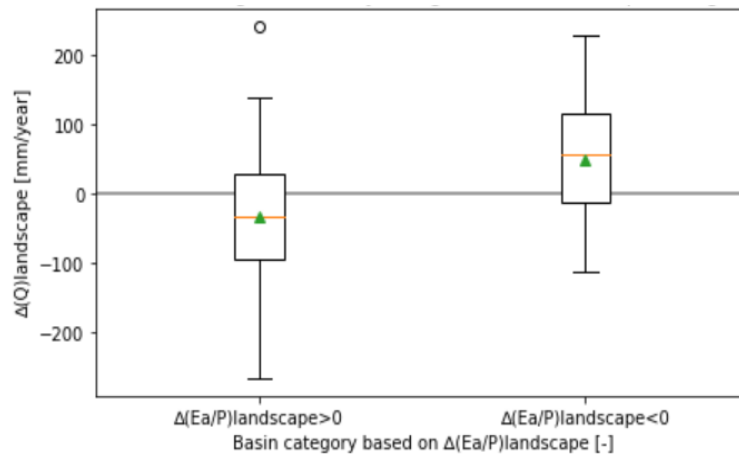


Figure 4.23: Changes in river runoff induced by drought-related landscape change between pre-drought period (5 years before extreme drought event) and post-drought period (5 years after extreme drought event) in basins with landscape-driven increases (left) and landscape-driven decreases (right). The horizontal orange line in boxplot represents the median of the changes. The green triangle represents the mean value of the changes. The black circles represent the outliers. The gray line represents the marginal line where runoff change ($\Delta Q_{\text{landscape}}$) is equal to 0

Vegetation greenness recovered relatively quickly in basins with both decreased aridity and evaporative index (87.5% of these basins recovered no more than two years). Around 79.2% of basins with decreased aridity index and increased evaporative index had a recovery time of vegetation greenness within two years. Water stress was mitigated by increased precipitation and then increased soil moisture in these two types of basins which became wetter in post-drought period implied by the decreased aridity index. Plentiful precipitation after drought is the precondition for vegetation to restore its physiological activity (Schwalm et al., 2017). Under high water availability and better water conditions, vegetation might regrow and recover rapidly in post-drought period with intense photosynthesis and respiration, which could result in the increased vegetation transpiration. Therefore, the increase in vegetation transpiration ascribed to the relatively rapid vegetation recovery might lead to an increasing landscape effect.

5 Discussion

This chapter further discusses the results and their consistency to the findings of previous studies discussed in Chapter 2. Section 5.1 discusses issues related to the definition of the three sub-periods analyzed in this study. The drought recovery of the basins and its possible factors are discussed in section 5.2. Section 5.3 and 5.4 further discuss the climatic drivers and landscape drivers with their effects on changes in catchment precipitation partitioning respectively. Section 5.5 describes some other landscape drivers, except for drought-related vegetation change, and their potential impacts on catchment precipitation partitioning change. The limitation and uncertainty of this study are presented in the final section.

5.1 Definition of pre-drought, drought and post-drought periods

In this study, the time series of SPEI at a 12-month time scale was utilized to identify extreme drought events. A SPEI value is based on the cumulative difference between precipitation and potential evaporation. Negative SPEI means the water deficit, while positive SPEI means the water surplus. In this study, drought event is defined to start in the month when SPEI is equal to or less than -1. When SPEI is below 0, the water deficit begins. The more negative SPEI is, the more severe the water shortage will be. Using -1 as truncation threshold has an inevitable shortage that a few months with negative SPEI before the drought event are included in pre-drought period. During these months, slight water deficit has already occurred. This might have an influence on the analysis of the hydrological condition in pre-drought period, especially for the conditions when there are relatively more months with SPEI between 0 and -1 before drought (e.g. Figure. B1). If there is only one month with negative SPEI before drought included in pre-drought period, the impact is relatively small (e.g. Figure. B3). Furthermore, as shown in Figure. B15, there are only two months with positive SPEI between the bottom in 1999 and the bottom in 2002 among SPEI time series. Based on the drought definition method in this study, the period of 1999-2000 with the bottom in 1999 was included in the pre-drought period. In this case, too much water shortage has already occurred in the pre-drought period. Therefore, it could be better to ignore the influence of the two months with positive SPEI on drought definition and extend the drought period forward to capture the catchment hydrological condition in pre-drought period exactly. Similarly, there is only one month with positive SPEI between the bottom in 2002 and the bottom in 2003 among SPEI time series as indicated in Figure. B5. The latter bottom was included in post-drought period, which indicates that water deficit still occurred in a few months after drought, affecting the analysis of the hydrological condition in post-drought period. It could be better to extend drought period afterward. Therefore, for the analysis of a large set of basins, it might need to make appropriate adjustments for drought definition according to different situations.

Additionally, the value of SPEI for a given month is computed based on the cumulative water surplus or deficit. The cumulative calculation method for the computation of SPEI at a certain timescale is accomplished by accumulating the differences between precipitation and potential evaporation for previous months up until the difference for the datum month. However, using only the so-called past data might have an influence on capturing the exact wet or dry condition implied by SPEI value for a given month in a basin. It could be better to apply central positioning, which uses the values of the differences for months before and after the datum month. This requires using a time scale with an odd number of months for the SPEI calculation. Nevertheless,

the fluctuation of the hydrological condition is gradual, and the impact of the positioning of the cumulative calculation is not great and usually ignored. Therefore, almost all the studies so far have used accumulated difference between precipitation and potential evaporation over preceding months for the computation of monthly SPEI at different time scales.

5.2 Drought recovery of ecohydrological system

Ecohydrological system has the ability to recover from drought. Schwalm et al. (2017) proposed that climatic, hydrological and land cover conditions can restore from drought within six months in most parts of the world. However, the basins did not experience complete recovery in the five years after extreme drought events in this study. As shown in Figure 4.12, 13 and 17, the catchment water balance behavior and its climatic and landscape components did not revert entirely to their pre-drought level. The magnitudes of hydroclimatic movements driven by the combined effect and driven by each single effect also did not reach zero or relatively small value in five years after drought (Figure 4.18, 19 and 20). Therefore, there were always differences in hydrological, climatic and landscape conditions of the basins before and after extreme droughts.

The drought recovery of ecohydrological system is controlled by climatic and landscape drivers. From the perspective of climatic drivers, the climate condition did not revert to its pre-drought state completely as shown in Figure 4.14, which led to the existence of climate-driven change in the evaporative index in the 1-5 years after drought. In terms of landscape drivers, especially drought-related vegetation change, vegetation greenness is able to revert from drought effects to pre-drought state within six months (Schwalm et al., 2017). However, the recovery time could be longer (e.g. over five years in this study). Vegetation that cannot recover rapidly might be in the face of various additional adverse impacts except for water deficit, including soil nutrient deficiency, forest fire, pests and carbohydrate reserves (Van der Molen et al., 2011; Brando et al., 2014). Furthermore, drought legacy effects might have an impact on vegetation recovery and regrowth for 1-4 years after drought. The patterns of vegetation recovery, including its degradation and repaid or slow recovery, affected the recovery of the basins, leading the variation in landscape-driven change in the evaporative index over time in post-drought period.

Except for the climatic and landscape drivers, the characteristic of drought events, drought severity in particular, could also affect drought recovery. Severe or extreme drought events could have a more adverse impact on ecohydrological system, which could lead to longer recovery after drought. The incomplete recovery of the basins might be the result of the extreme drought events that have caused a more serious impact on hydroclimatic conditions of these basins. Besides, ecohydrological system might transition to a new stable state that consists of new hydrological, climatic and landscape conditions, instead of reverting completely to its pre-drought condition (Luo et al., 2015). Therefore, it is expected that these 63 basins might have restored to a different stable state from pre-drought state.

5.3 Drought-related climate change and climatic effect

The result of this study demonstrates that with the impact of drought-related climate change alone most of these 63 basins became wetter in the post-drought period implied by decreased aridity index, which was mainly ascribed to precipitation increase before and after extreme drought event. This post-drought climate

change led to more precipitation partitioned into streamflow and less into evaporation. The increase in precipitation directly led to an increase in river runoff. This result is consistent with the theoretical hydrological and climatic shift from wet condition to dry condition then to wet condition. Some previous studies also found precipitation increased after drought and even extreme precipitation events occurred (Alpert, 2002; Feng et al., 2014). However, there were still some basins suffering more arid conditions and experiencing less precipitation and higher temperature after drought, which led to more precipitation partitioned into evaporation and less into streamflow. This post-drought climate change led to a decrease in river runoff accompanied by increased evaporation. This ties well with the previous study that less precipitation and higher temperature after drought led to a reduction of streamflow in the United States (Vose et al., 2016). In this study, there are no general patterns of the relationship between drought-related climate change in these basins and potential factors, including drought severity, land use and landcover and catchment properties, which still needs further exploration. The dominant contribution of precipitation to the impact of drought-induced climate change presented in this study is nicely consistent with the findings of Huo et al. (2013), but be opposite to the findings that potential evaporation plays a predominant role in climatic variables in studies of Sun et al. (2017) and Y. Li et al. (2017) mentioned in Chapter 2. This might be the result of the various catchment hydrological conditions and catchment properties of the study areas in different studies.

5.4 Vegetation-related landscape effect on precipitation partitioning

In this study, the vegetation greenness reverted to its pre-drought level in most basins. Signs of the post-drought vegetation greenness recovery are nicely consistent with findings in the United States, Africa and Southwest China (Pennington and Collins, 2007; Anyamba and Tucker, 2005; Li et al., 2019). Drought-related vegetation changes, especially vegetation recovery, regeneration and further degradation after drought, could have an influence on precipitation partitioning in the post-drought period. Landscape-driven change in precipitation partitioning might be the result of changes in vegetation transpiration and vegetation-related changes in streamflow. In post-drought period, vegetation greenness restored to its pre-drought state within three years in most of the 63 basins, which implies that vegetation has high resilience to drought. The rapid vegetation recovery after drought may result in an increase in vegetation transpiration (Han et al., 2018). Furthermore, as mentioned in Chapter 2.4, vegetation neighbors also affect vegetation recovery in the post-drought period (Callaway and Walker, 1997). Vegetation die-off induced by drought might lead to less vegetation competition. The vegetation recovery might be enhanced by the improvement of environmental conditions and more moisture availability due to less competition among vegetation communities. Besides, vegetation experienced a rapid recovery even in a more arid condition in post-drought period (Figure 4.22, A), as the competition for the limited resources (such as light, minerals, nutrients and water) might be mitigated after drought. Vegetation transpiration might therefore be increased by the growth improvement of vegetation survivors, which, thus, can lead to the landscape-driven increases. On the other hand, streamflow change induced by vegetation change might be another possible factor for landscape-driven increases. Basins with increased evaporative index driven by landscape change experienced a decrease in river runoff between pre- and post-drought periods as indicated in Figure 4.23. Lower river runoff might be the result of a post-drought shift in the species composition to the species which can extract water more efficiently (Vicente-Serrano et al., 2013). Similarly, the landscape-driven decreases in the evaporative index might be mainly the result of decreased vegetation transpiration and increased river runoff associated with vegetation change, both of which were caused by slow recovery. This assumption based on the result in this study ties well with

previous studies that less vegetation cover due to slow regrowth and recovery after drought reduces vegetation transpiration and increases river runoff (Hadley et al., 2008; Bosch and Hewlett, 1982).

5.5 Other possible landscape drivers

Apart from vegetation change induced by extreme droughts, there might be other landscape drivers that could explain the landscape-driven change in precipitation partitioning in these basins. Vegetation greenness recovered relatively rapidly in basins with both decreased aridity and evaporative index, which might lead to vegetation-related landscape-driven increases. However, the result of the separation of climate and landscape impacts indicates that these basins experienced a decreasing landscape-driven change. It could be hypothesized that the landscape-driven decreases may be the result of a combination of multiple landscape-driven changes. Changes in precipitation partitioning driven by various landscape effects might counteract and enhance each other and lead to the overall landscape-driven change. In addition, some of the basins with both increased aridity index and evaporative index are mainly covered by cultivated cropland as shown in Appendix A. Agricultural development possibly responsible for landscape-driven increases has been suggested in some studies (Van der Velde et al., 2013; Jaramillo and Destouni, 2014). Therefore, irrigated agriculture development (e.g. drainage practices) might lead to an increase in $(Ea/P)_{\text{landscape}}$ in these basins. Furthermore, hydropower development has been shown to be a suggested reason for the landscape-driven increases in the evaporative index (Levi et al., 2015; Jaramillo and Destouni, 2014; Destouni et al., 2013). Nevertheless, all 63 basins utilized for analysis in this study are the ones with minimal human water disturbances. Therefore, precipitation partitioning in these 63 basins may not be affected by the hydropower development. Besides, the landscape-driven decreases might be the result of groundwater changes and water phase condition changes (Smith et al., 2007; Jaramillo and Destouni, 2014). The deforestation, afforestation, pests and forest fire, etc. can also lead to change in catchment precipitation partitioning. It is hard to distinguish the impact of the drought-induced landscape change on catchment precipitation partitioning change from the effect of other landscape changes. This needs more and further explorations.

5.6 Uncertainty and limitation

Lack of data and inaccuracy of data are common problems in hydrology research. In the process of data collection, weekly Normalized Difference Vegetation Index (NDVI) composites based on 1-km AVHRR data from 1989 to present were obtained. However, it is found that there is a lack of NDVI before the 1990s for most of the basins. To finish the analysis of vegetation-related landscape effects on catchment precipitation partitioning, basins with drought events from 1990 to 2013 were selected as study areas, which reduced the numbers of basins studied. This might cause the results to be less general and more specific. Indeed, this is a common limitation of large dataset analysis. Additionally, the result of vegetation change shows that there was a reduction in vegetation greenness during extreme drought and a rise in vegetation greenness after extreme drought. However, as a result of lack of data, it is difficult to separate vegetation change induced by drought, pests, forest fire, afforestation and deforestation, which needs more explorations. Therefore, it was hypothesized that drought is the main factor for vegetation greenness reduction and its recovery in this study to analyze the vegetation-related landscape effects on the hydrological change before and after extreme drought event. Besides, except for drought-induced vegetation change, there might be some other landscape changes affecting precipitation partitioning change in these basins, which still exists uncertainty and needs

more investigation.

In this study, the meteorological data processing is based on the calendar year, instead of the hydrological year (water year) usually defined as the 12 months between October 1st of a year and September 30th of the following year. Using calendar year might have an influence on the estimation of mean annual actual evaporation based on water balance. Using hydrological year can reflect the cycle of hydrological conditions. The beginning of a hydrological year means the water storage is minimum and surface runoff is the lowest. Then the precipitation begins to replenish water in the ground and reservoirs, and the hydrological cycle changes from loss to gain. For basins with sufficient precipitation in 12 months of a year, the difference between precipitation for the hydrological year and calendar year is relatively small. Using calendar year may not have a massive impact on the computation for actual evaporation. However, for the general basins, using the calendar year may not be a good idea, since it might split the wet or dry seasons and precipitation cycle into different years and destroy the integrity of the hydrological cycle. Besides, it could also split the cycle of winter snow accumulation and snowmelt in basins where river runoff is partly originated from snowmelt. Using calendar year might have an effect on the estimation of actual evaporation and then the relevant analysis of extreme drought.

In addition, generally speaking, SPEI can be calculated on a range of time scales from 1 to 48 months. SPEI with different time scales can be utilized for the analysis of various kinds of drought and cumulative water deficit at different time scales. In most previous studies about vegetation response to drought, SPEI at shorter timescales (1-month or 3-month) was widely used to capture water condition important for vegetation growth at a short or medium timescale, considering growth season of vegetation (Li et al., 2019; George et al., 2017; Serra-Maluquer et al., 2018). However, this study focuses on how hydroclimatic conditions change and how catchment hydrological conditions respond to climate and landscape changes under the effect of extreme drought events in ecohydrological system. In order to capture annual water condition and hydrological effects, SPEI with a 12-month timescale was selected to identify important characteristics, including the start, end, duration, intensity and severity, of extreme drought events for different basins. Using 12-month SPEI to characterize drought event might have some limitations for investigation of vegetation response to extreme drought. This might affect the findings of the vegetation-related landscape effect on catchment precipitation partitioning in this study.

6 Conclusion

This study applied Budyko framework to detect hydroclimatic change before and after extreme drought events in 63 basins in the United States through studying hydroclimatic movements in Budyko space. To further explore the causes of hydrological change, the climate impact on changes in catchment precipitation partitioning was separated from the landscape effect that relates to changes in vegetation in particular. The objective of this study was achieved by answering five sub-research questions mentioned in Chapter 1.2. The conclusion for each sub-question is given below, followed by the final conclusion of this study and recommendations for future research.

How do hydroclimatic conditions change before and after extreme drought event?

The hydroclimatic movements in Budyko space illustrate the hydroclimatic changes of the basins under the effects of extreme drought events. There was no general pattern of hydroclimatic movements in Budyko space in all these 63 basins across the United States. Basins moved either upward or downward, and either leftward or rightward in Budyko space, which means that after extreme drought events these basins experienced either wetter or drier conditions, and more precipitation partitioned into either evaporation or streamflow. The different changes in water and energy balance behavior in response to drought implied by variations in aridity and evaporative index led to the movements of these basins in all directions in Budyko space. In addition to the different directions of the hydroclimatic movements, the magnitudes of movements that represent the extent of hydroclimate change also differed between these basins. Basins with larger magnitudes of movements experienced greater climate and landscape changes induced by extreme droughts.

Overall, most of the 63 basins experienced more precipitation partitioned into evaporation and less into streamflow after extreme drought events. Compared with pre-drought period, these basins experienced a significant reduction in streamflow in post-drought period, enhanced by more water loss through evaporation, including vegetation transpiration, canopy interception and soil evaporation. The change in streamflow was relatively greater than change in evaporation. Besides, 63.5 % of all basins experienced wetter and more energy limited conditions after drought implied by the decrease in aridity index, which is the representation of wet-dry-wet hydrological shift. Additionally, different climatic regions show various patterns of hydroclimatic change under extreme drought. For the 63 basins, semi-arid/arid basins were more likely to experience increased aridity and evaporative index after drought, while basins with a more humid climate were more likely to experience decreased aridity and evaporative index.

The different hydroclimatic changes between pre- and post-drought periods in the 63 basins represent the different catchment responses to extreme droughts and various impacts of extreme droughts on basins. The occurrence of different trajectories highlights that basins had different and unique responses to extreme drought events. The response of ecohydrological system to extreme drought event and the directly displayed hydroclimatic change strongly differ among catchment properties, long-term hydrological and climatic conditions and land cover type.

What are the relationship and interaction between climate and landscape effects on change in catchment precipitation partitioning?

The wind rose of climate-driven hydroclimatic movements differs markedly from that of total hydroclimatic

movements. The occurrence of movements outside the range of theoretical climate-driven movements denotes that the drought-related climate change that is alterations of climatic variables, is not the only driver of the hydrological change before and after extreme drought events in the 63 basins. It is not possible to explain or predict hydrological change between pre- and post-drought periods and the impacts of extreme drought events based on the information about the climatic impact alone, without pertinent explanation and account of landscape drivers. The catchment precipitation partitioning was affected by the combination of drought-related climate and landscape changes in these basins.

Basins with similar patterns of hydroclimatic changes between the two comparative periods had similar patterns of the relationship and interaction between climate and landscape effects on change in catchment precipitation partitioning. In these basins, the climate-driven increases were either enhanced by landscape-driven increases or counteracted by landscape-driven decreases. Similarly, the climate-driven decreases were either enhanced by landscape-driven decreases or counteracted by landscape-driven increases. Overall, the drought-related climate and landscape effects on change in catchment water balance behavior can either enhance or offset each other. Nevertheless, generally, landscape impact contributed more to changes in precipitation partitioning between pre- and post-drought periods than climatic impact. Therefore, landscape change is likely to play a dominant role in catchment precipitation partitioning change before and after extreme drought event in the 63 basins in the United States.

How does drought-related climate change affect catchment precipitation partitioning?

The effect of drought-related climate change on precipitation partitioning change is related to the changes in aridity index which are directly induced by the variations of climatic variables, namely precipitation and potential evaporation. For basins without landscape impact, wetter climate conditions after drought implied by a decrease in aridity index could only lead to precipitation partitioned more into river runoff and less into evaporation. Basins with a post-drought wetter condition experienced a relatively obvious rise in precipitation, which directly resulted in the increase in river runoff and thus decreased evaporative index. In contrast, drier conditions after drought implied by an increase in aridity index could only lead to more precipitation partitioned into evaporation. Basins still suffering from more arid conditions after drought experienced a decrease in precipitation accompanied by a relatively significant rise in mean temperature, which resulted in the reduction in streamflow, and thus increased evaporative index. The streamflow reduction might be enhanced by more water resources on land released through soil evaporation, vegetation transpiration and open water evaporation due to higher temperature.

Between the two comparative periods, the changes in precipitation were relatively larger than the changes in potential evaporation. The increased aridity index was mainly the result of precipitation reduction in the basins. Likewise, the decreased aridity index was mainly ascribed to the increase in precipitation. Precipitation is more critical than potential evaporation for dominating the variation of aridity index in these basins. The changes in catchment precipitation partitioning driven by drought-related climate change were therefore caused by the changes in streamflow and evaporation which were mainly due to precipitation alteration before and after extreme drought event in these 63 basins.

How does drought-related vegetation change affect catchment precipitation partitioning?

Climate change affects precipitation partitioning by altering potential evaporation and precipitation, whereas landscape change has an immediate effect on precipitation partitioning, leading to changes in evaporation

and streamflow. As an important part of ecohydrological system, vegetation is one of the crucial drivers of energy and water cycles in ecohydrological system. For a basin with a natural and unregulated condition, drought-induced vegetation change plays a vital role in landscape change under extreme drought. From pre-drought to in-drought then to post-drought periods, all these basins experienced an obvious shift in vegetation greenness from decreasing to increasing. The extreme drought events triggered a substantial reduction in aboveground productivity and vegetation biomass implied by decreased NDVI. Due to the inherent resilience of vegetation and the improvement of hydroclimatic condition after drought, NDVI gradually reverted to its pre-drought level within three years after drought in most of the basins, which could denote that vegetation experienced recovery and regeneration in post-drought period.

The landscape-driven increases in the evaporative index could be mainly the result of the increase in vegetation transpiration due to rapid vegetation recovery and recruitment after drought. Water stress was alleviated by increased precipitation and then increased soil moisture in the basins under wetter conditions after drought, which might lead to rapid vegetation recovery and recruitment. Vegetation transpiration might increase during the process of rapid recovery and regeneration due to an increase in vegetation biomass and productivity through intense photosynthesis and respiration. In addition, vegetation greenness was able to recover rapidly in basins still suffering water shortage in post-drought period, which could be explained by high vegetation resilience to drought. The mitigation of competition of resources for growth among vegetation survivors due to vegetation degradation during extreme drought events could be another possible reason. Apart from increased transpiration, the landscape-driven increases in the evaporative index are also expected to be related to lower runoff ascribed to a possible shift of vegetation species towards the species extracting water more efficiently.

The landscape-driven decreases in evaporative index might be the result of less vegetation transpiration compared with pre-drought period due to slow recovery and reduction of regrowth. Vegetation greenness showed recovery but could not revert to its pre-drought level in five years after drought in some basins. The slow recovery of vegetation greenness might be due to the growth characteristics of the vegetation within these basins, namely inherent slow growth. The possible legacy effects of extreme drought events (e.g. further water deficit after drought and loss of nutrients in soil induced by drought) and other possible factors (e.g. forest fire, deforestation and pests) might also lead to slower recovery or even prolonged vegetation degradation in post-drought period, thus less vegetation transpiration. Besides, the slow recovery could lead to lower water holding capacity of soil due to the reduction in vegetation cover, causing higher river runoff and enhancing landscape-driven decreases.

Moreover, basins with both decreased aridity and evaporative index experienced landscape-driven decreases in the evaporative index. However, the rapid recovery of vegetation in these basins might lead to an increase in transpiration, thus an increased evaporative index. Therefore, there might be changes in precipitation partitioning driven by other landscape changes that could counteract the drought-related vegetation driven changes. The landscape-driven changes in catchment precipitation partitioning between pre- and post-drought periods are, therefore, actually caused by a combination of multiple landscape-driven changes. Apart from drought-related vegetation change, other possible landscape changes, including agricultural development, drought-related groundwater changes and water phase condition changes, afforestation, deforestation, pests and forest fire, are expected to lead to changes in catchment precipitation partitioning simultaneously, which still needs further exploration.

What are the patterns of post-drought ecohydrological system recovery?

Ecohydrological system has ability to self-regulate to recover to pre-drought state after drought. All the basins experienced gradual recovery from extreme drought effects. In post-drought period, the absolute values of change in the evaporative index and its climate-driven and landscape-driven components showed a decreasing trend regardless of the increase or decrease in the partitioning of precipitation into evaporation in the basins. The water balance behavior of the basins gradually returned to its pre-drought level over time after extreme drought. Besides, the magnitudes of hydroclimatic movements in Budyko space driven by the combined effect of climate change and landscape change and driven by the two individual effects decreased significantly over time in post-drought period. The climate change and landscape change related to extreme droughts in these basins weakened over time after extreme drought events. The differences between pre- and post-drought states of these basins diminished gradually over time. However, these differences have not entirely disappeared. All the basins did not restore completely to their pre-drought conditions. The drought recovery of ecohydrological system depends on the recovery of climate conditions and vegetation within the system. Both the differences in climate conditions that persisted over time and the patterns of vegetation recovery might lead to the incomplete recovery of water balance behavior in these basins. Besides, extreme drought events could also be one of the possible reasons for the incomplete recovery. Extreme drought events could have more adverse and prolonged impacts on ecohydrological system, leading to longer recovery after drought. Furthermore, it is likely that these basins might reach new stable states, instead of reverting completely to their pre-drought states.

Under the impacts of extreme droughts, there were great hydroclimate changes in the 63 basins before and after extreme drought event. The basins had the resilience to recover gradually from extreme drought impacts. The drought-induced hydroclimatic changes represent the alterations of the response of ecohydrological system to variations in water fluxes and water resources on land induced by drought. The hydrological change is caused by the combination of climate change and landscape change. Climate-driven change in catchment precipitation partitioning is the result of the drought-induced variations in climatic variables, including precipitation and potential evaporation, among which precipitation contributed more to climatic effect. The vegetation responses to extreme droughts, namely rapid or slow recovery, regrowth and even further degradation in post-drought period, lead to different landscape-driven changes in catchment water balance behavior through directly changing vegetation transpiration and streamflow. The two drivers of changes can both enhance and counteract each other. The landscape drivers play a dominant role in hydrological changes between pre- and post-drought periods. For the 63 basins in the United States, most basins experienced an increase in the evaporative index under the impact of extreme drought, which was mainly due to the landscape change, especially vegetation change. On the one hand, due to the improvement of environment (e.g. increased water availability and nutrients) and the reduced competition for resources required for growth among the survivors of vegetation die-off induced by drought, the vegetation transpiration increases during the rapid recovery and regeneration of vegetation in post-drought period. On the other hand, the possible substitution in species composition after drought to species that extract water more efficiently might lead to lower river runoff. Therefore, the increased transpiration and vegetation-related runoff reduction might result in the increase in the proportion of precipitation partitioned into evaporation.

Several recommendations for future research can be given based on the conclusions and limitations of this study. This study focuses on the effects of extreme drought based on the medium-term tendency of water

deficit and annual water condition. It is recommended to further explore seasonal climatic and hydrological changes between pre- and post-drought periods by firstly using SPEI with shorter timescale (e.g. 1, 3 or 6 months) to define drought events. This could also help to further understand the effect of drought-related vegetation change on catchment precipitation partitioning in growing period and non-growing period. Furthermore, conclusions related to the landscape-driven changes in catchment precipitation partitioning, drought-related vegetation-driven change in particular, are based on the results and relevant previous research, which might need more field sampling or simulation models for further exploration and verification. It would also be recommended to further explore the landscape effects on change in catchment precipitation partitioning and try to distinguish the impacts of drought-induced vegetation change and other possible landscape changes. In this study, it was assumed that all the vegetation change was induced by extreme drought events. However, pests, forest fire, afforestation and deforestation can also have an influence on vegetation. Combined with the extreme drought events, all of these might lead to the change in catchment precipitation partitioning before and after drought in these basins. Possible separation of the effects of different landscape changes might be better for understanding the effect of drought-related landscape change alone on catchment water balance behavior.

References

- Abramowitz, M., & Stegun, I. A. (Eds.). (1948). *Handbook of mathematical functions with formulas, graphs, and mathematical tables* (Vol. 55). US Government printing office.
- Adams, H. D., Luce, C. H., Breshears, D. D., Allen, C. D., Weiler, M., Hale, V. C., Smith, A. M. S., & Huxman, T. E. (2012). Ecohydrological consequences of drought- and infestation- triggered tree die-off: insights and hypotheses. *Ecohydrology*, 5(2), 145–159.
- Alpert, P. (2002). The paradoxical increase of Mediterranean extreme daily rainfall in spite of decrease in total values. *Geophysical Research Letters*, 29(11), 1536.
- Anderegg, W. R. L., Schwalm, C., Biondi, F., Camarero, J. J., Koch, G., Litvak, M., Ogle, K., Shaw, J. D., Shevliakova, E., Williams, A. P., Wolf, A., Ziaco, E., & Pacala, S. (2015). Pervasive drought legacies in forest ecosystems and their implications for carbon cycle models. *Science*, 349(6247), 528–532.
- Anyamba, A., & Tucker, C. J. (2005). Analysis of Sahelian vegetation dynamics using NOAA-AVHRR NDVI data from 1981-2003. *Journal of Arid Environments*, 63(3), 596–614.
- Arora, V. K. (2002). The use of the aridity index to assess climate change effect on annual runoff. *Journal of Hydrology*, 265(1–4), 164–177.
- Bêche, L. A., Connors, P. G., Resh, V. H., & Merenlender, A. M. (2009). Resilience of fishes and invertebrates to prolonged drought in two California streams. *Ecography*, 32(5), 778–788.
- Beniston, M., & Stephenson, D. B. (2004). Extreme climatic events and their evolution under changing climatic conditions. *Global and Planetary Change*, 44(1–4), 1–9.
- Blodgett, D. L., Booth, N. L., Kunicki, T. C., Walker, J. I., & Viger, R. J. (2011). Description and testing of the Geo Data Portal: Data integration framework and Web processing services for environmental science collaboration. In *Open-File Report*.
- Bosch, J. M., & Hewlett, J. D. (1982). A review of catchment experiments to determine the effect of vegetation changes on water yield and evapotranspiration. In *Journal of Hydrology* (Vol. 55, Issues 1–4, pp. 3–23).
- Brando, P. M., Balch, J. K., Nepstad, D. C., Morton, D. C., Putz, F. E., Coe, M. T., Silvério, D., Macedo, M. N., Davidson, E. A., Nóbrega, C. C., Alencar, A., & Soares-Filho, B. S. (2014). Abrupt increases in Amazonian tree mortality due to drought-fire interactions. *Proceedings of the National Academy of Sciences of the United States of America*, 111(17), 6347–6352.
- Brown, A. E., Zhang, L., McMahon, T. A., Western, A. W., & Vertessy, R. A. (2005). A review of paired catchment studies for determining changes in water yield resulting from alterations in vegetation. *Journal of Hydrology*, 310(1–4), 28–61.
- Budyko, M. I. (1974). *Climate And Life*.
- Callaway, R. M., & Walker, L. R. (1997). Competition and facilitation: a synthetic approach to interactions in plant communities. *Ecology*, 78(7), 1958–1965.
- Camarero, J. J., Bigler, C., Linares, J. C., & Gil-Pelegrín, E. (2011). Synergistic effects of past historical logging and drought on the decline of Pyrenean silver fir forests. *Forest Ecology and Management*, 262(5), 759–769.
- Cavin, L., Mountford, E. P., Peterken, G. F., & Jump, A. S. (2013). Extreme drought alters competitive dominance within and between tree species in a mixed forest stand. *Functional Ecology*, 27(6), 1424–1435.
- Choat, B., Brodribb, T. J., Brodersen, C. R., Duursma, R. A., López, R., & Medlyn, B. E. (2018). Triggers

- of tree mortality under drought. In *Nature* (Vol. 558, Issue 7711, pp. 531–539).
- Creed, I. F., Spargo, A. T., Jones, J. A., Buttle, J. M., Adams, M. B., Beall, F. D., Booth, E. G., Campbell, J. L., Clow, D., Elder, K., Green, M. B., Grimm, N. B., Miniati, C., Ramlal, P., Saha, A., Sebestyen, S., Spittlehouse, D., Sterling, S., Williams, M. W., ... Yao, H. (2014). Changing forest water yields in response to climate warming: results from long-term experimental watershed sites across North America. *Global Change Biology*, 20(10), 3191–3208.
- Dai, A. (2011). Characteristics and trends in various forms of the Palmer Drought Severity Index during 1900–2008. *Journal of Geophysical Research*, 116(D12), D12115.
- Dai, A. (2013). Increasing drought under global warming in observations and models. *Nature Climate Change*, 3(1), 52–58.
- Destouni, G., Jaramillo, F., & Prieto, C. (2013). Hydroclimatic shifts driven by human water use for food and energy production. *Nature Climate Change*, 3(3), 213–217.
- Espinoza, J. C., Ronchail, J., Guyot, J. L., Junquas, C., Vauchel, P., Lavado, W., Drapeau, G., & Pombosa, R. (2011). Climate variability and extreme drought in the upper Solimões River (western Amazon Basin): Understanding the exceptional 2010 drought. *Geophysical Research Letters*, 38(13), n/a-n/a.
- Feng, J., Yan, D., Li, C., Gao, Y., & Liu, J. (2014). Regional Frequency Analysis of Extreme Precipitation after Drought Events in the Heihe River Basin, Northwest China. *Journal of Hydrologic Engineering*, 19(6), 1101–1112.
- Gazol, A., Camarero, J. J., Anderegg, W. R. L., & Vicente-Serrano, S. M. (2017). Impacts of droughts on the growth resilience of Northern Hemisphere forests. *Global Ecology and Biogeography*, 26(2), 166–176.
- Gazol, Antonio, & Camarero, J. J. (2016). Functional diversity enhances silver fir growth resilience to an extreme drought. *Journal of Ecology*, 104(4), 1063–1075.
- George, J.-P., Grabner, M., Karanitsch-Ackerl, S., Mayer, K., Weißenbacher, L., Schueler, S., & Mäkelä, A. (2017). Genetic variation, phenotypic stability, and repeatability of drought response in European larch throughout 50 years in a common garden experiment. *Tree Physiology*, 37(1), 33–46.
- George, J. P., Grabner, M., Karanitsch-Ackerl, S., Mayer, K., Weißenbacher, L., Schueler, S., & Mäkelä, A. (2017). Genetic variation, phenotypic stability, and repeatability of drought response in European larch throughout 50 years in a common garden experiment. *Tree Physiology*, 37(1), 33–46.
- Gessler, A., Schaub, M., & McDowell, N. G. (2017). The role of nutrients in drought-induced tree mortality and recovery. In *New Phytologist* (Vol. 214, Issue 2, pp. 513–520).
- Guardiola-Claramonte, M., Troch, P. A., Breshears, D. D., Huxman, T. E., Switanek, M. B., Durcik, M., & Cobb, N. S. (2011). Decreased streamflow in semi-arid basins following drought-induced tree die-off: A counter-intuitive and indirect climate impact on hydrology. *Journal of Hydrology*, 406(3–4), 225–233.
- Gudmundsson, L., Greve, P., & Seneviratne, S. I. (2016). The sensitivity of water availability to changes in the aridity index and other factors-A probabilistic analysis in the Budyko space. *Geophysical Research Letters*, 43(13), 6985–6994.
- Hadley, J. L., Kuzeja, P. S., Daley, M. J., Phillips, N. G., Mulcahy, T., & Singh, S. (2008). Water use and carbon exchange of red oak- and eastern hemlock-dominated forests in the northeastern USA: implications for ecosystem-level effects of hemlock woolly adelgid. *Tree Physiology*, 28(4), 615–627.
- Han, D., Wang, G., Liu, T., Xue, B. L., Kuczera, G., & Xu, X. (2018). Hydroclimatic response of evapotranspiration partitioning to prolonged droughts in semiarid grassland. *Journal of Hydrology*, 563, 766–777.
- Helman, D., Lensky, I. M., Yakir, D., & Osem, Y. (2017). Forests growing under dry conditions have higher

- hydrological resilience to drought than do more humid forests. *Global Change Biology*, 23(7), 2801–2817.
- Hoover, D. L., Knapp, A. K., & Smith, M. D. (2014). Resistance and resilience of a grassland ecosystem to climate extremes. *Ecology*, 95(9), 2646–2656.
- Huo, Z., Dai, X., Feng, S., Kang, S., & Huang, G. (2013). Effect of climate change on reference evapotranspiration and aridity index in arid region of China. *Journal of Hydrology*, 492, 24–34.
- Jaramillo, F., Cory, N., Arheimer, B., Laudon, H., Van Der Velde, Y., Hasper, T. B., Teutschbein, C., & Uddling, J. (2018). Dominant effect of increasing forest biomass on evapotranspiration: interpretations of movement in Budyko space. *Hydrol. Earth Syst. Sci*, 22, 567–580.
- Jaramillo, F., & Destouni, G. (2014). Developing water change spectra and distinguishing change drivers worldwide. *Geophysical Research Letters*, 41(23), 8377–8386.
- Julio Camarero, J., Gazol, A., Sangüesa-Barreda, G., Cantero, A., Sánchez-Salguero, R., Sánchez-Miranda, A., Granda, E., Serra-Maluquer, X., & Ibáñez, R. (2018). Forest Growth Responses to Drought at Short- and Long-Term Scales in Spain: Squeezing the Stress Memory from Tree Rings. *Frontiers in Ecology and Evolution*, 6(FEB), 9. <https://doi.org/10.3389/fevo.2018.00009>
- Levi, L., Jaramillo, F., Andričević, R., & Destouni, G. (2015). Hydroclimatic changes and drivers in the Sava River Catchment and comparison with Swedish catchments. *Ambio*, 44(7), 624–634.
- Li, X., Li, Y., Chen, A., Gao, M., Slette, I. J., & Piao, S. (2019). The impact of the 2009/2010 drought on vegetation growth and terrestrial carbon balance in Southwest China. *Agricultural and Forest Meteorology*, 269–270, 239–248.
- Li, Y., Feng, A., Liu, W., Ma, X., & Dong, G. (2017). Variation of Aridity Index and the Role of Climate Variables in the Southwest China. *Water*, 9(10), 743.
- Liang, E., Shao, X., Kong, Z., & Lin, J. (2003). The extreme drought in the 1920s and its effect on tree growth deduced from tree ring analysis: a case study in North China. *Ann. For. Sci*, 60, 145–152.
- Liu, X., Liu, W., & Xia, J. (2013). Comparison of the streamflow sensitivity to aridity index between the Danjiangkou Reservoir basin and Miyun Reservoir basin, China. *Theoretical and Applied Climatology*, 111(3–4), 683–691.
- Luo, Y., Keenan, T. F., & Smith, M. (2015). Predictability of the terrestrial carbon cycle. *Global Change Biology*, 21(5), 1737–1751.
- Marengo, J. A., & Espinoza, J. C. (2016). Extreme seasonal droughts and floods in Amazonia: causes, trends and impacts. *International Journal of Climatology*, 36(3), 1033–1050.
- Martorell, S., Diaz-Espejo, A., Medrano, H., Ball, M. C., & Choat, B. (2014). Rapid hydraulic recovery in *Eucalyptus pauciflora* after drought: Linkages between stem hydraulics and leaf gas exchange. *Plant, Cell and Environment*, 37(3), 617–626.
- Mckee, T. B., Doesken, N. J., & Kleist, J. (1993). The relationship of drought frequency and duration to time scales. In *Eighth Conference on Applied Climatology*.
- Mishra, A. K., & Singh, V. P. (2010). A review of drought concepts. In *Journal of Hydrology* (Vol. 391, Issues 1–2, pp. 202–216).
- Mueller, R. C., Scudder, C. M., Porter, M. E., Talbot Trotter, R., Gehring, C. A., & Whitham, T. G. (2005). Differential tree mortality in response to severe drought: evidence for long-term vegetation shifts. *Journal of Ecology*, 93(6), 1085–1093.
- Nalbantis, I., & Tsakiris, G. (2009). Assessment of hydrological drought revisited. *Water Resources Management*, 23(5), 881–897.
- Newman, A. J., Clark, M. P., Sampson, K., Wood, A., Hay, L. E., Bock, A., Viger, R. J., Blodgett, D., Brekke,

- L., Arnold, J. R., Hopson, T., & Duan, Q. (2015). Development of a large-sample watershed-scale hydrometeorological data set for the contiguous USA: data set characteristics and assessment of regional variability in hydrologic model performance. *Hydrol. Earth Syst. Sci*, *19*, 209–223.
- Oudin, L., Andréassian, V., Lerat, J., & Michel, C. (2008). Has land cover a significant impact on mean annual streamflow? An international assessment using 1508 catchments. *Journal of Hydrology*, *357*(3–4), 303–316.
- Pennington, D. D., & Collins, S. L. (2007). Response of an aridland ecosystem to interannual climate variability and prolonged drought. *Landscape Ecology*, *22*(6), 897–910.
- Ponce, V. M., Pandey, R. P., & Ercan, S. (2000). Characterization of Drought across Climatic Spectrum. *Journal of Hydrologic Engineering*, *5*(2), 222–224.
- Potter, N. J., & Chiew, F. H. S. (2011). An investigation into changes in climate characteristics causing the recent very low runoff in the southern Murray-Darling Basin using rainfall-runoff models. *Water Resources Research*, *47*(12).
- Renner, M., Seppelt, R., & Bernhofer, C. (2012). Hydrology and Earth System Sciences Evaluation of water-energy balance frameworks to predict the sensitivity of streamflow to climate change. *Hydrol. Earth Syst. Sci*, *16*, 1419–1433.
- Roderick, M. L., & Farquhar, G. D. (2011). A simple framework for relating variations in runoff to variations in climatic conditions and catchment properties. *Water Resources Research*, *47*(12).
- Saft, M., Western, A. W., Zhang, L., Peel, M. C., & Potter, N. J. (2015). The influence of multiyear drought on the annual rainfall-runoff relationship: An Australian perspective. *Water Resources Research*, *51*(4), 2444–2463.
- Schlesinger, W. H., & Jasechko, S. (2014). Transpiration in the global water cycle. *Agricultural and Forest Meteorology*, *189–190*, 115–117.
- Schwalm, C. R., Anderegg, W. R. L., Michalak, A. M., Fisher, J. B., Biondi, F., Koch, G., Litvak, M., Ogle, K., Shaw, J. D., Wolf, A., Huntzinger, D. N., Schaefer, K., Cook, R., Wei, Y., Fang, Y., Hayes, D., Huang, M., Jain, A., & Tian, H. (2017). Global patterns of drought recovery. *Nature*, *548*(7666), 202–205.
- Serra-Maluquer, X., Mencuccini, M., & Martínez-Vilalta, J. (2018). Changes in tree resistance, recovery and resilience across three successive extreme droughts in the northeast Iberian Peninsula. *Oecologia*, *187*(1), 343–354.
- Sheffield, J. (2004). A simulated soil moisture based drought analysis for the United States. *Journal of Geophysical Research*, *109*(D24), D24108.
- Sheffield, J., & Wood, E. F. (2008). Projected changes in drought occurrence under future global warming from multi-model, multi-scenario, IPCC AR4 simulations. *Climate Dynamics*, *31*(1), 79–105.
- Silvio, Karanitsch-Ackerl, George, J. P., Schueler, S., Mayer, K., Klumpp, R. T., & Grabner, M. (2015). Inter- and intra-specific variation in drought sensitivity in *Abies spec.* and its relation to wood density and growth traits. *Agricultural and Forest Meteorology*, *214–215*, 430–443.
- Singh, V. P., Guo, H., & Yu, F. X. (1993). Parameter estimation for 3-parameter log-logistic distribution (LLD3) by Pome. *Stochastic Hydrology and Hydraulics*, *7*(3), 163–177.
- Sivapalan, M., Thompson, S. E., Harman, C. J., Basu, N. B., & Kumar, P. (2011). Water cycle dynamics in a changing environment: Improving predictability through synthesis. *Water Resour. Res*, *47*, 0–01. <https://doi.org/10.1029/2011WR011377>
- Smith, L. C., Pavelsky, T. M., MacDonald, G. M., Shiklomanov, A. I., & Lammers, R. B. (2007). Rising minimum daily flows in northern Eurasian rivers: A growing influence of groundwater in the high-

- latitude hydrologic cycle. *Journal of Geophysical Research: Biogeosciences*, 112(G4).
- Spinoni, J., Naumann, G., Carrao, H., Barbosa, P., & Vogt, J. (2014). World drought frequency, duration, and severity for 1951-2010. *International Journal of Climatology*, 34(8), 2792–2804.
- Spinoni, J., Naumann, G., & Vogt, J. V. (2017). Pan-European seasonal trends and recent changes of drought frequency and severity. *Global and Planetary Change*, 148, 113–130.
- Sun, S., Chen, H., Ju, W., Wang, G., Sun, G., Huang, J., Ma, H., Gao, C., Hua, W., & Yan, G. (2017). On the coupling between precipitation and potential evapotranspiration: contributions to decadal drought anomalies in the Southwest China. *Climate Dynamics*, 48(11–12), 3779–3797. <https://doi.org/10.1007/s00382-016-3302-5>
- Tomer, M. D., & Schilling, K. E. (2009). A simple approach to distinguish land-use and climate-change effects on watershed hydrology. *Journal of Hydrology*, 376(1–2), 24–33.
- Van der Molen, M. K., Dolman, A. J., Ciais, P., Eglin, T., Gobron, N., Law, B. E., Meir, P., Peters, W., Phillips, O. L., Reichstein, M., Chen, T., Dekker, S. C., Doubkova, M., Friedl, M. A., Jung, M., van den Hurk, B. J. J. M., de Jeu, R. A. M., Kruijt, B., Ohta, T., ... Wang, G. (2011). Drought and ecosystem carbon cycling. In *Agricultural and Forest Meteorology* (Vol. 151, Issue 7, pp. 765–773).
- Van der Velde, Y., Lyon, S. W., & Destouni, G. (2013). Data-driven regionalization of river discharges and emergent land cover-evapotranspiration relationships across Sweden. *Journal of Geophysical Research: Atmospheres*, 118(6), 2576–2587.
- Van der Velde, Y., Vercauteren, N., Jaramillo, F., Dekker, S. C., Destouni, G., & Lyon, S. W. (2014). Exploring hydroclimatic change disparity via the Budyko framework. *Hydrological Processes*, 28(13), 4110–4118.
- Vicente-Serrano, S. M., Beguería, S., & López-Moreno, J. I. (2010). A Multiscalar Drought Index Sensitive to Global Warming: The Standardized Precipitation Evapotranspiration Index. *Journal of Climate*, 23(7), 1696–1718.
- Vicente-Serrano, S. M., Gouveia, C., Camarero, J. J., Beguería, S., Trigo, R., López-Moreno, J. I., Azorín-Molina, C., Pasho, E., Lorenzo-Lacruz, J., Revuelto, J., Morán-Tejeda, E., & Sanchez-Lorenzo, A. (2013). Response of vegetation to drought time-scales across global land biomes. *Proceedings of the National Academy of Sciences of the United States of America*, 110(1), 52–57.
- Vose, J. M., Miniati, C. F., Luce, C. H., Asbjornsen, H., Caldwell, P. V., Campbell, J. L., Grant, G. E., Isaak, D. J., Loheide, S. P., & Sun, G. (2016). Ecohydrological implications of drought for forests in the United States. *Forest Ecology and Management*, 380, 335–345.
- Wang, D., & Hejazi, M. (2011). Quantifying the relative contribution of the climate and direct human impacts on mean annual streamflow in the contiguous United States. *Water Resources Research*, 47(10). <https://doi.org/10.1029/2010WR010283>
- Williams, C. A., Reichstein, M., Buchmann, N., Baldocchi, D., Beer, C., Schwalm, C., Wohlfahrt, G., Hasler, N., Bernhofer, C., Foken, T., Papale, D., Schymanski, S., & Schaefer, K. (2012). Climate and vegetation controls on the surface water balance: Synthesis of evapotranspiration measured across a global network of flux towers. *Water Resources Research*, 48(6). <https://doi.org/10.1029/2011WR011586>
- Wu, H., Svoboda, M. D., Hayes, M. J., Wilhite, D. A., & Wen, F. (2007). Appropriate application of the standardized precipitation index in arid locations and dry seasons. *International Journal of Climatology*, 27(1), 65–79.
- Wu, X., Liu, H., Li, X., Ciais, P., Babst, F., Guo, W., Zhang, C., Magliulo, V., Pavelka, M., Liu, S., Huang, Y., Wang, P., Shi, C., & Ma, Y. (2018). Differentiating drought legacy effects on vegetation growth over the temperate Northern Hemisphere. *Global Change Biology*, 24(1), 504–516.

- Xu, X., Yang, D., Yang, H., & Lei, H. (2014). Attribution analysis based on the Budyko hypothesis for detecting the dominant cause of runoff decline in Haihe basin. *Journal of Hydrology*, 510, 530–540.
- Yang, H., & Yang, D. (2011). Derivation of climate elasticity of runoff to assess the effects of climate change on annual runoff. *Water Resources Research*, 47(7).
- Yang, Y., McVicar, T. R., Donohue, R. J., Zhang, Y., Roderick, M. L., Chiew, F. H. S., Zhang, L., & Zhang, J. (2017). Lags in hydrologic recovery following an extreme drought: Assessing the roles of climate and catchment characteristics. *Water Resources Research*, 53(6), 4821–4837.
- Yevjevich, V. (1969). An objective approach to definitions and investigations of continental hydrologic droughts. *Journal of Hydrology*, 7(3), 353.
- Yin, J., & Bauerle, T. L. (2017). A global analysis of plant recovery performance from water stress. *Oikos*, 126(10), 1377–1388. <https://doi.org/10.1111/oik.04534>
- Young, D. J. N., Stevens, J. T., Earles, J. M., Moore, J., Ellis, A., Jirka, A. L., & Latimer, A. M. (2017). Long-term climate and competition explain forest mortality patterns under extreme drought. *Ecology Letters*, 20(1), 78–86.
- Zhang, L., Dawes, W. R., & Walker, G. R. (2001). Response of mean annual evapotranspiration to vegetation changes at catchment scale. *Water Resources Research*, 37(3), 701–708.
- Zhang, Lu, Potter, N., Hickel, K., Zhang, Y., & Shao, Q. (2008). Water balance modeling over variable time scales based on the Budyko framework – Model development and testing. *Journal of Hydrology*, 360(1–4), 117–131.
- Zhao, X., Wei, H., Liang, S., Zhou, T., He, B., Tang, B., & Wu, D. (2015). Responses of Natural Vegetation to Different Stages of Extreme Drought during 2009–2010 in Southwestern China. *Remote Sensing*, 7(10), 14039–14054.

Appendix

Appendix A: Catchment characteristics of 63 basins

Table A: Hydrological, geographical and land cover characteristics of 63 basins.

NO.	Basin ID	Size [km ²]	Elevation [m]	Slope [m/km ⁻¹]	P [mm/yr]	Q [mm/yr]	Ep [mm/yr]	T [°C]	Land cover
1	1022500	620	93	17.8	1329	783	767	7	Forest
2	1031500	767	248	29.6	1270	738	752	5	Forest
3	1139000	260	373	43.1	1143	589	767	5	Forest
4	1139800	25	518	41.0	1195	651	771	5	Forest
5	1169000	234	375	49.5	1417	817	819	7	Forest
6	1181000	246	418	33.3	1376	763	823	7	Forest
7	1411300	79	15	2.0	1160	445	922	13	Forest
8	1439500	306	307	22.3	1319	731	851	9	Forest
9	1440000	172	234	28.8	1290	652	851	9	Forest
10	1440400	179	334	26.5	1337	761	847	8	Forest
11	1451800	149	180	14.9	1281	630	879	10	Hay/Pasture
12	1542810	14	493	45.6	1231	577	824	7	Forest
13	1543000	704	543	36.5	1219	589	827	7	Forest
14	1547700	115	354	43.0	1142	472	851	9	Forest
15	1568000	536	266	34.5	1204	514	880	10	Forest
16	1580000	247	174	12.4	1249	475	917	12	Hay/Pasture
17	1620500	61	786	75.0	1207	566	921	9	Forest
18	1634500	264	344	47.4	1070	357	917	11	Forest
19	1638480	234	156	16.9	1100	374	931	12	Hay/Pasture
20	1644000	860	187	24.0	1102	353	932	12	forest
21	2011400	410	784	73.9	1180	358	926	10	Forest
22	2011460	236	878	77.1	1220	511	917	9	Forest
23	2013000	436	692	70.9	1104	360	946	11	Forest
24	2046000	291	87	6.0	1196	299	993	14	Forest
25	2064000	428	192	10.0	1127	321	1073	13	Forest
26	2065500	253	170	10.1	1141	330	1349	14	Forest
27	2300700	86	25	2.9	1405	507	1296	23	Cropland
28	2374500	458	110	7.4	1571	514	1583	18	Forest
29	2422500	600	145	11.1	1446	462	1121	17	Forest
30	2450250	243	255	12.3	1575	597	1090	16	Forest
31	2469800	423	78	9.9	1484	458	1215	18	Forest
32	2472500	789	114	6.8	1560	475	1588	18	Forest
33	2481000	250	52	5.6	1716	692	1171	19	Forest
34	2481510	801	64	5.1	1672	634	1170	19	Forest

Table A (continued)

NO.	Basin ID	Size [km ²]	Elevation [m]	Slope [m/km ⁻¹]	P [mm/yr]	Q [mm/yr]	Ep [mm/yr]	T [°C]	Land cover
35	3011800	101	629	19.8	1298	703	819	7	Forest
36	3015500	831	493	22.0	1309	702	822	8	Forest
37	3021350	249	485	20.0	1345	848	823	8	Forest
38	3026500	20	577	15.8	1284	652	822	7	Forest
39	3028000	166	569	18.3	1260	715	823	7	Forest
40	3574500	859	338	47.7	1563	683	1039	15	Forest
41	4015330	226	338	19.2	822	378	711	4	Forest
42	4127997	504	357	12.2	930	392	1048	6	Forest
43	4161580	67	277	7.5	907	220	845	9	Forest
44	4216418	197	534	22.3	1147	521	812	7	Forest
45	4221000	752	658	27.1	1129	464	824	7	Forest
46	4296000	301	391	40.5	1311	618	782	5	Forest
47	6431500	428	1890	36.2	704	139	1056	5	Forest
48	7184000	515	281	3.5	1168	339	1002	14	Hay/Pasture
49	7196900	107	430	35.1	1326	411	1041	15	Hay/Pasture
50	7261000	456	198	14.4	1361	507	1057	15	Forest
51	8086290	733	476	7.9	705	33	1542	18	Grassland
52	8164300	865	103	5.8	991	132	1719	21	Grassland
53	8269000	163	2791	117.2	582	141	1475	4	Forest
54	10205030	151	2489	76.2	634	109	1477	5	Shrubland
55	11224500	325	658	70.0	453	23	1248	14	Grassland
56	11253310	236	802	88.1	404	23	1088	14	Grassland
57	12390700	470	1415	115.2	1130	408	992	5	Forest
58	12411000	866	1146	92.5	1271	697	765	6	Forest
59	13161500	990	2059	60.0	503	89	929	6	Shrubland
60	14141500	60	652	96.7	2710	2144	781	8	Forest
61	14154500	550	922	108.8	1719	951	827	9	Forest
62	14185000	450	977	116.2	2180	1650	863	7	Forest
63	14316700	588	952	119.1	1695	1102	825	9	Forest

The meteorological data (precipitation, streamflow, potential evaporation and average temperature) is long-term mean annual data over period 1981-2013. The land cover type was summarized based on land use and land cover map of the United States obtained from USGS Science Data Catalog (SDC) (<https://www.sciencebase.gov/catalog/item/5b96c2f9e4b0702d0e826f6d>). The land cover type of each basin in this table is the dominant land cover type within that basin.

Appendix B: Time series of monthly SPEI at a 12-month timescale of 63

basins

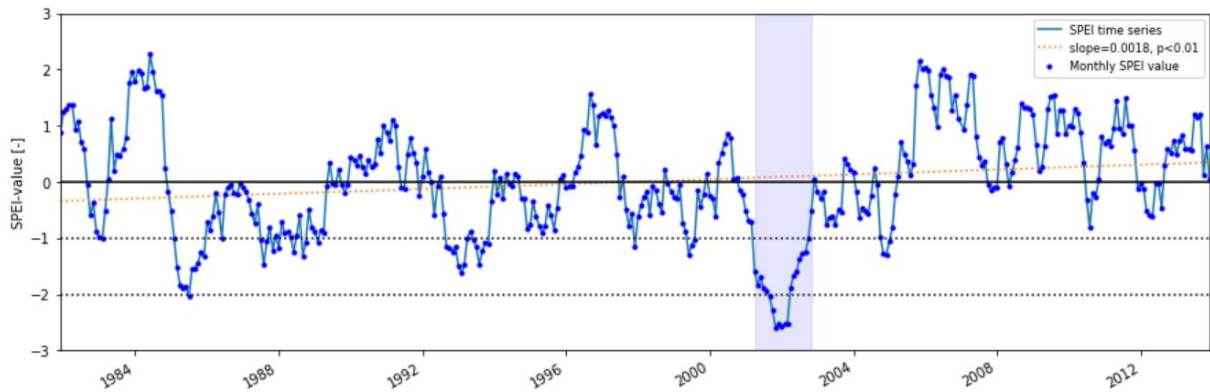


Figure B1: Time series of monthly SPEI at a 12-month time scale for the period of 1981-2013 of basin 1022500. The blue points represent the monthly SPEI values. The blue block represents times series of SPEI of the extreme drought event analyzed for this basin. The orange dashed line represents the linear regression line. The line regression equation here is: $y=0.0018x-0.3446$, $p < 0.01$.

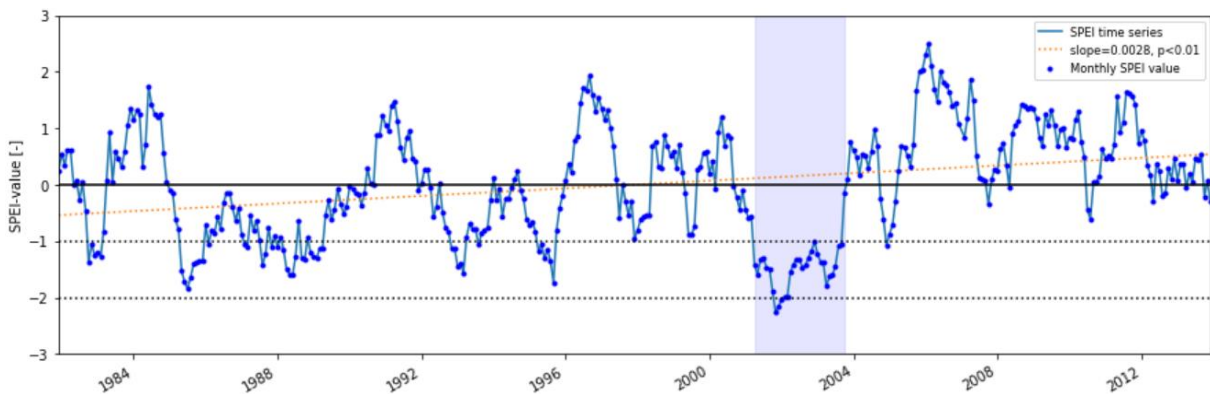


Figure B2: Time series of monthly SPEI at a 12-month time scale for the period of 1981-2013 of basin 1031500. The blue points represent the monthly SPEI values. The blue block represents times series of SPEI of the extreme drought event analyzed for this basin. The orange dashed line represents the linear regression line. The line regression equation here is: $y=0.0028x-0.5408$, $p < 0.01$.

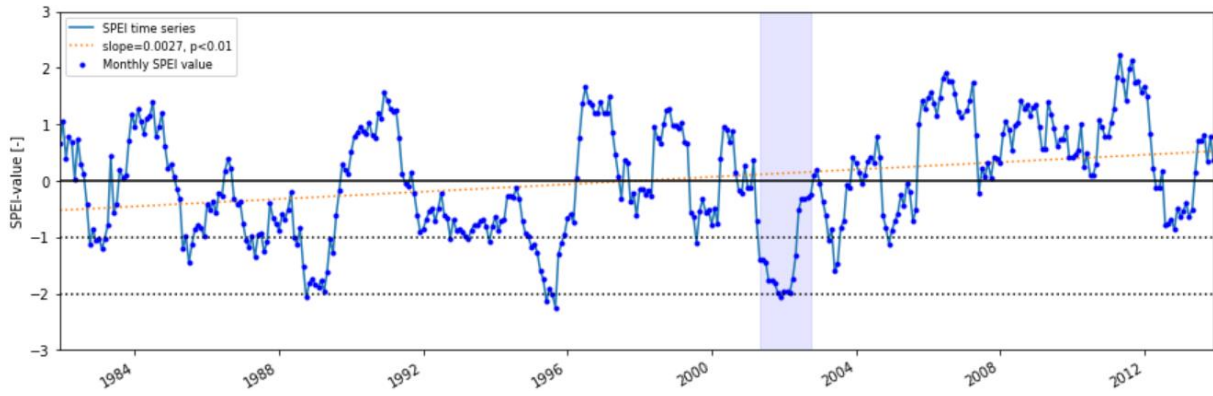


Figure B3: Time series of monthly SPEI at a 12-month time scale for the period of 1981-2013 of basin 1139000. The blue points represent the monthly SPEI values. The blue block represents times series of SPEI of the extreme drought event analyzed for this basin. The orange dashed line represents the linear regression line. The line regression equation here is: $y=0.0027x-0.5257$, $p < 0.01$.

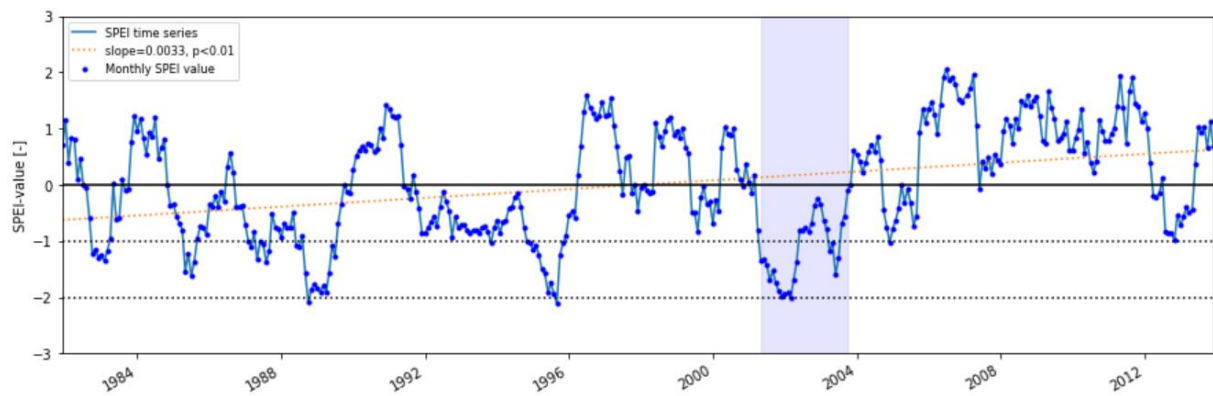


Figure B4: Time series of monthly SPEI at a 12-month time scale for the period of 1981-2013 of basin 1139800. The blue points represent the monthly SPEI values. The blue block represents times series of SPEI of the extreme drought event analyzed for this basin. The orange dashed line represents the linear regression line. The line regression equation here is: $y=0.0033x-0.6302$, $p < 0.01$.

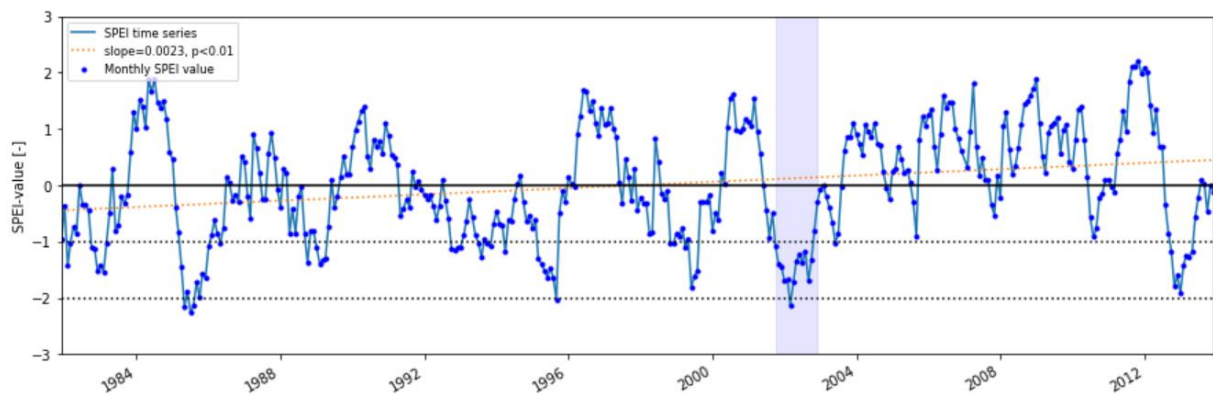


Figure B5: Time series of monthly SPEI at a 12-month time scale for the period of 1981-2013 of basin 1169000. The blue points represent the monthly SPEI values. The blue block represents times series of SPEI of the extreme drought event analyzed for this basin. The orange dashed line represents the linear regression line. The line regression equation here is: $y=0.0023x-0.4465$, $p < 0.01$.

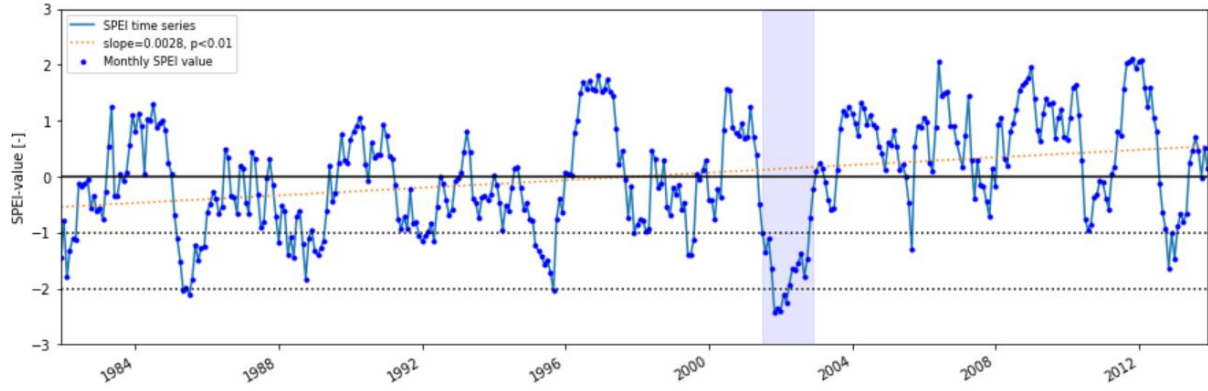


Figure B6: Time series of monthly SPEI at a 12-month time scale for the period of 1981-2013 of basin 1181000. The blue points represent the monthly SPEI values. The blue block represents times series of SPEI of the extreme drought event analyzed for this basin. The orange dashed line represents the linear regression line. The line regression equation here is: $y=0.0028x-0.5436$, $p < 0.01$.

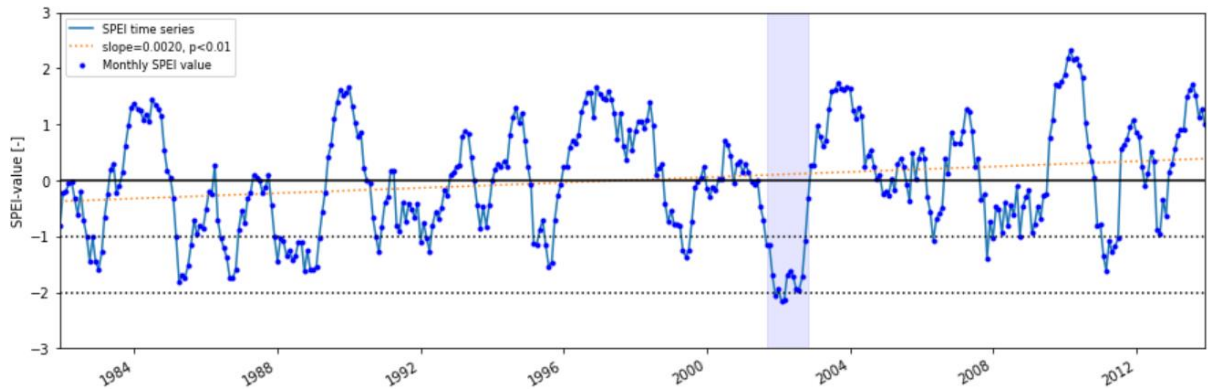


Figure B7: Time series of monthly SPEI at a 12-month time scale for the period of 1981-2013 of basin 1411300. The blue points represent the monthly SPEI values. The blue block represents times series of SPEI of the extreme drought event analyzed for this basin. The orange dashed line represents the linear regression line. The line regression equation here is: $y=0.002x-0.3763$, $p < 0.01$.

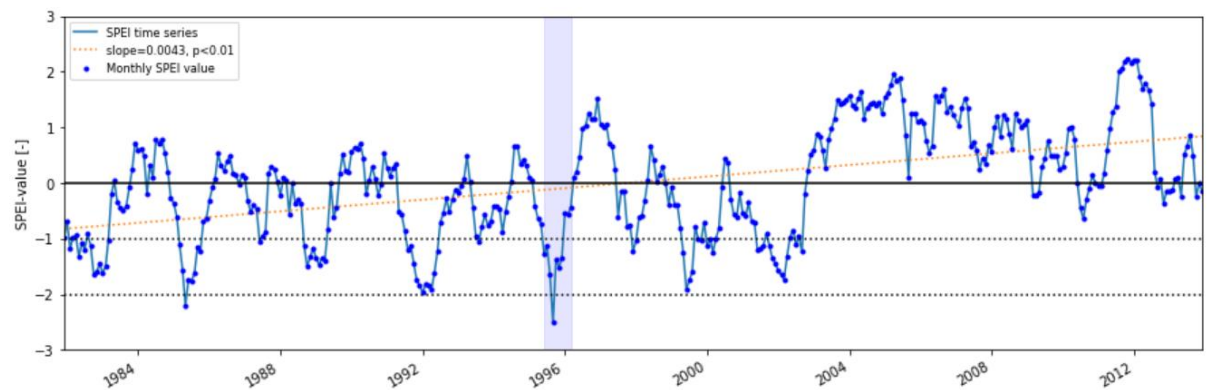


Figure B8: Time series of monthly SPEI at a 12-month time scale for the period of 1981-2013 of basin 1439500. The blue points represent the monthly SPEI values. The blue block represents times series of SPEI of the extreme drought event analyzed for this basin. The orange dashed line represents the linear regression line. The line regression equation here is: $y=0.0043x-0.8286$, $p < 0.01$.

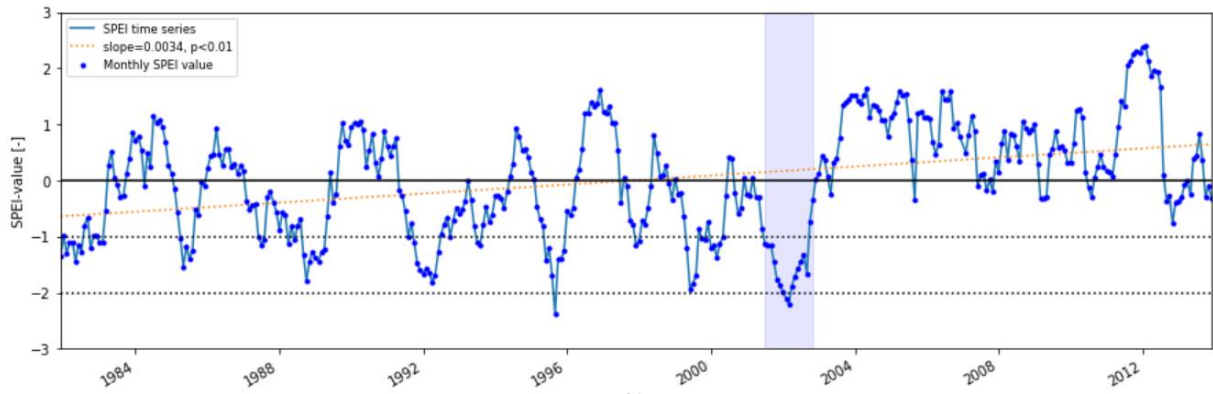


Figure B9: Time series of monthly SPEI at a 12-month time scale for the period of 1981-2013 of basin 1440000. The blue points represent the monthly SPEI values. The blue block represents times series of SPEI of the extreme drought event analyzed for this basin. The orange dashed line represents the linear regression line. The line regression equation here is: $y=0.0034x-0.6426$ $p < 0.01$.

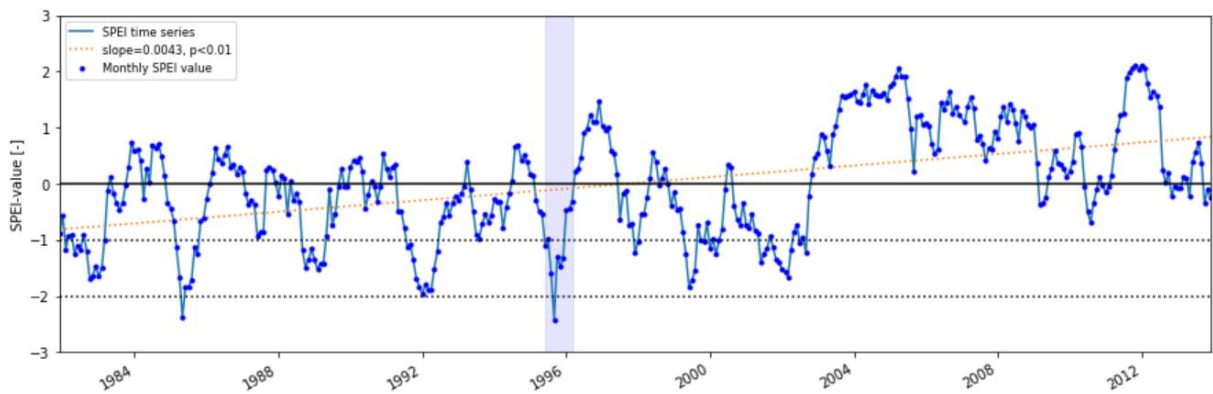


Figure B10: Time series of monthly SPEI at a 12-month time scale for the period of 1981-2013 of basin 1440400. The blue points represent the monthly SPEI values. The blue block represents times series of SPEI of the extreme drought event analyzed for this basin. The orange dashed line represents the linear regression line. The line regression equation here is: $y=0.0043x-0.8171$, $p < 0.01$.

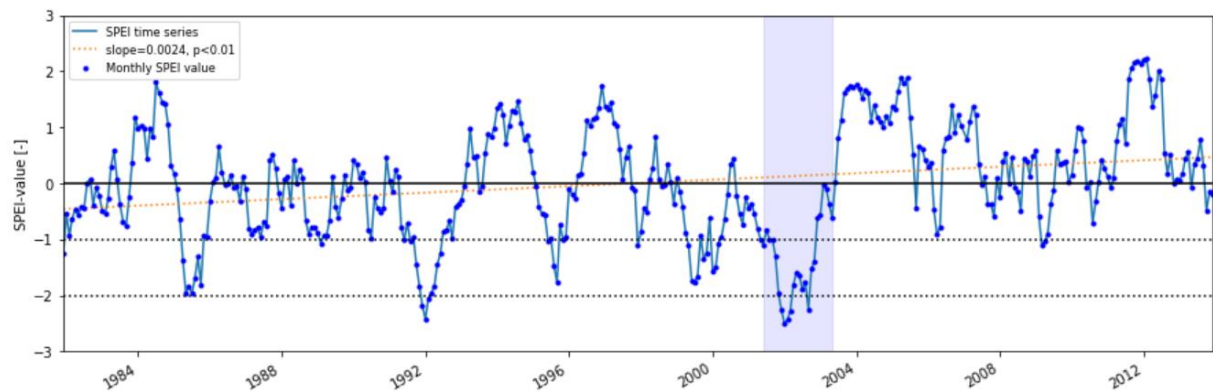


Figure B11: Time series of monthly SPEI at a 12-month time scale for the period of 1981-2013 of basin 1451800. The blue points represent the monthly SPEI values. The blue block represents times series of SPEI of the extreme drought event analyzed for this basin. The orange dashed line represents the linear regression line. The line regression equation here is: $y=0.0024x-0.4603$, $p < 0.01$.

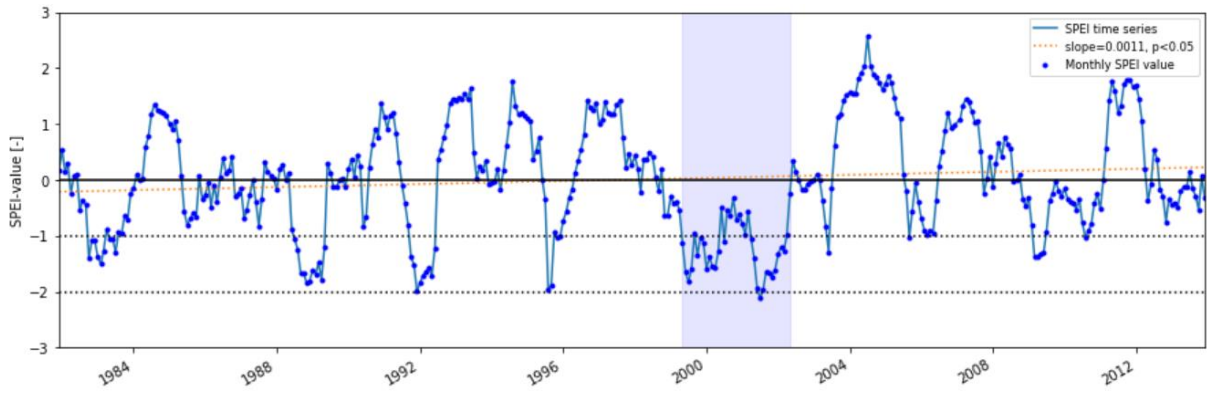


Figure B12: Time series of monthly SPEI at a 12-month time scale for the period of 1981-2013 of basin 1542810. The blue points represent the monthly SPEI values. The blue block represents times series of SPEI of the extreme drought event analyzed for this basin. The orange dashed line represents the linear regression line. The line regression equation here is: $y=0.0011x-0.2127$, $p < 0.05$.

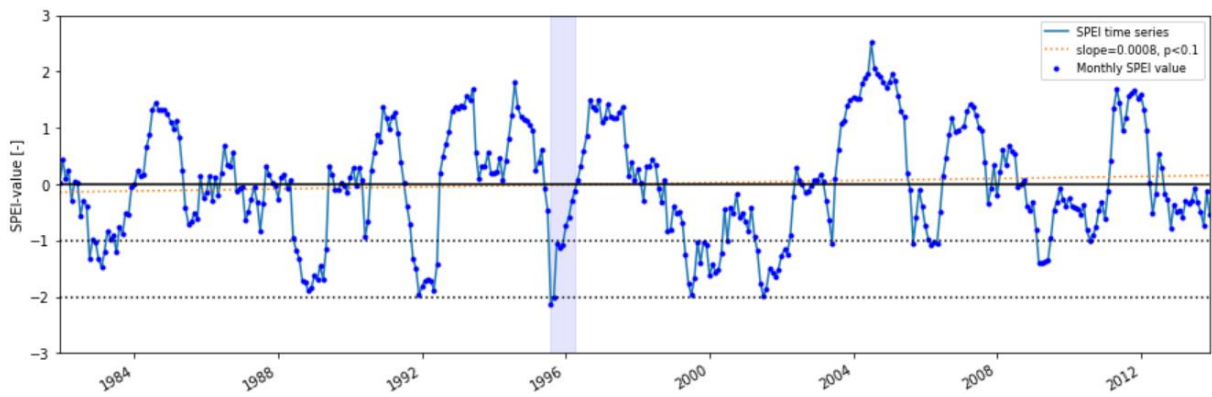


Figure B13: Time series of monthly SPEI at a 12-month time scale for the period of 1981-2013 of basin 1543000. The blue points represent the monthly SPEI values. The blue block represents times series of SPEI of the extreme drought event analyzed for this basin. The orange dashed line represents the linear regression line. The line regression equation here is: $y=0.0008x-0.1421$, $p < 0.1$.

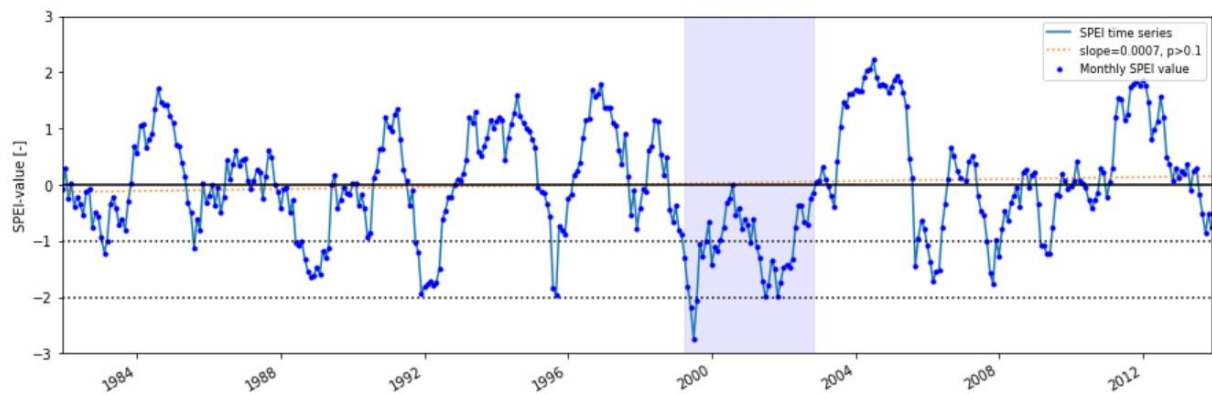


Figure B14: Time series of monthly SPEI at a 12-month time scale for the period of 1981-2013 of basin 1547700. The blue points represent the monthly SPEI values. The blue block represents times series of SPEI of the extreme drought event analyzed for this basin. The orange dashed line represents the linear regression line. The line regression equation here is: $y=0.0007x-0.131$, $p > 0.1$.

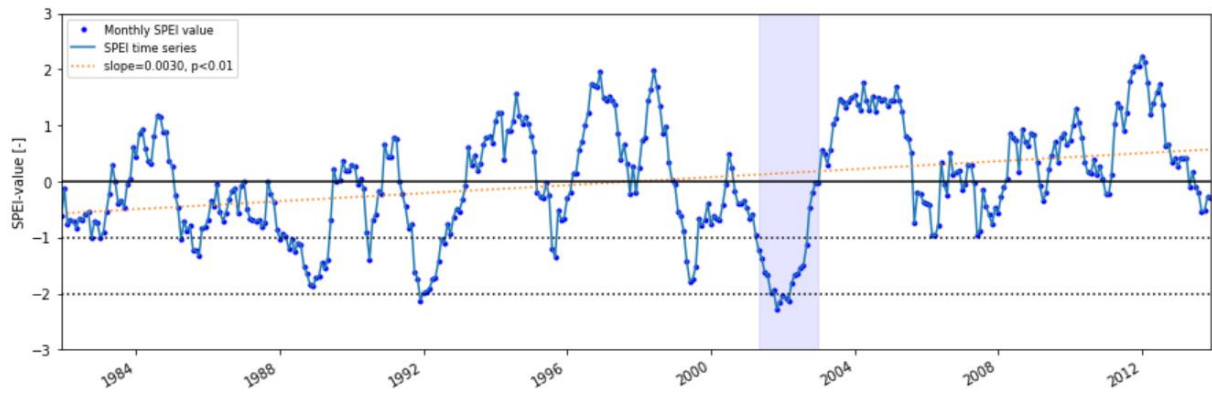


Figure B15: Time series of monthly SPEI at a 12-month time scale for the period of 1981-2013 of basin 1568000. The blue points represent the monthly SPEI values. The blue block represents times series of SPEI of the extreme drought event analyzed for this basin. The orange dashed line represents the linear regression line. The line regression equation here is: $y=0.003x-0.5717$, $p < 0.01$.

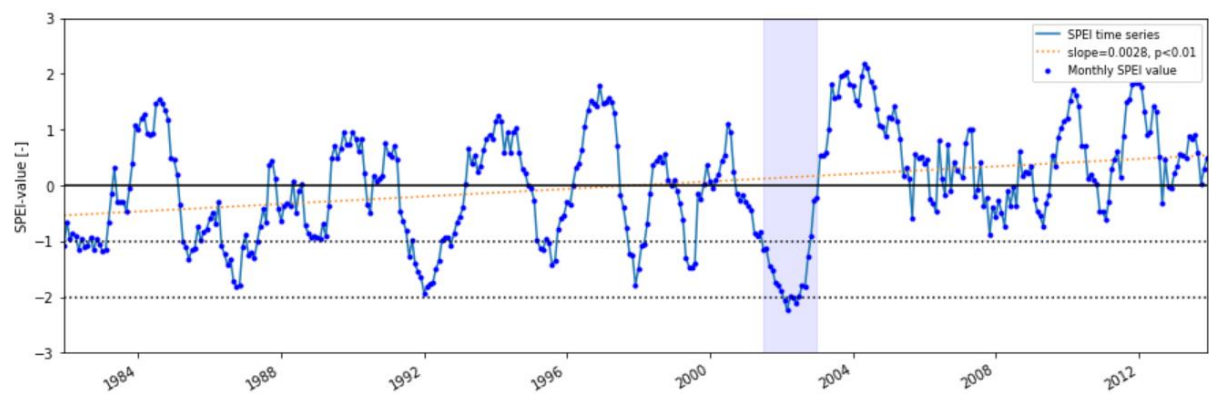


Figure B16: Time series of monthly SPEI at a 12-month time scale for the period of 1981-2013 of basin 1580000. The blue points represent the monthly SPEI values. The blue block represents times series of SPEI of the extreme drought event analyzed for this basin. The orange dashed line represents the linear regression line. The line regression equation here is: $y=0.0028x-0.534$, $p < 0.01$.

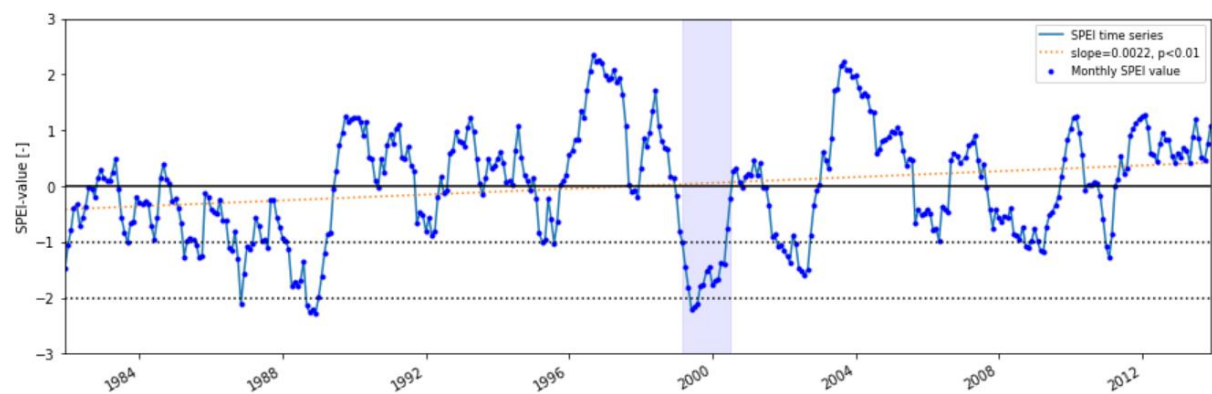


Figure B17: Time series of monthly SPEI at a 12-month time scale for the period of 1981-2013 of basin 1620500. The blue points represent the monthly SPEI values. The blue block represents times series of SPEI of the extreme drought event analyzed for this basin. The orange dashed line represents the linear regression line. The line regression equation here is: $y=0.0022x-0.4178$, $p < 0.01$.

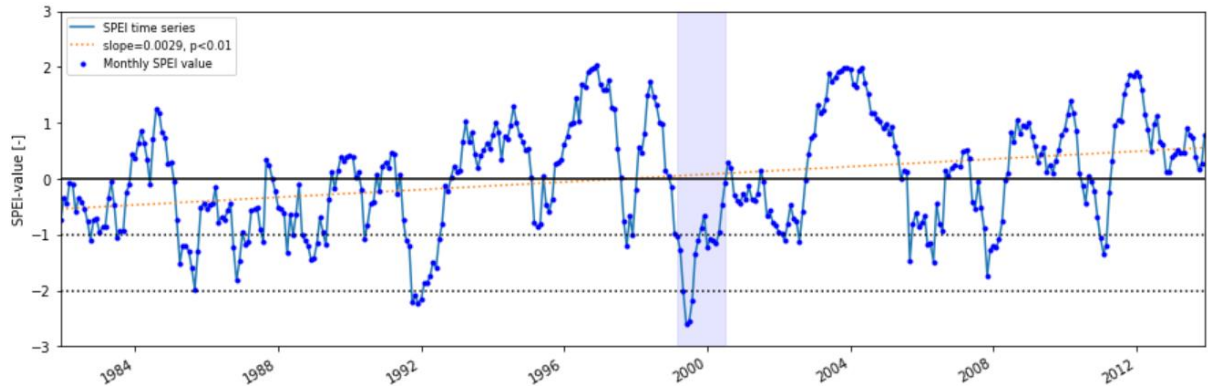


Figure B18: Time series of monthly SPEI at a 12-month time scale for the period of 1981-2013 of basin 1634500. The blue points represent the monthly SPEI values. The blue block represents times series of SPEI of the extreme drought event analyzed for this basin. The orange dashed line represents the linear regression line. The line regression equation here is: $y=0.0029x-0.5436$, $p < 0.01$.

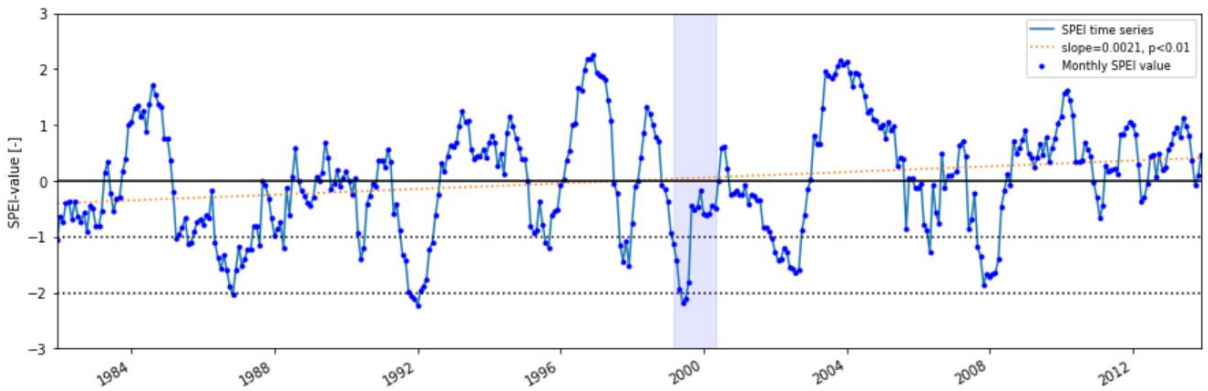


Figure B19: Time series of monthly SPEI at a 12-month time scale for the period of 1981-2013 of basin 1638480. The blue points represent the monthly SPEI values. The blue block represents times series of SPEI of the extreme drought event analyzed for this basin. The orange dashed line represents the linear regression line. The line regression equation here is: $y=0.0021x-0.4044$, $p < 0.01$.

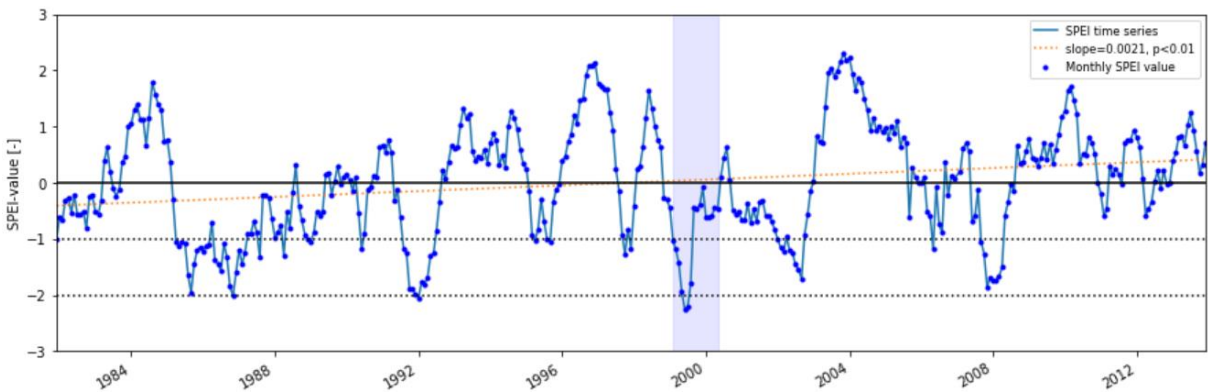


Figure B20: Time series of monthly SPEI at a 12-month time scale for the period of 1981-2013 of basin 1644000. The blue points represent the monthly SPEI values. The blue block represents times series of SPEI of the extreme drought event analyzed for this basin. The orange dashed line represents the linear regression line. The line regression equation here is: $y=0.0021x-0.4105$, $p < 0.01$.

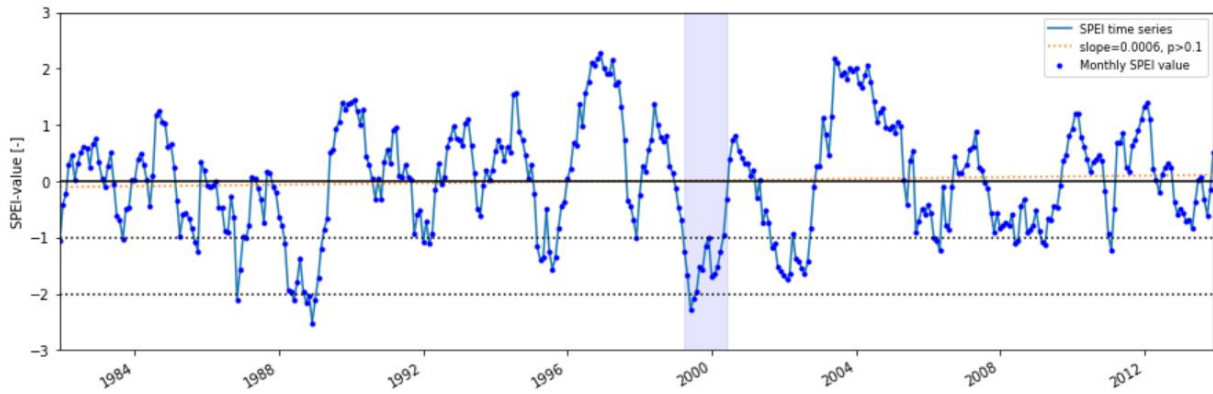


Figure B21: Time series of monthly SPEI at a 12-month time scale for the period of 1981-2013 of basin 2011400. The blue points represent the monthly SPEI values. The blue block represents times series of SPEI of the extreme drought event analyzed for this basin. The orange dashed line represents the linear regression line. The line regression equation here is: $y=0.0006x-0.1036$, $p > 0.1$.

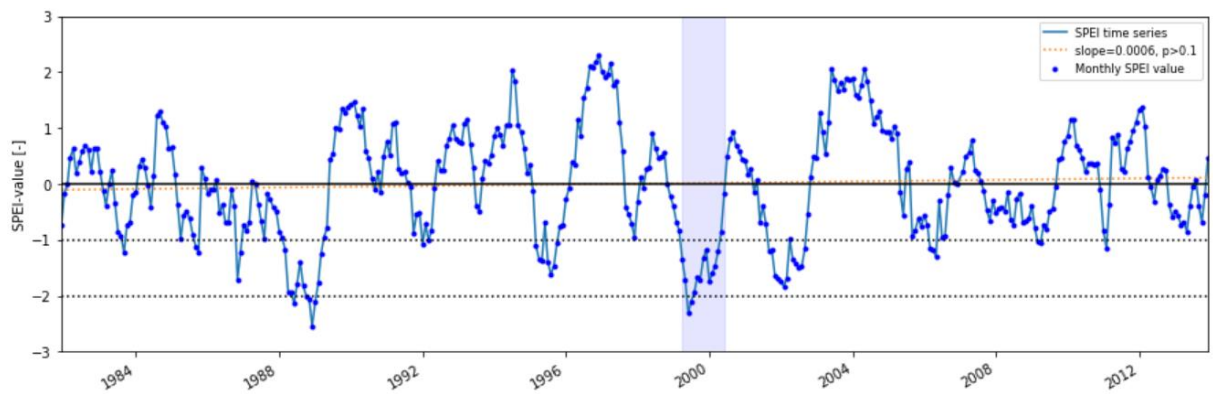


Figure B22: Time series of monthly SPEI at a 12-month time scale for the period of 1981-2013 of basin 2011460. The blue points represent the monthly SPEI values. The blue block represents times series of SPEI of the extreme drought event analyzed for this basin. The orange dashed line represents the linear regression line. The line regression equation here is: $y=0.0006x-0.1056$, $p > 0.1$.

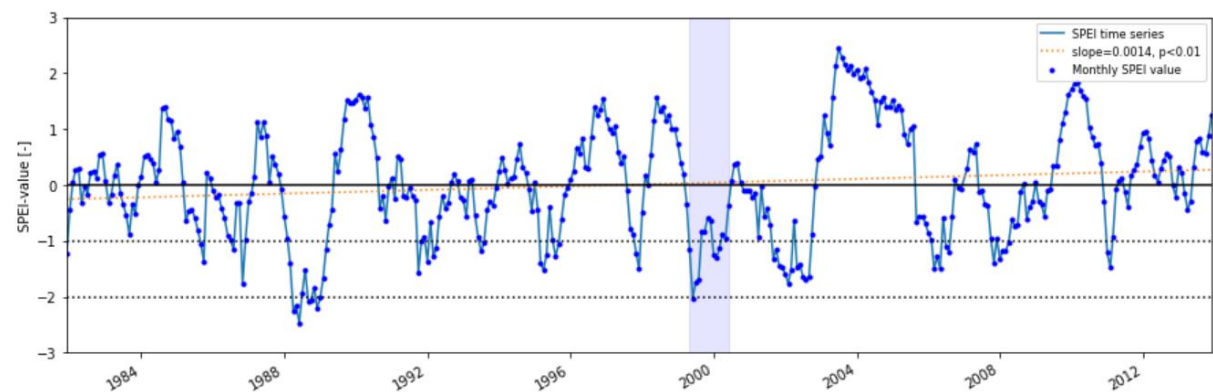


Figure B23: Time series of monthly SPEI at a 12-month time scale for the period of 1981-2013 of basin 2013000. The blue points represent the monthly SPEI values. The blue block represents times series of SPEI of the extreme drought event analyzed for this basin. The orange dashed line represents the linear regression line. The line regression equation here is: $y=0.0014x-0.2555$, $p < 0.01$.

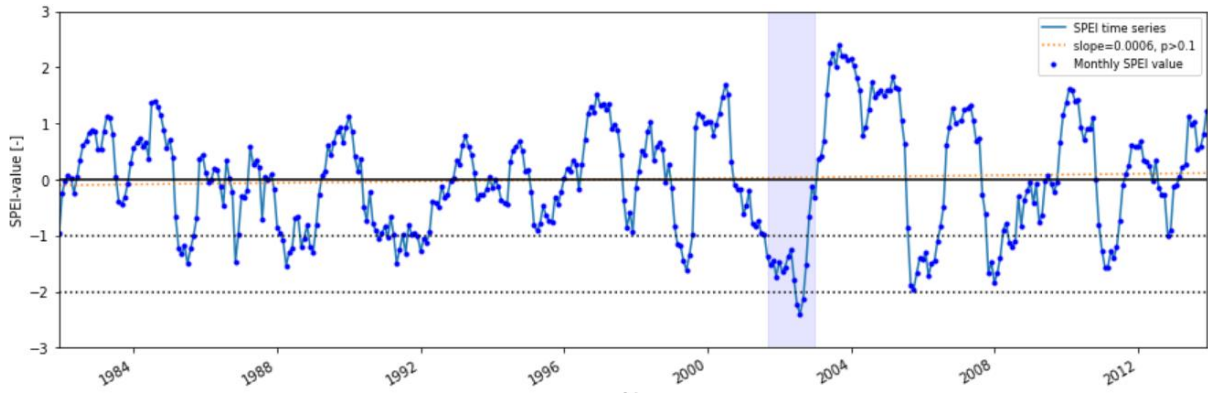


Figure B24: Time series of monthly SPEI at a 12-month time scale for the period of 1981-2013 of basin 2046000. The blue points represent the monthly SPEI values. The blue block represents times series of SPEI of the extreme drought event analyzed for this basin. The orange dashed line represents the linear regression line. The line regression equation here is: $y=0.0006x-0.1013$, $p > 0.1$.

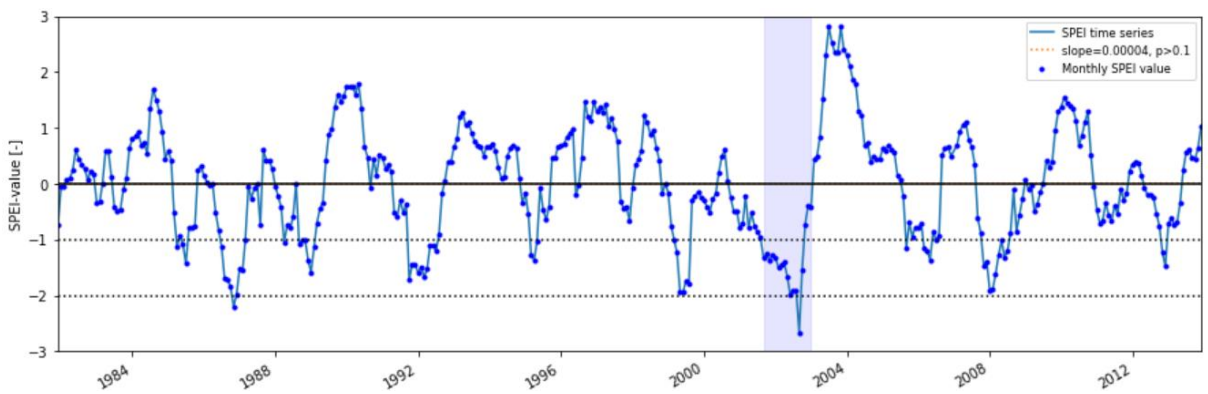


Figure B25: Time series of monthly SPEI at a 12-month time scale for the period of 1981-2013 of basin 2064000. The blue points represent the monthly SPEI values. The blue block represents times series of SPEI of the extreme drought event analyzed for this basin. The orange dashed line represents the linear regression line. The line regression equation here is: $y=0.00004x-0.0049$, $p > 0.1$.

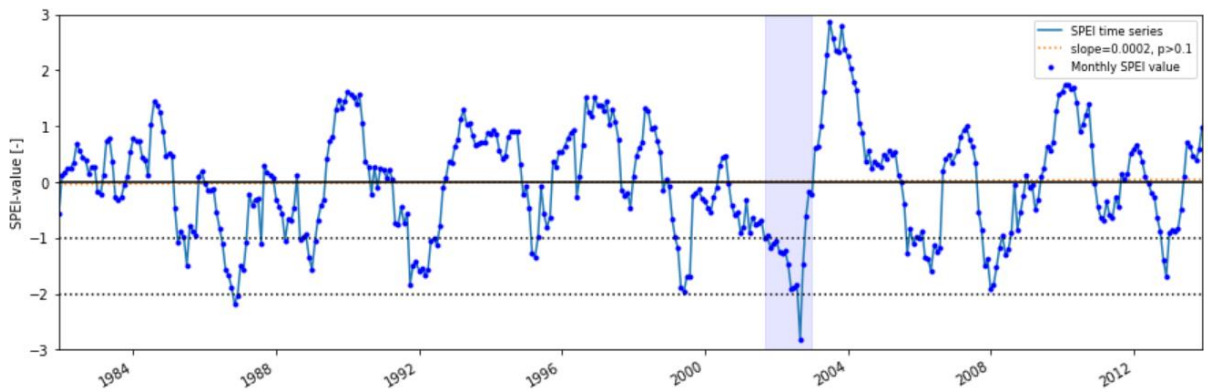


Figure B26: Time series of monthly SPEI at a 12-month time scale for the period of 1981-2013 of basin 2065500. The blue points represent the monthly SPEI values. The blue block represents times series of SPEI of the extreme drought event analyzed for this basin. The orange dashed line represents the linear regression line. The line regression equation here is: $y=0.0002x-0.0405$, $p > 0.1$.

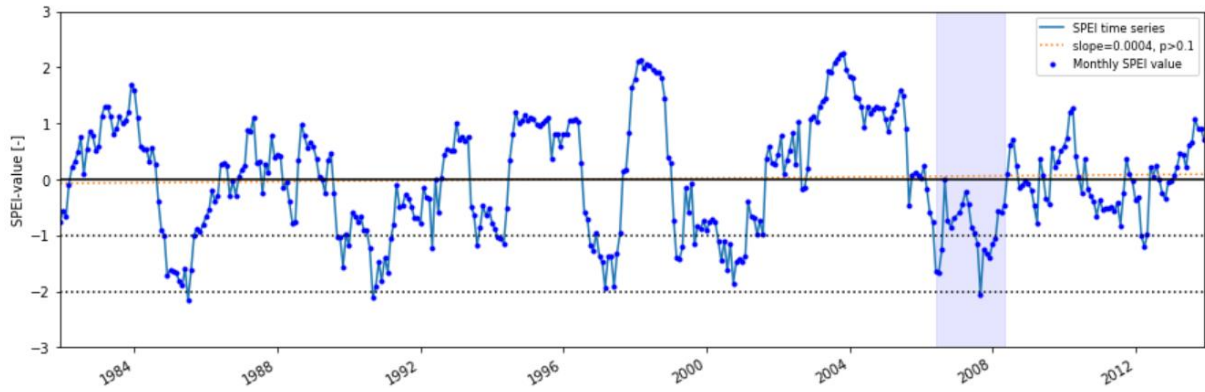


Figure B27: Time series of monthly SPEI at a 12-month time scale for the period of 1981-2013 of basin 2300700. The blue points represent the monthly SPEI values. The blue block represents times series of SPEI of the extreme drought event analyzed for this basin. The orange dashed line represents the linear regression line. The line regression equation here is: $y=0.0004x-0.0714$, $p > 0.1$.

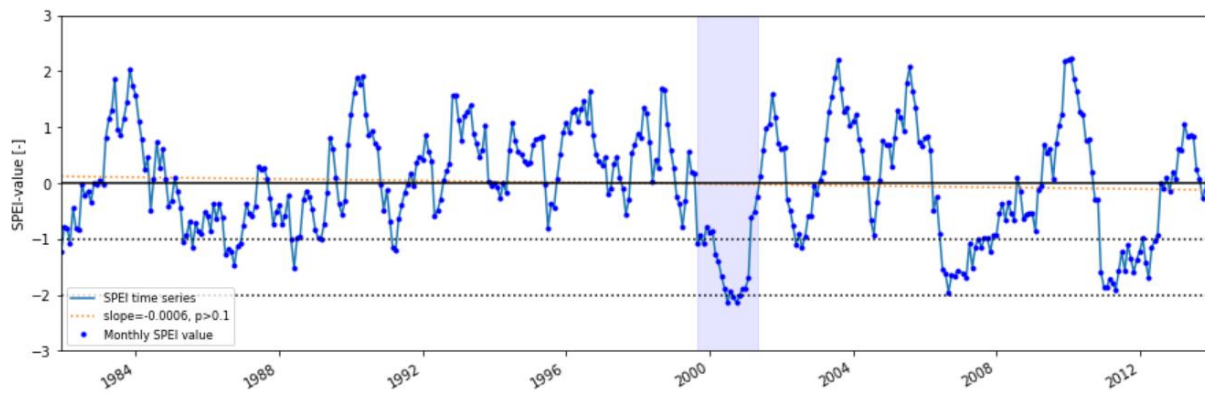


Figure B28: Time series of monthly SPEI at a 12-month time scale for the period of 1981-2013 of basin 2374800. The blue points represent the monthly SPEI values. The blue block represents times series of SPEI of the extreme drought event analyzed for this basin. The orange dashed line represents the linear regression line. The line regression equation here is: $y=-0.0006x+0.1199$, $p > 0.1$.

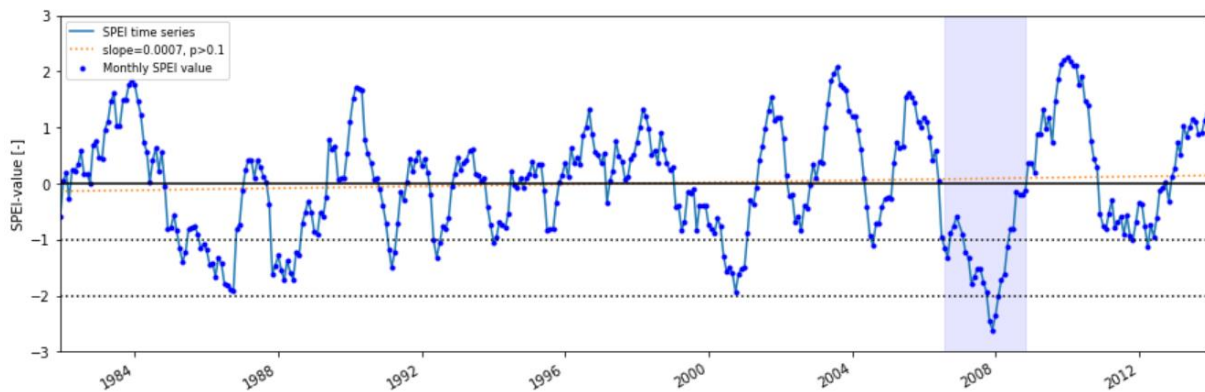


Figure B29: Time series of monthly SPEI at a 12-month time scale for the period of 1981-2013 of basin 2422500. The blue points represent the monthly SPEI values. The blue block represents times series of SPEI of the extreme drought event analyzed for this basin. The orange dashed line represents the linear regression line. The line regression equation here is: $y=0.0007x-0.1387$, > 0.1 .

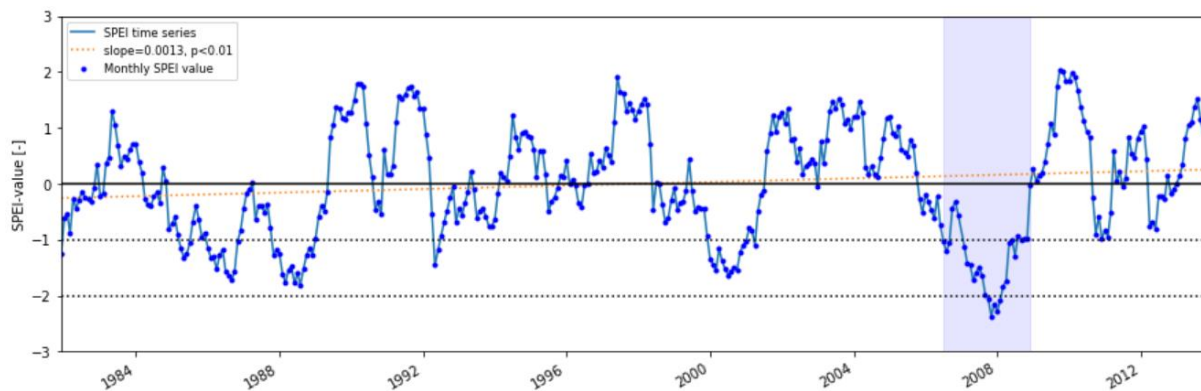


Figure B30: Time series of monthly SPEI at a 12-month time scale for the period of 1981-2013 of basin 2450250. The blue points represent the monthly SPEI values. The blue block represents times series of SPEI of the extreme drought event analyzed for this basin. The orange dashed line represents the linear regression line. The line regression equation here is: $y=0.0013x-0.2569$, $p < 0.01$.

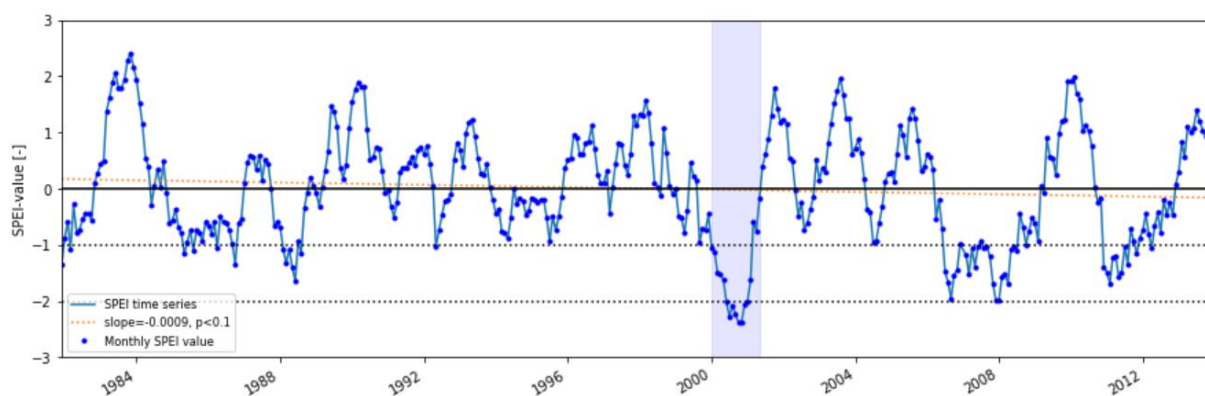


Figure B31: Time series of monthly SPEI at a 12-month time scale for the period of 1981-2013 of basin 2469800. The blue points represent the monthly SPEI values. The blue block represents times series of SPEI of the extreme drought event analyzed for this basin. The orange dashed line represents the linear regression line. The line regression equation here is: $y=-0.0009x+0.1721$ $p < 0.1$.

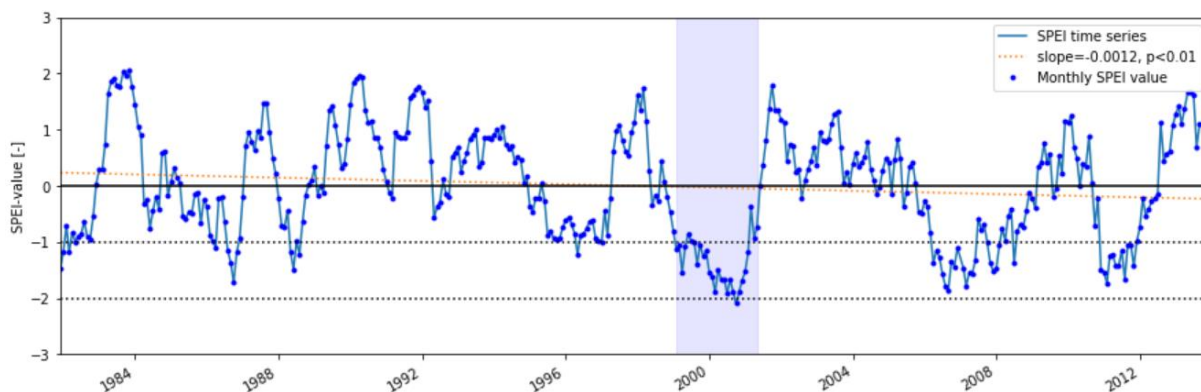


Figure B32: Time series of monthly SPEI at a 12-month time scale for the period of 1981-2013 of basin 2472500. The blue points represent the monthly SPEI values. The blue block represents times series of SPEI of the extreme drought event analyzed for this basin. The orange dashed line represents the linear regression line. The line regression equation here is: $y=-0.0012x+0.2354$, $p < 0.01$.

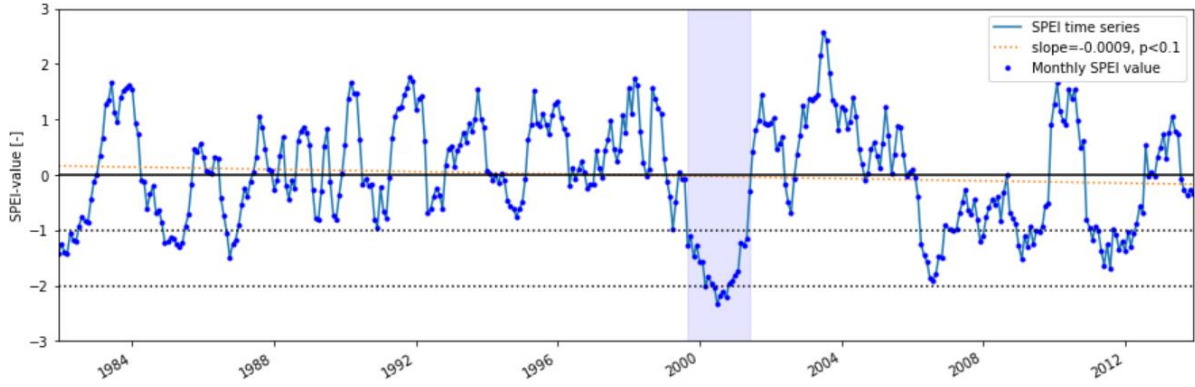


Figure B33: Time series of monthly SPEI at a 12-month time scale for the period of 1981-2013 of basin 2481000. The blue points represent the monthly SPEI values. The blue block represents times series of SPEI of the extreme drought event analyzed for this basin. The orange dashed line represents the linear regression line. The line regression equation here is: $y = -0.0009x + 0.1624$, $p < 0.1$.

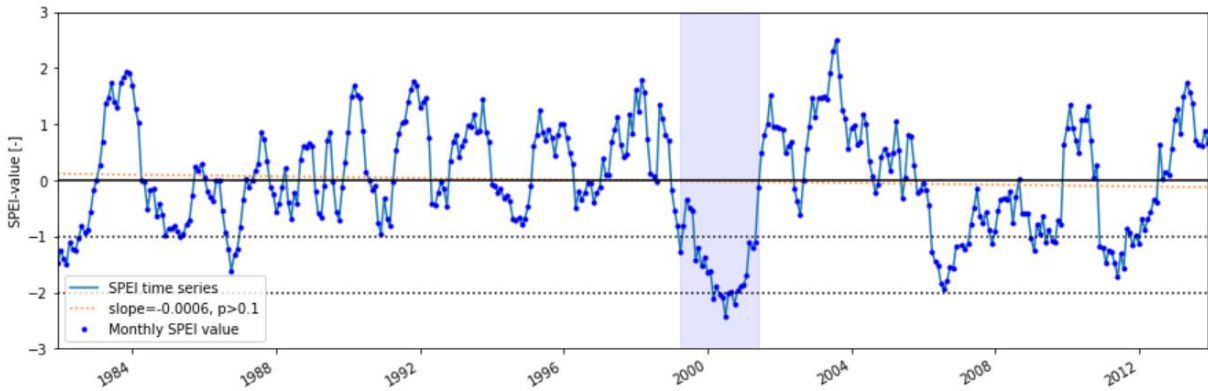


Figure B34: Time series of monthly SPEI at a 12-month time scale for the period of 1981-2013 of basin 2481510. The blue points represent the monthly SPEI values. The blue block represents times series of SPEI of the extreme drought event analyzed for this basin. The orange dashed line represents the linear regression line. The line regression equation here is: $y = -0.0006x + 0.1179$, $p > 0.1$.

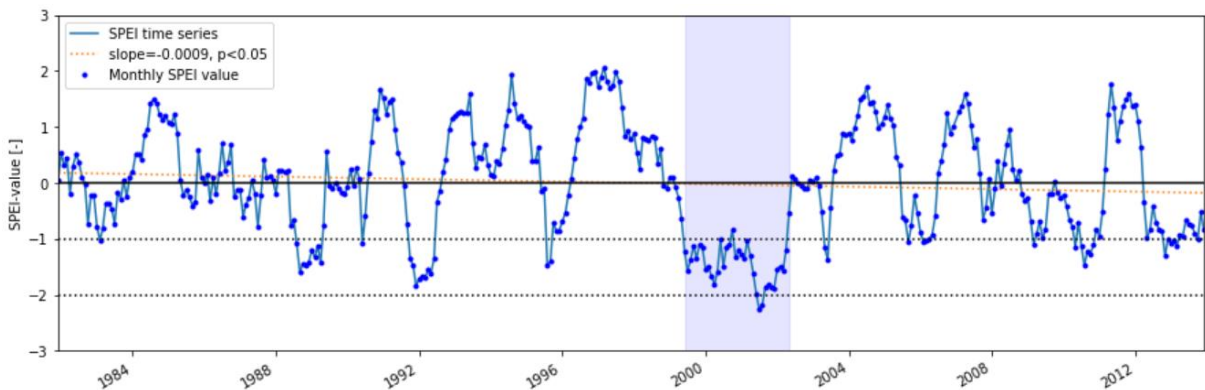


Figure B35: Time series of monthly SPEI at a 12-month time scale for the period of 1981-2013 of basin 3011800. The blue points represent the monthly SPEI values. The blue block represents times series of SPEI of the extreme drought event analyzed for this basin. The orange dashed line represents the linear regression line. The line regression equation here is: $y = -0.0009x + 0.1813$, $p < 0.05$.

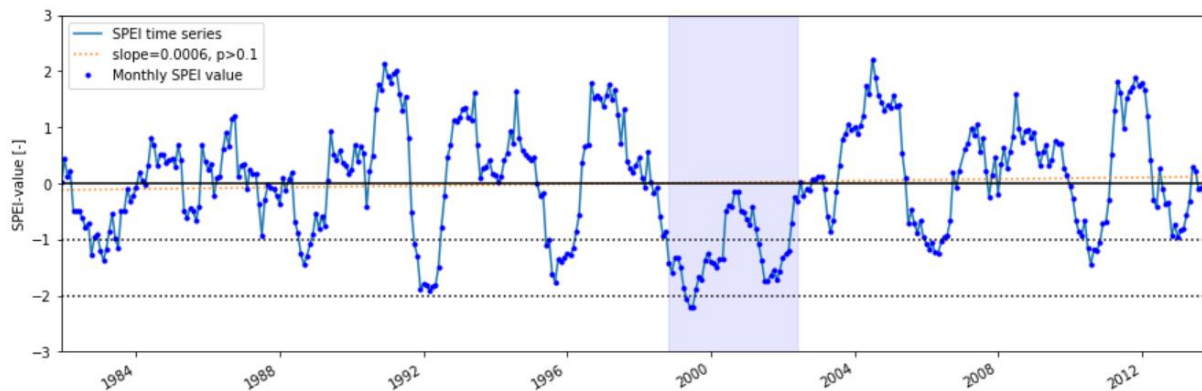


Figure B36: Time series of monthly SPEI at a 12-month time scale for the period of 1981-2013 of basin 3015500. The blue points represent the monthly SPEI values. The blue block represents times series of SPEI of the extreme drought event analyzed for this basin. The orange dashed line represents the linear regression line. The line regression equation here is: $y=0.0006x-0.1185$, $p > 0.1$.

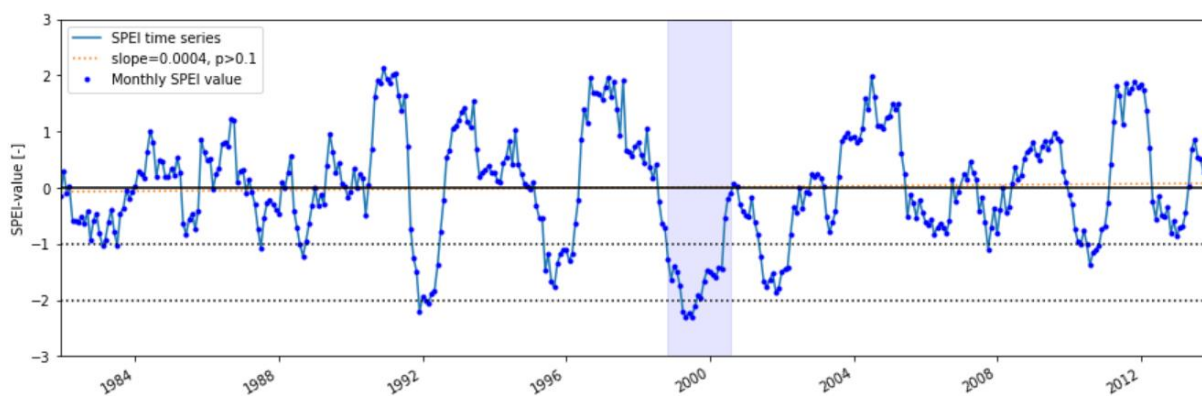


Figure B37: Time series of monthly SPEI at a 12-month time scale for the period of 1981-2013 of basin 3021350. The blue points represent the monthly SPEI values. The blue block represents times series of SPEI of the extreme drought event analyzed for this basin. The orange dashed line represents the linear regression line. The line regression equation here is: $y=0.0004x-0.0714$, $p > 0.1$.

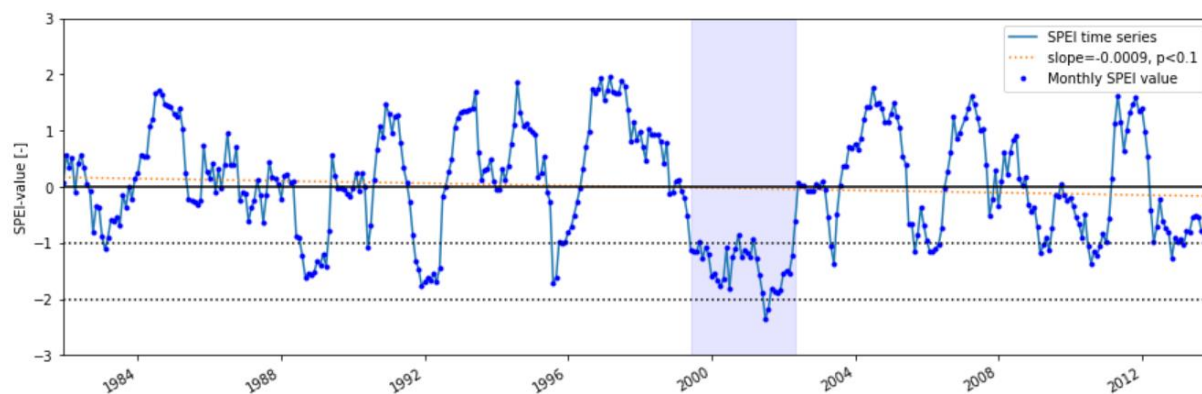


Figure B38: Time series of monthly SPEI at a 12-month time scale for the period of 1981-2013 of basin 1022500. The blue points represent the monthly SPEI values. The blue block represents times series of SPEI of the extreme drought event analyzed for this basin. The orange dashed line represents the linear regression line. The line regression equation here is: $y=-0.0009x+0.1679$, $p < 0.1$.

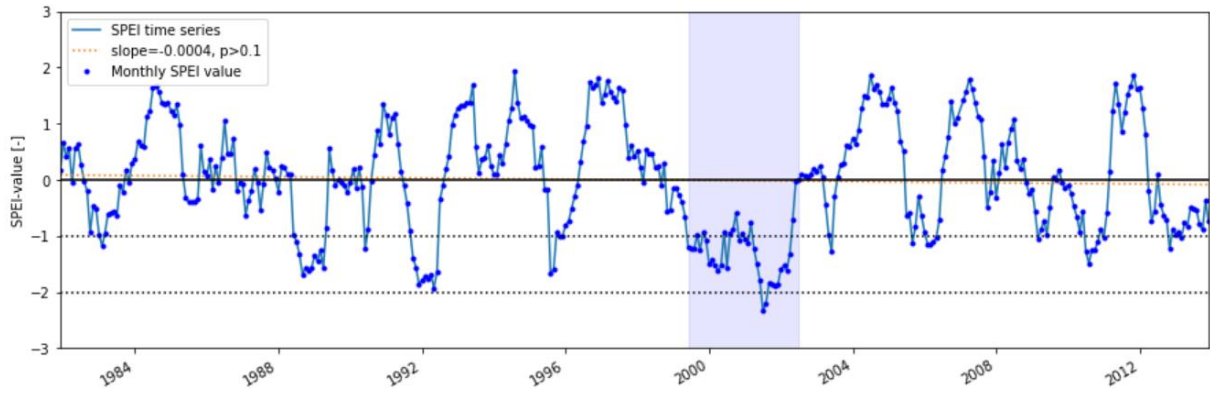


Figure B39: Time series of monthly SPEI at a 12-month time scale for the period of 1981-2013 of basin 3028000. The blue points represent the monthly SPEI values. The blue block represents times series of SPEI of the extreme drought event analyzed for this basin. The orange dashed line represents the linear regression line. The line regression equation here is: $y = -0.0004x + 0.0863$, $p > 0.1$.

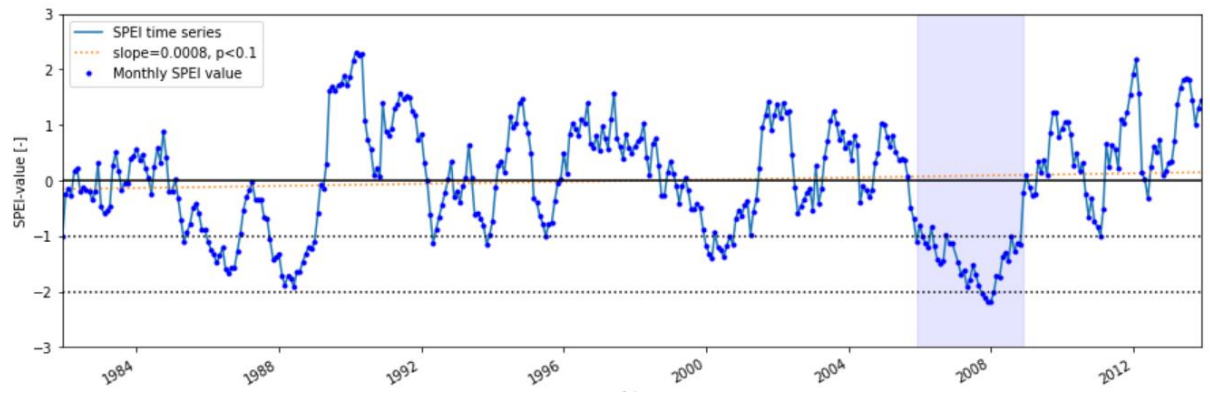


Figure B40: Time series of monthly SPEI at a 12-month time scale for the period of 1981-2013 of basin 3574500. The blue points represent the monthly SPEI values. The blue block represents times series of SPEI of the extreme drought event analyzed for this basin. The orange dashed line represents the linear regression line. The line regression equation here is: $y = 0.0008x - 0.1569$, $p < 0.1$.

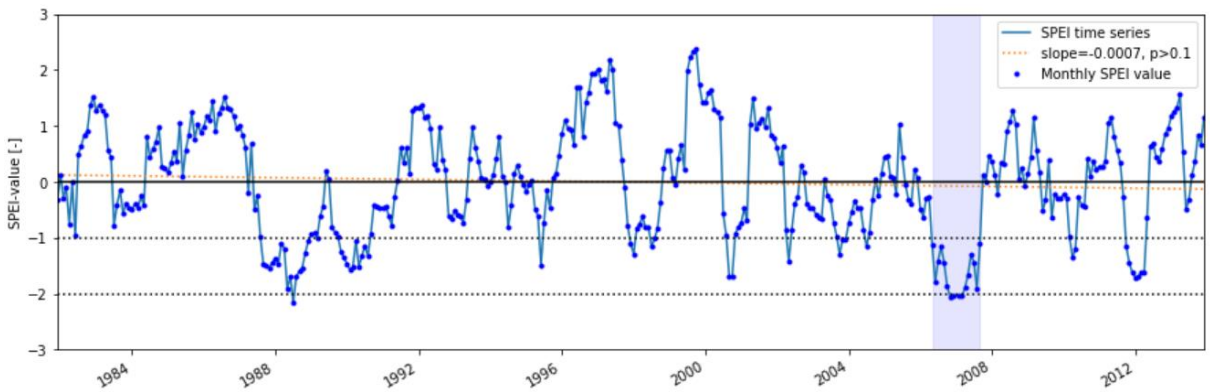


Figure B41: Time series of monthly SPEI at a 12-month time scale for the period of 1981-2013 of basin 4015330. The blue points represent the monthly SPEI values. The blue block represents times series of SPEI of the extreme drought event analyzed for this basin. The orange dashed line represents the linear regression line. The line regression equation here is: $y = -0.0007x + 0.1241$, $p > 0.1$.

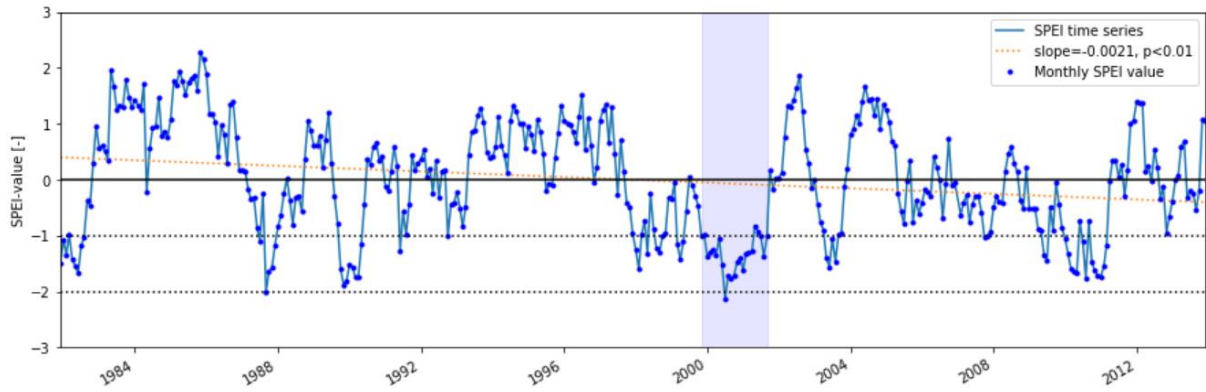


Figure B42: Time series of monthly SPEI at a 12-month time scale for the period of 1981-2013 of basin 4127997. The blue points represent the monthly SPEI values. The blue block represents times series of SPEI of the extreme drought event analyzed for this basin. The orange dashed line represents the linear regression line. The line regression equation here is: $y = -0.0021x + 0.402$, $p < 0.01$.

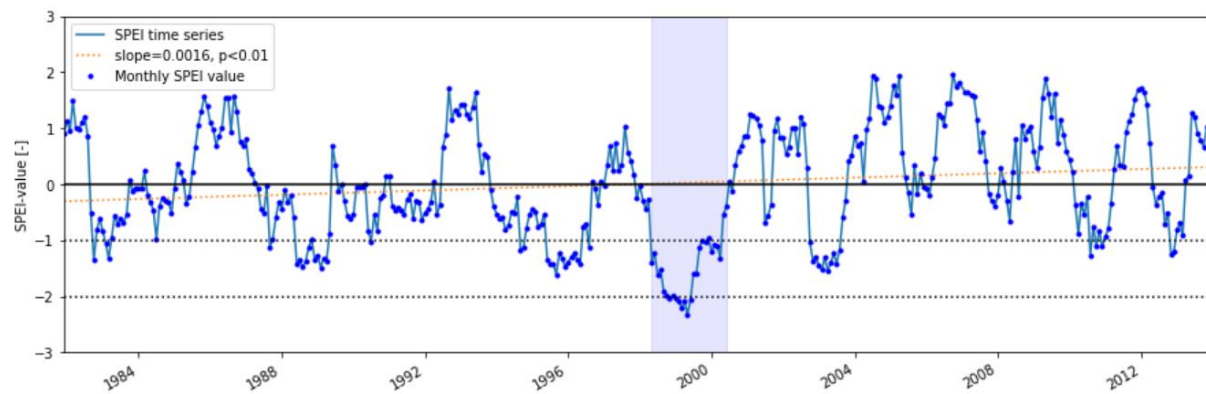


Figure B43: Time series of monthly SPEI at a 12-month time scale for the period of 1981-2013 of basin 4161580. The blue points represent the monthly SPEI values. The blue block represents times series of SPEI of the extreme drought event analyzed for this basin. The orange dashed line represents the linear regression line. The line regression equation here is: $y = 0.0016x - 0.3048$, $p < 0.01$.

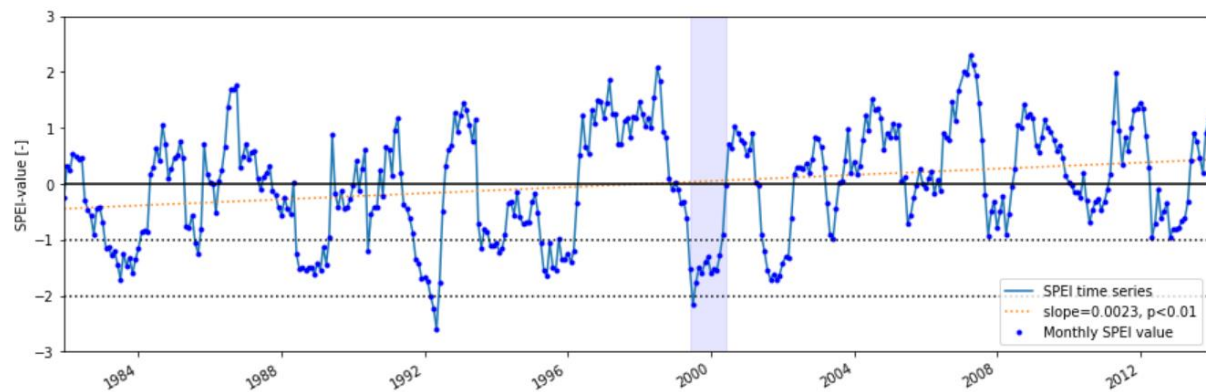


Figure B44: Time series of monthly SPEI at a 12-month time scale for the period of 1981-2013 of basin 4216418. The blue points represent the monthly SPEI values. The blue block represents times series of SPEI of the extreme drought event analyzed for this basin. The orange dashed line represents the linear regression line. The line regression equation here is: $y = 0.0023x - 0.4468$, $p < 0.01$.

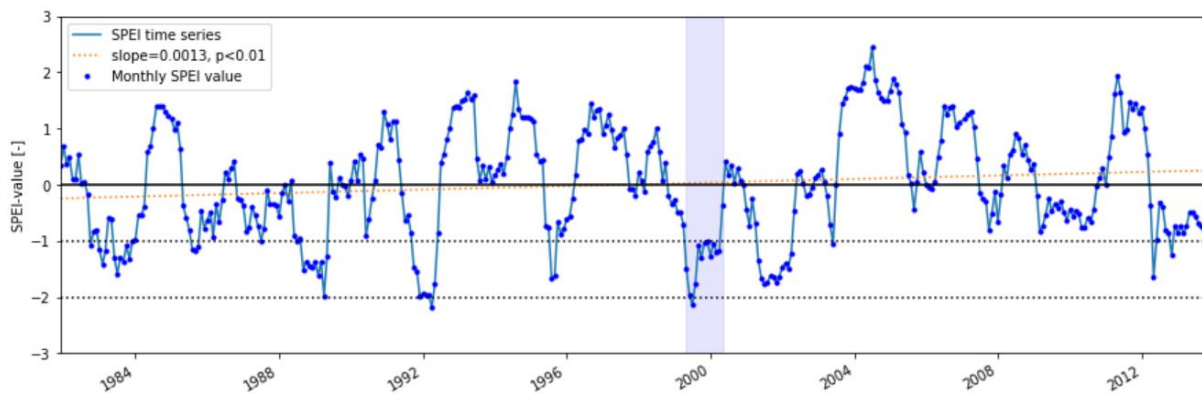


Figure B45: Time series of monthly SPEI at a 12-month time scale for the period of 1981-2013 of basin 4221000. The blue points represent the monthly SPEI values. The blue block represents times series of SPEI of the extreme drought event analyzed for this basin. The orange dashed line represents the linear regression line. The line regression equation here is: $y=0.0013x-2456$, $p < 0.01$.

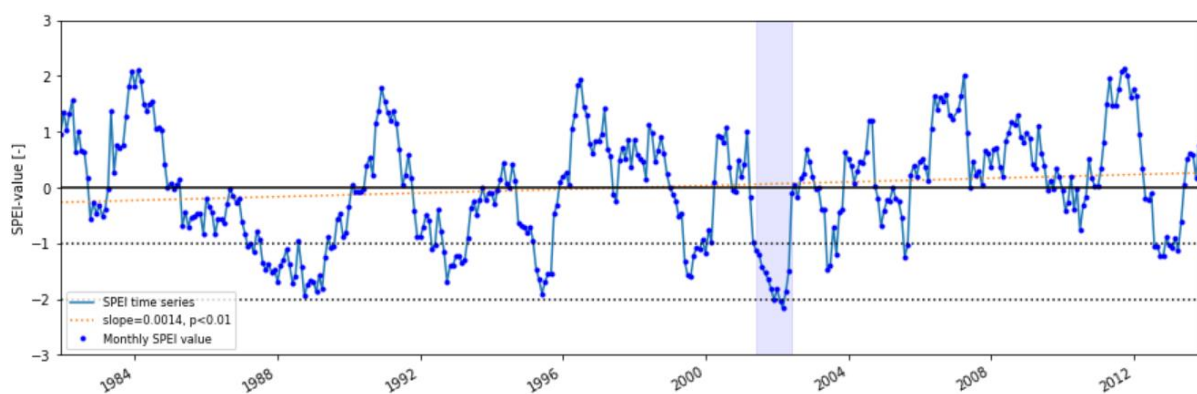


Figure B46: Time series of monthly SPEI at a 12-month time scale for the period of 1981-2013 of basin 4296000. The blue points represent the monthly SPEI values. The blue block represents times series of SPEI of the extreme drought event analyzed for this basin. The orange dashed line represents the linear regression line. The line regression equation here is: $y=0.0014x-0.2664$, $p < 0.01$.

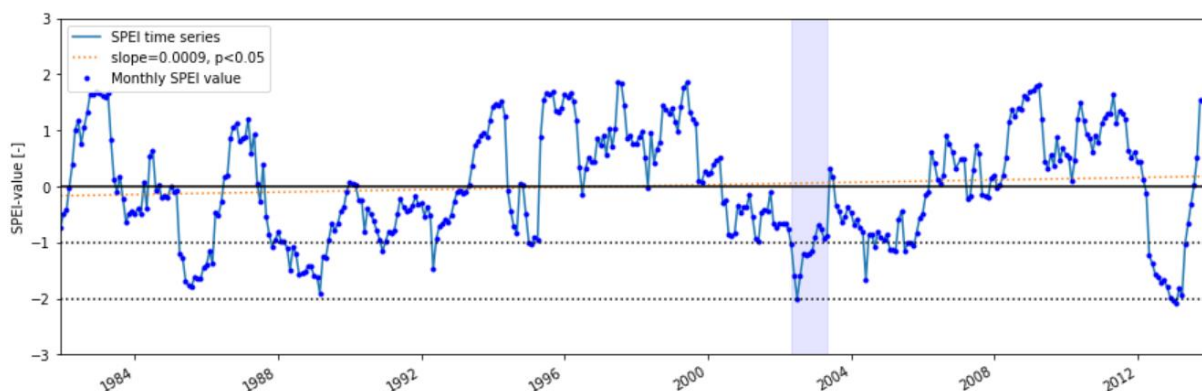


Figure B47: Time series of monthly SPEI at a 12-month time scale for the period of 1981-2013 of basin 6431500. The blue points represent the monthly SPEI values. The blue block represents times series of SPEI of the extreme drought event analyzed for this basin. The orange dashed line represents the linear regression line. The line regression equation here is: $y=0.0009x-0.1683$, $p < 0.05$.

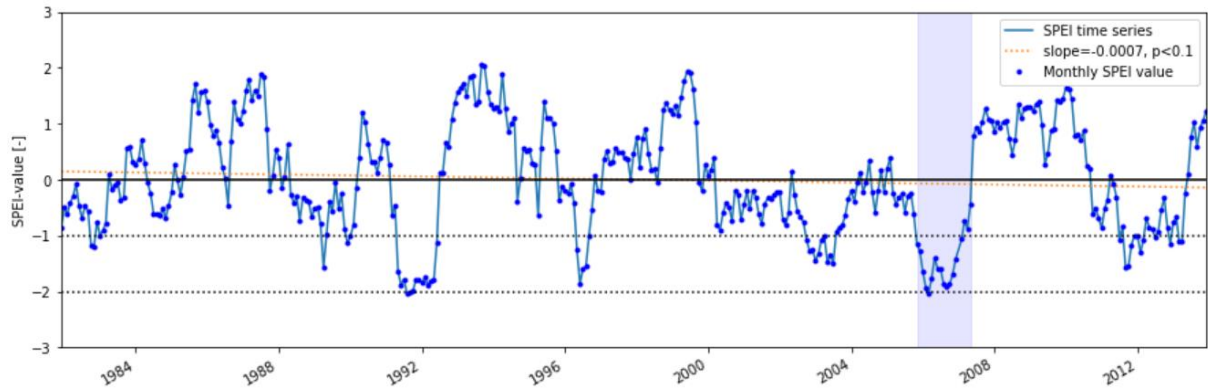


Figure B48: Time series of monthly SPEI at a 12-month time scale for the period of 1981-2013 of basin 7184000. The blue points represent the monthly SPEI values. The blue block represents times series of SPEI of the extreme drought event analyzed for this basin. The orange dashed line represents the linear regression line. The line regression equation here is: $y = -0.0007x + 0.1485$, $p < 0.1$.

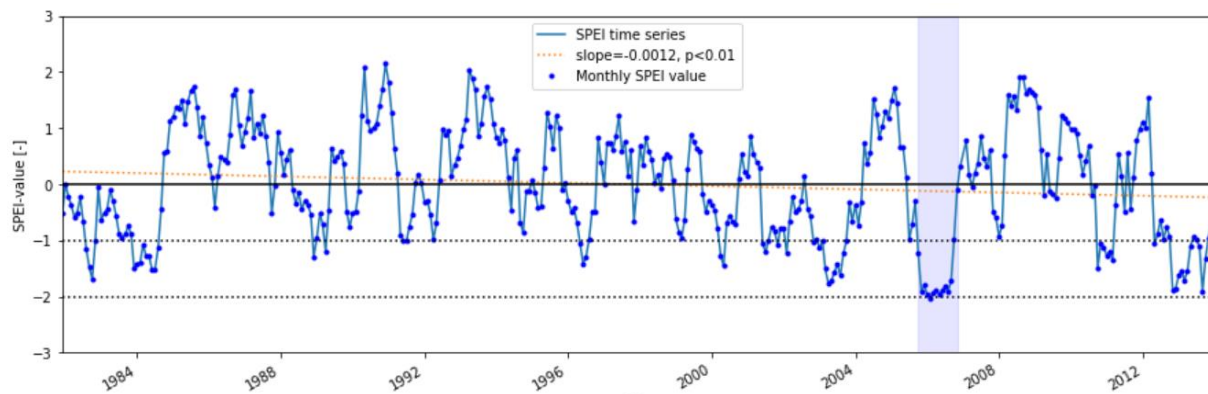


Figure B49: Time series of monthly SPEI at a 12-month time scale for the period of 1981-2013 of basin 7196900. The blue points represent the monthly SPEI values. The blue block represents times series of SPEI of the extreme drought event analyzed for this basin. The orange dashed line represents the linear regression line. The line regression equation here is: $y = -0.0012x + 0.2296$, $p < 0.01$.

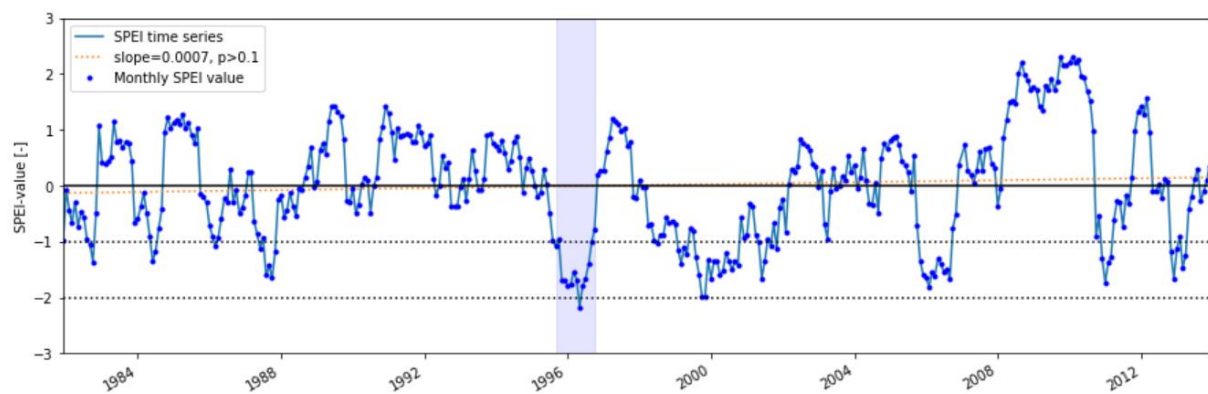


Figure B50: Time series of monthly SPEI at a 12-month time scale for the period of 1981-2013 of basin 7261000. The blue points represent the monthly SPEI values. The blue block represents times series of SPEI of the extreme drought event analyzed for this basin. The orange dashed line represents the linear regression line. The line regression equation here is: $y = 0.0007x - 0.1321$, $p > 0.1$.

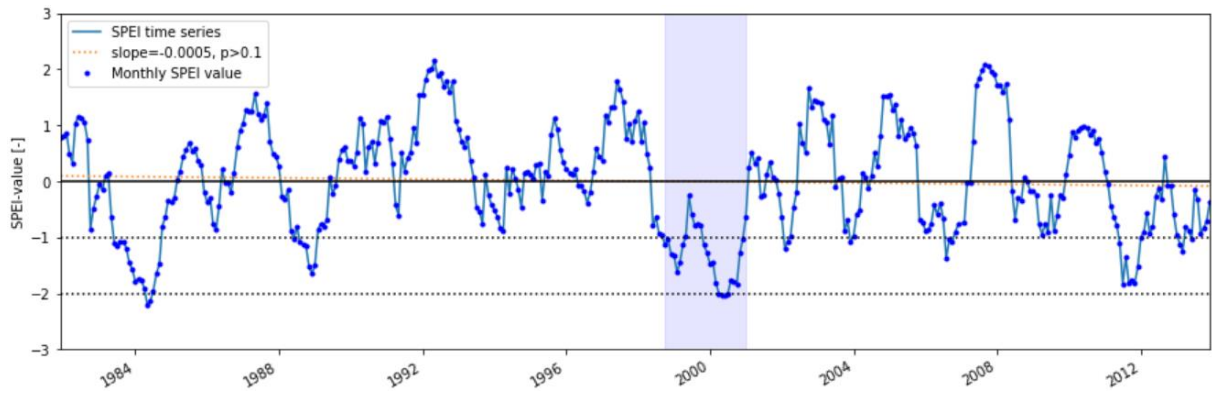


Figure B51: Time series of monthly SPEI at a 12-month time scale for the period of 1981-2013 of basin 8086290. The blue points represent the monthly SPEI values. The blue block represents times series of SPEI of the extreme drought event analyzed for this basin. The orange dashed line represents the linear regression line. The line regression equation here is: $y = -0.0005x + 0.0963$, $p > 0.1$.

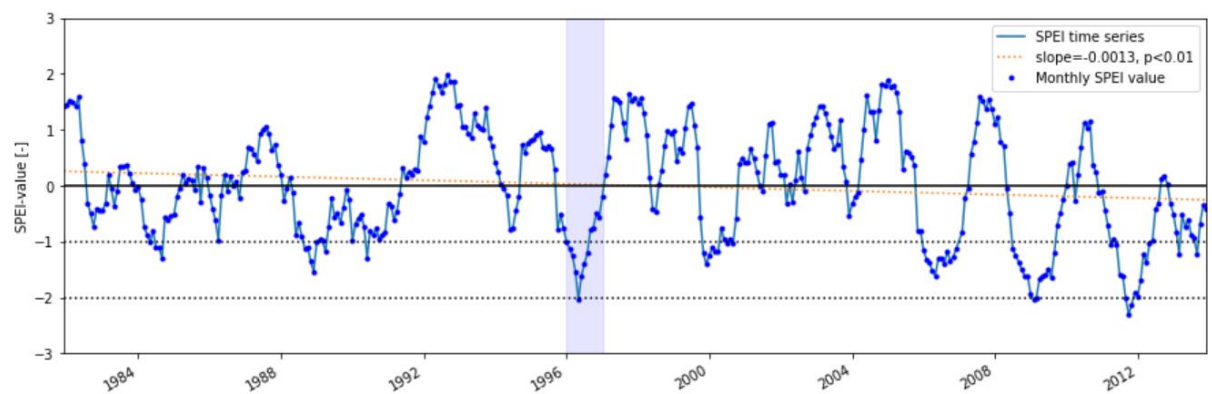


Figure B52: Time series of monthly SPEI at a 12-month time scale for the period of 1981-2013 of basin 8164300. The blue points represent the monthly SPEI values. The blue block represents times series of SPEI of the extreme drought event analyzed for this basin. The orange dashed line represents the linear regression line. The line regression equation here is: $y = -0.0013x + 0.259$, $p < 0.01$.

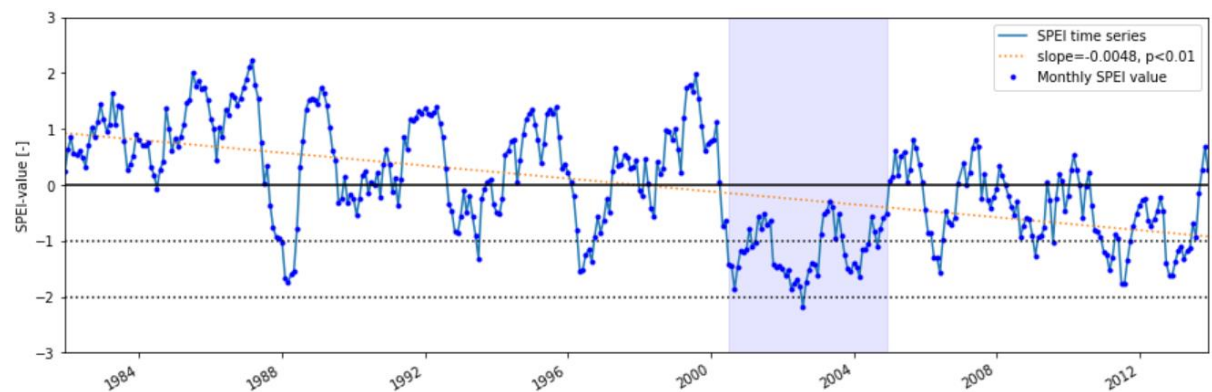


Figure B53: Time series of monthly SPEI at a 12-month time scale for the period of 1981-2013 of basin 8269000. The blue points represent the monthly SPEI values. The blue block represents times series of SPEI of the extreme drought event analyzed for this basin. The orange dashed line represents the linear regression line. The line regression equation here is: $y = -0.0048x + 0.9309$, $p < 0.01$.

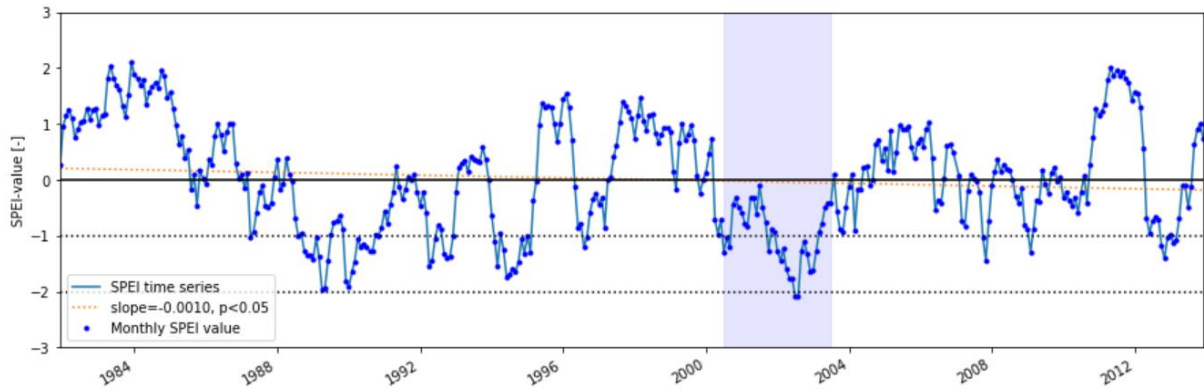


Figure B54: Time series of monthly SPEI at a 12-month time scale for the period of 1981-2013 of basin 10205030. The blue points represent the monthly SPEI values. The blue block represents times series of SPEI of the extreme drought event analyzed for this basin. The orange dashed line represents the linear regression line. The line regression equation here is: $y = -0.001x + 0.2069$, $p < 0.05$.

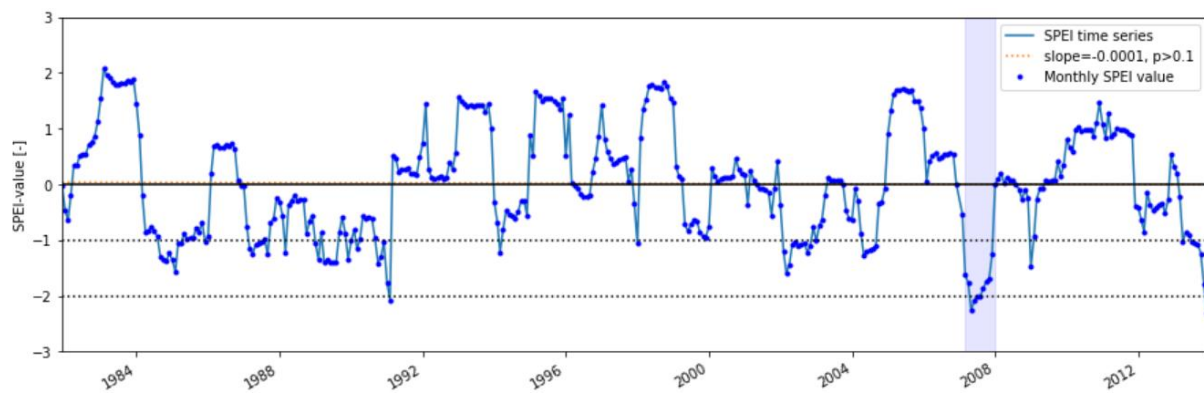


Figure B55: Time series of monthly SPEI at a 12-month time scale for the period of 1981-2013 of basin 11224500. The blue points represent the monthly SPEI values. The blue block represents times series of SPEI of the extreme drought event analyzed for this basin. The orange dashed line represents the linear regression line. The line regression equation here is: $y = -0.0001x + 0.0391$, $p > 0.1$.

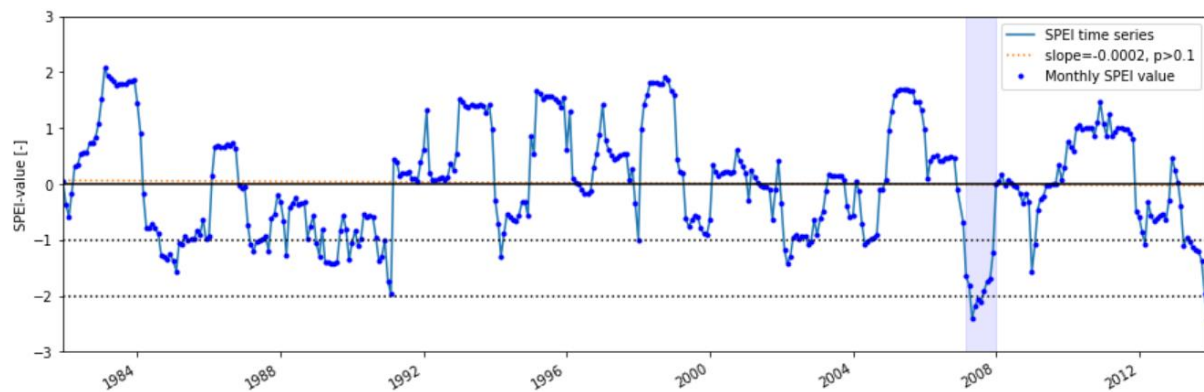


Figure B56: Time series of monthly SPEI at a 12-month time scale for the period of 1981-2013 of basin 11253310. The blue points represent the monthly SPEI values. The blue block represents times series of SPEI of the extreme drought event analyzed for this basin. The orange dashed line represents the linear regression line. The line regression equation here is: $y = -0.0002x + 0.0649$, $p > 0.1$.

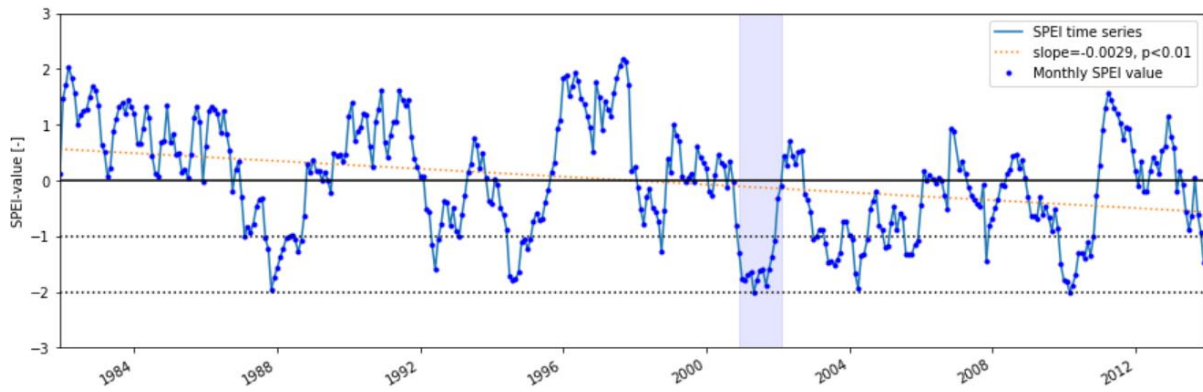


Figure B57: Time series of monthly SPEI at a 12-month time scale for the period of 1981-2013 of basin 12390700. The blue points represent the monthly SPEI values. The blue block represents times series of SPEI of the extreme drought event analyzed for this basin. The orange dashed line represents the linear regression line. The line regression equation here is: $y = -0.0029x + 0.5658$, $p < 0.01$.

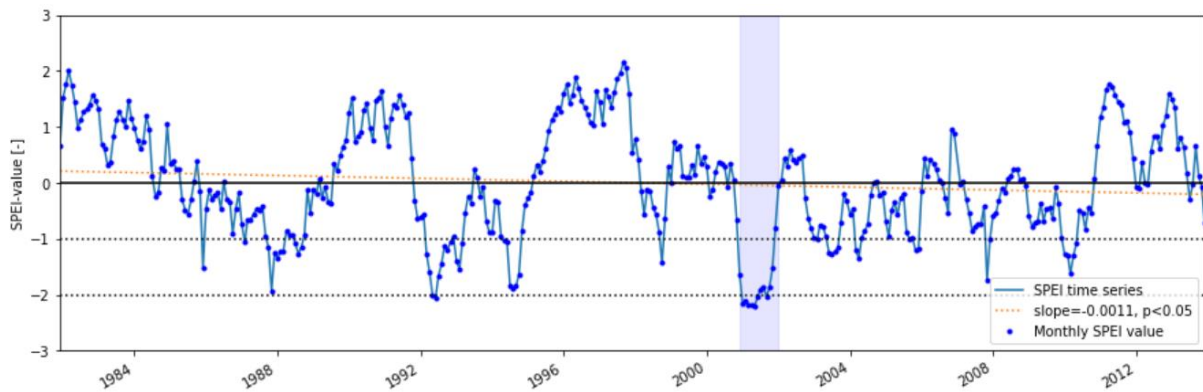


Figure B58: Time series of monthly SPEI at a 12-month time scale for the period of 1981-2013 of basin 12411000. The blue points represent the monthly SPEI values. The blue block represents times series of SPEI of the extreme drought event analyzed for this basin. The orange dashed line represents the linear regression line. The line regression equation here is: $y = -0.0011x + 0.2116$, $p < 0.05$.

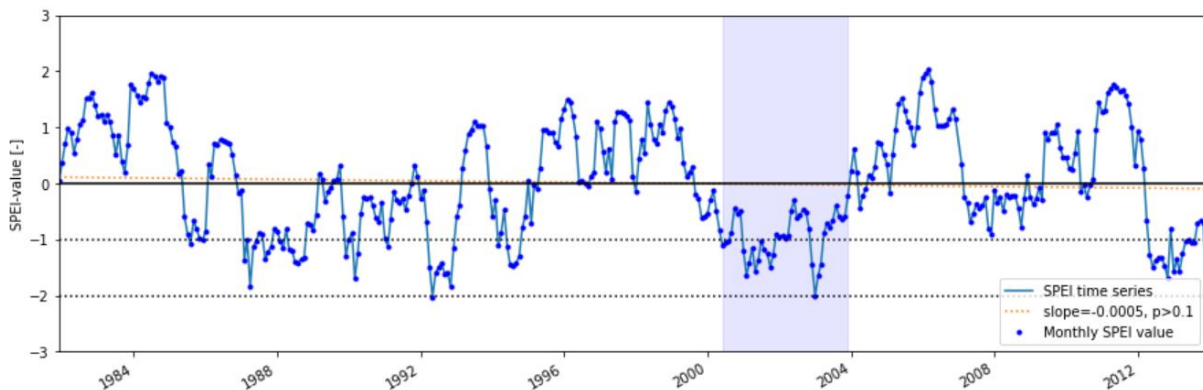


Figure B59: Time series of monthly SPEI at a 12-month time scale for the period of 1981-2013 of basin 13161500. The blue points represent the monthly SPEI values. The blue block represents times series of SPEI of the extreme drought event analyzed for this basin. The orange dashed line represents the linear regression line. The line regression equation here is: $y = -0.0005x + 0.1118$, $p > 0.1$.

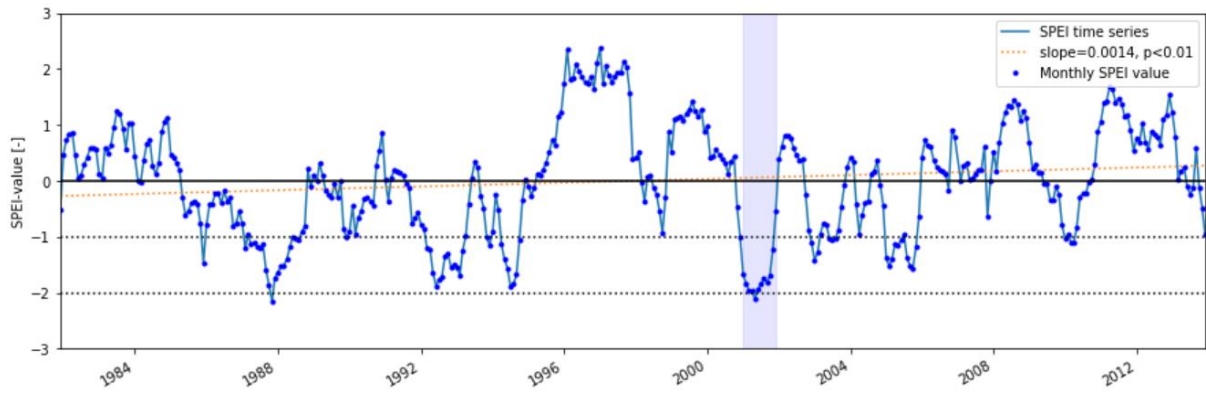


Figure B60: Time series of monthly SPEI at a 12-month time scale for the period of 1981-2013 of basin 14141500. The blue points represent the monthly SPEI values. The blue block represents times series of SPEI of the extreme drought event analyzed for this basin. The orange dashed line represents the linear regression line. The line regression equation here is: $y=0.0014x-0.2713$, $p < 0.01$.

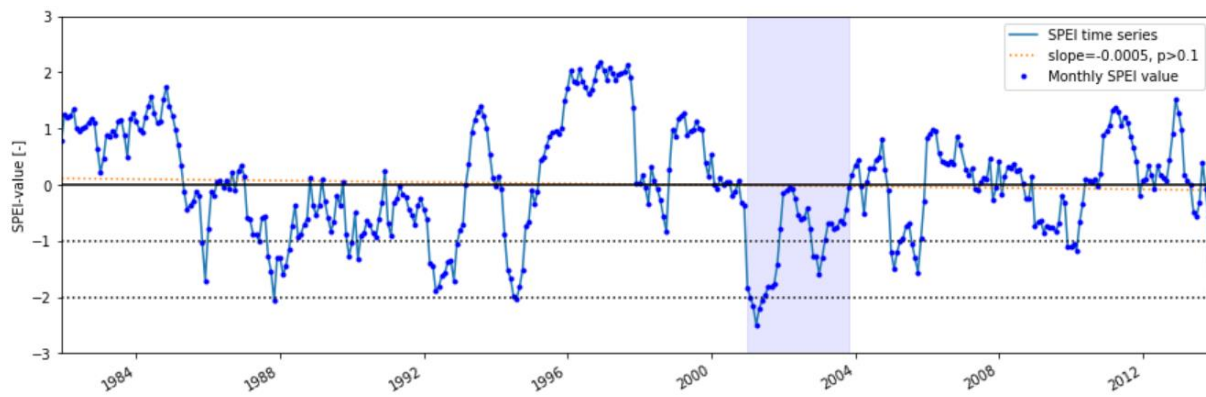


Figure B61: Time series of monthly SPEI at a 12-month time scale for the period of 1981-2013 of basin 14154500. The blue points represent the monthly SPEI values. The blue block represents times series of SPEI of the extreme drought event analyzed for this basin. The orange dashed line represents the linear regression line. The line regression equation here is: $y=-0.0005x+0.1131$, $p > 0.1$.

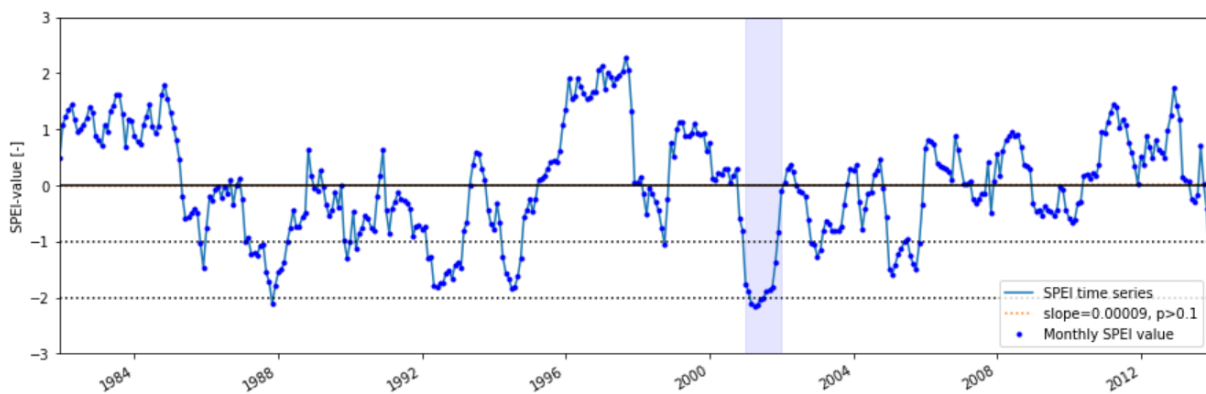


Figure B62: Time series of monthly SPEI at a 12-month time scale for the period of 1981-2013 of basin 14185000. The blue points represent the monthly SPEI values. The blue block represents times series of SPEI of the extreme drought event analyzed for this basin. The orange dashed line represents the linear regression line. The line regression equation here is: $y=0.00009x-0.0158$, $p > 0.1$.

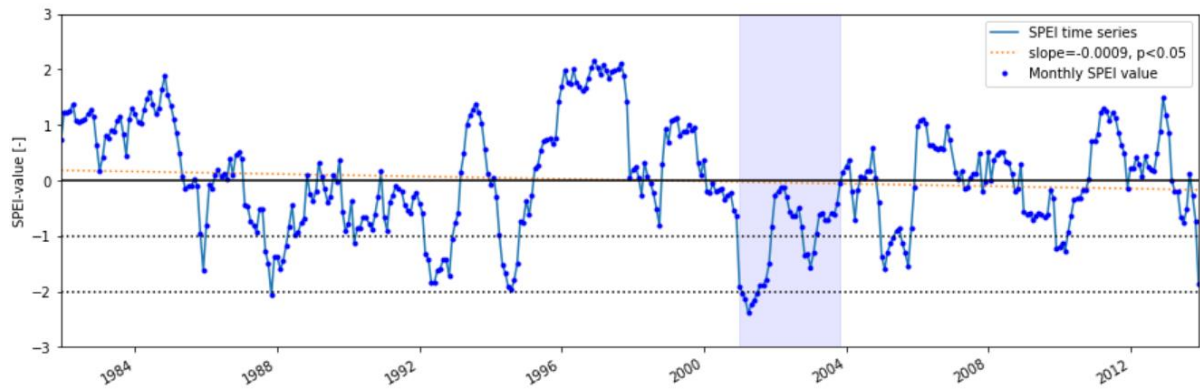


Figure B63: Time series of monthly SPEI at a 12-month time scale for the period of 1981-2013 of basin 14316700. The blue points represent the monthly SPEI values. The blue block represents times series of SPEI of the extreme drought event analyzed for this basin. The orange dashed line represents the linear regression line. The line regression equation here is: $y = -0.0009x + 0.1841$, $p < 0.05$.

Appendix C: Drought characteristics and pre- and post-drought periods

Table C: The start, end, duration, severity and intensity of extreme drought event (1990-2013) in each basin and overview of pre-drought period (5 years before the extreme drought event) and post-drought period (5 years after the extreme drought event)

No.	Basin ID	Start	End	Duration [Month]	Severity [-]	Intensity [-]	Pre-drought period	Post-drought period
1	1022500	Apr,2001	Dec,2002	20	-36.6	-2.60	Apr,1996-Mar,2001	Dec,2002-Nov,2007
2	1031500	Apr,2001	Nov,2003	31	-45.5	-2.26	Apr,1996-Mar,2001	Nov,2003-Oct,2008
3	1139000	May,2001	Nov,2002	18	-24.3	-2.05	May,1996-Apr,2001	Nov,2002-Oct,2007
4	1139800	May,2001	Nov,2003	30	-34.6	-2.01	May,1996-Apr,2001	Nov,2003-Oct,2008
5	1169000	Oct,2001	Feb,2003	16	-20.5	-2.13	Oct,1996-Sep,2001	Feb,2003-Jan,2008
6	1181000	Jul,2001	Jan,2003	18	-29.0	-2.43	Jul,1996-Jun,2001	Jan,2003-Dec,2007
7	1411300	Sep,2001	Dec,2002	15	-24.3	-2.16	Sep,1996-Aug,2001	Dec,2002-Nov,2007
8	1439500	Jun,1995	Apr,1996	10	-12.4	-2.51	Jun,1990-May,1995	Apr,1996-Mar,2001
9	1440000	Jul,2001	Dec,2002	17	-25.5	-2.20	Jul,1996-Jun,2001	Dec,2002-Nov,2007
10	1440400	Jun,1995	Apr,1996	10	-11.4	-2.42	Jun,1990-May,1995	Apr,1996-Mar,2001
11	1451800	Jun,2001	Jun,2003	24	-32.8	-2.50	Jun,1996-May,2001	Jun,2003-May,2008
12	1542810	May,1999	Jun,2002	37	-44.8	-2.12	May,1994-Apr,1999	Jun,2002-May,2007
13	1543000	Aug,1995	May,1996	9	-9.1	-2.12	Aug,1990-Jul,1995	May,1996-Apr,2001
14	1547700	Apr,1999	Dec,2002	44	-48.3	-2.75	Apr,1994-Mar,1999	Dec,2002-Nov,2007
15	1568000	May,2001	Feb,2003	21	-30.5	-2.28	May,1996-Apr,2001	Feb,2003-Jan,2008
16	1580000	Jul,2001	Feb,2003	19	-29.3	-2.24	Jul,1996-Jun,2001	Feb,2003-Jan,2008
17	1620500	Mar,1999	Aug,2000	17	-26.2	-2.20	Mar,1994-Feb,1999	Aug,2000-Jul,2005
18	1634500	Mar,1999	Aug,2000	17	-21.7	-2.61	Mar,1994-Feb,1999	Aug,2000-Jul,2005
19	1638480	Mar,1999	Jun,2000	15	-14.9	-2.17	Mar,1994-Feb,1999	Jun,2000-May,2005
20	1644000	Feb,1999	Jun,2000	16	-15.9	-2.26	Feb,1994-Jan,1999	Jun,2000-May,2005
21	2011400	Apr,1999	Jul,2000	15	-21.8	-2.27	Apr,1994-Mar,1999	Jul,2000-Jun,2005
22	2011460	Apr,1999	Jul,2000	15	-22.3	-2.32	Apr,1994-Mar,1999	Jul,2000-Jun,2005
23	2013000	May,1999	Jul,2000	14	-15.4	-2.02	May,1994-Apr,1999	Jul,2000-Jun,2005
24	2046000	Sep,2001	Feb,2003	17	-24.6	-2.39	Sep,1996-Aug,2001	Feb,2003-Jan,2008
25	2064000	Sep,2001	Feb,2003	17	-24.1	-2.67	Sep,1996-Aug,2001	Feb,2003-Jan,2008
26	2065500	Sep,2001	Feb,2003	17	-21.5	-2.82	Sep,1996-Aug,2001	Feb,2003-Jan,2008
27	2300700	Jun,2006	Jun,2008	24	-21.8	-2.07	Jun,2001-May,2006	Jun,2008-May,2013
28	2374500	Sep,1999	Jun,2001	21	-28.9	-2.14	Sep,1994-Aug,1999	Jun,2001-May,2006
29	2422500	Aug,2006	Dec,2008	28	-35.2	-2.61	Aug,2001-Jul,2006	Dec,2008-Nov,2013
30	2450250	Jul,2006	Jan,2009	30	-39.6	-2.37	Jul,2001-Jun,2006	Jan,2009-Dec,2008
31	2469800	Jan,2000	Jun,2001	17	-27.4	-2.38	Jan,1995-Dec,1999	Jun,2001-May,2006
32	2472500	Feb,1999	Jun,2001	28	-38.2	-2.10	Feb,1994-Jan,1999	Jun,2001-May,2006
33	2481000	Sep,1999	Jul,2001	22	-36.3	-2.33	Sep,1994-Aug,1999	Jul,2001-Jun,2006
34	2481510	Apr,1999	Jul,2001	27	-40.0	-2.42	Apr,1994-Mar,1999	Jul,2001-Jun,2006
35	3011800	Jun,1999	Jun,2002	36	-51.9	-2.26	Jun,1994-May,1999	Jun,2002-May,2007
36	3015500	Nov,1998	Jul,2002	44	-53.1	-2.20	Nov,1993-Oct,1998	Jul,2002-Jun,2007
37	3021350	Nov,1998	Sep,2000	22	-34.1	-2.31	Nov,1993-Oct,1998	Sep,2000-Aug,2005
38	3026500	Jun,1999	Jun,2002	36	-51.1	-2.35	Jun,1994-May,1999	Jun,2002-May,2007

Table C (continued)

No.	Basin ID	Start	End	Duration [Month]	Severity [-]	Intensity [-]	Pre-drought period	Post-drought period
39	3028000	Jun,1999	Aug,2002	38	-48.7	-2.33	Jun,1994-May,1999	Aug,2002-Jul,2007
40	3574500	Dec,2005	Jan,2009	37	-52.7	-2.19	Dec,2000-Nov,2005	Jan,2009-Dec,2008
41	4015330	May,2006	Oct,2007	17	-28.2	-2.06	May,2001-Apr,2006	Oct,2007-Sep,2012
42	4127997	Nov,1999	Oct,2001	23	-30.7	-2.13	Nov,1994-Oct,1999	Oct,2001-Sep,2006
43	4161580	May,1998	Jul,2000	26	-39.4	-2.32	May,1993-Apr,1998	Jul,2000-Jun,2005
44	4216418	Jun,1999	Jul,2000	13	-18.1	-2.16	Jun,1994-May,1999	Jul,2000-Jun,2005
45	4221000	May,1999	Jun,2000	13	-16.8	-2.14	May,1994-Apr,1999	Jun,2000-May,2005
46	4296000	Jun,2001	Jul,2002	13	-20.3	-2.16	Jun,1996-May,2001	Jul,2002-Jun,2007
47	6431500	May,2002	Jun,2003	13	-27.5	-2.00	May,1997-Apr,2002	Jun,2003-May,2008
48	7184000	Nov,2005	Jun,2007	19	-25.1	-2.04	Nov,2000-Oct,2005	Jun,2007-May,2012
49	7196900	Oct,2005	Dec,2006	14	-23.1	-2.04	Oct,2000-Sep,2005	Dec,2006-Nov,2011
50	7261000	Sep,1995	Nov,1996	14	-21.0	-2.17	Sep,1990-Aug,1995	Nov,1996-Oct,2001
51	8086290	Oct,1998	Feb,2001	28	-36.7	-2.05	Oct,1993-Sep,1998	Feb,2001-Jan,2006
52	8164300	Jan,1996	Feb,1997	13	-14.0	-2.04	Jan,1991-Dec,1995	Feb,1997-Jan,2002
53	8269000	Jul,2000	Jan,2005	54	-63.3	-2.18	Jul,1995-Jun,2000	Jan,2005-Dec,2009
54	10205030	Jul,2000	Aug,2003	37	-37.2	-2.09	Jul,1995-Jun,2000	Aug,2003-Jul,2008
55	11224500	Mar,2007	Feb,2008	11	-18.3	-2.25	Mar,2002-Feb,2007	Feb,2008-Jan,2013
56	11253310	Mar,2007	Feb,2008	11	-18.8	-2.40	Mar,2002-Feb,2007	Feb,2008-Jan,2013
57	12390700	Dec,2000	Mar,2002	15	-21.6	-2.00	Dec,1995-Nov,2000	Mar,2002-Feb,2007
58	12411000	Dec,2000	Feb,2002	14	-24.6	-2.21	Dec,1995-Nov,2000	Feb,2002-Jan,2007
59	13161500	Jun,2000	Jan,2004	43	-40.6	-2.01	Jun,1995-May,2000	Jan,2004-Dec,2008
60	14141500	Jan,2001	Jan,2002	12	-20.3	-2.10	Jan,1996-Dec,2000	Jan,2002-Dec,2006
61	14154500	Jan,2001	Dec,2003	35	-37.1	-2.50	Jan,1996-Dec,2000	Dec,2003-Nov,2008
62	14185000	Jan,2001	Feb,2002	13	-21.9	-2.16	Jan,1996-Dec,2000	Feb,2002-Jan,2007
63	14316700	Jan,2001	Dec,2003	35	-37.7	-2.39	Jan,1996-Dec,2000	Dec,2003-Nov,2008
Average				22	-29.7	-2.26		

Appendix D: Relative changes of streamflow and evaporation

Table D: Relative changes of streamflow and evaporation induced by the combination effect of drought-related climate and landscape changes

No.	Basin ID	Q RC [%]	Ea RC [%]
1	1022500	20.3	7.8
2	1031500	25.8	11.6
3	1139000	3.9	9.1
4	1139800	19.6	22.8
5	1169000	25.4	16.9
6	1181000	13.6	7.2
7	1411300	11.3	11.7
8	1439500	10.1	30.4
9	1440000	5.6	23.2
10	1440400	4.7	17.6
11	1451800	41.4	1.3
12	1542810	22.4	0.2
13	1543000	24.1	14.0
14	1547700	20.8	7.4
15	1568000	4.6	7.1
16	1580000	29.0	2.6
17	1620500	15.5	3.1
18	1634500	13.9	9.7
19	1638480	3.0	6.9
20	1644000	6.2	6.0
21	2011400	1.0	0.4
22	2011460	4.8	2.3
23	2013000	2.6	8.4
24	2046000	30.3	1.2
25	2064000	5.0	15.3
26	2065500	3.9	9.7
27	2300700	38.9	4.9
28	2374500	10.4	8.3
29	2422500	4.3	6.3
30	2450250	1.6	4.5
31	2469800	14.3	9.6
32	2472500	1.2	10.0
33	2481000	2.5	5.0
34	2481510	2.2	4.7
35	3011800	13.8	21.4
36	3015500	5.3	1.8
37	3021350	3.4	14.0
38	3026500	10.5	15.5

Table D (continued)

No.	Basin ID	Q RC [%]	Ea RC [%]
39	3028000	17.7	18.3
40	3574500	5.0	15.7
41	4015330	22.2	0.2
42	4127997	7.8	12.2
43	4161580	11.6	21.8
44	4216418	21.1	18.3
45	4221000	7.9	2.8
46	4296000	9.3	7.1
47	6431500	37.9	5.5
48	7184000	90.2	1.1
49	7196900	109.1	18.2
50	7261000	34.6	0.8
51	8086290	53.8	2.1
52	8164300	21.2	0.9
53	8269000	31.2	11.7
54	10205030	18.0	1.8
55	11224500	0.0	1.4
56	11253310	22.0	1.7
57	12390700	30.4	1.4
58	12411000	19.4	0.8
59	13161500	15.4	5.2
60	14141500	18.2	1.0
61	14154500	20.6	2.0
62	14185000	20.4	9.6
63	14316700	22.1	21.0
Mean change		18.2	8.6

The mean annual evaporation (Ea) in pre- and post-drought periods was estimated by $Ea = P - Q$ according to Equation 3.1, assuming that the storage change is negligible.